UNIVERSITY OF
BIRMINGHAM

DESIGN AND DEVELOPMENT OF WIRELESS UNDERGROUND SENSOR NETWORKS FOR PIPELINE MONITORING

By

Ali Mollazadeh Sadeghioon

A thesis submitted to
The University of Birmingham
For the degree of
Doctor of Philosophy

School of Mechanical Engineering
The University of Birmingham
October 2014

Abstract

Infrastructure monitoring, and specifically pipeline monitoring (e.g. water supply systems), is becoming crucial in order to achieve improved asset management and a more sustainable future. A vast amount of research has been carried out in the field of pipeline monitoring and various pipeline monitoring/assessment techniques have been developed. However, different drawbacks in each of these methods have prevented them from being widely used on water distribution systems. In this research a comprehensive review of the current state-of-the-art in pipeline monitoring is presented and the advantages and disadvantages of each of these methods are discussed in detail. The main disadvantages of current pipeline monitoring systems are their invasive nature (access to the inside of the pipe), their unsuitability for continuous, long-term monitoring and the lack of redundancy. Thus, an ultra-low power Wireless Underground Sensor Network (WUSN) has been carefully researched, designed, developed and presented as part of this project. The sensor system consists of discrete nodes with associated sensors communicating with each other and to more sparsely placed mother nodes. The power consumption of the nodes was minimised through multiple iterations of software and hardware design in order to achieve a long operational lifetime. A data management system was designed and developed in order to sort the data coming from the nodes and upload them to an internet server, which enables the data to be readily accessible from any internet connected device.

In addition, a novel non-invasive (to the pipe) relative pressure sensor assembly has been designed, modelled and developed based on Force Sensitive Resistors (FSR). The performance of this sensor is validated by comparison with commercial pressure sensors, and both laboratory and field trials. In these field trials the FSR-based

pressure sensor assemblies were used in conjunction with the developed sensor node to measure daily pressure variations and induced leaks. RF transmission through the soil is one of the main challenges in the field of WUSNs, particularly for buried pipelines, where data needs to be transmitted through the soil between nodes and to the ground surface. Various parameters affect RF signal attenuation in soil (i.e. transmission frequency, burial depth, soil dielectric properties, etc.). In this research existing models for RF transmission are reviewed and compared with measurements from field trials. In addition a modification to an existing method of extracting real and imaginary parts of permittivity is proposed in order to improve the accuracy of the existing RF propagation models.

The key achievements of the research therefore are:

- An ultra-low power sensor node developed specifically for buried pipeline monitoring.
- A novel non-invasive relative pressure sensor assembly based on Force Sensitive Resistors (FSR), validated by both laboratory and field trials.
- Successful burst detection based on non-absolute (relative) pressure measurements in laboratory tests and field trials.
- Improved model for approximation of RF signal attenuation in soil.

To my family without whom I am incomplete

Acknowledgements

This research and thesis was made possible with the fantastic support and help that I have received from a number of people and I would like to express my gratitude towards them.

Firstly I would like to especially thank my supervisory group: Dr. Nicole Metje, Dr. Carl Anthony, Dr. Mike Ward and Dr. David Chapman for their invaluable help, guidance and support through the course of my studies.

I would also like to thank all of my present and former colleagues and friends. Particularly I would like to thank Rob and Tom for the fantastic times I spent in the office. A special thank you also goes to Ali, Haseena and Aydin for making the office a lively and happy place.

This thesis was copy edited for conventions of language, spelling and grammar by Janet's Proofreading Service.

No words can convey my gratitude to my family, who has supported me in every step of my life. A very special thank you to my father Iraj; without his support I would not have been able to complete my studies and achieve any of my goals. I also wish to express my gratitude to my wonderful sisters, Ladan and Lida, who were always there to help me whenever I needed them. A big thank you goes to my fantastic wife Lana for her love, patience and support; she made tough times easier and filled my life with love. Finally, I want to give my biggest thank you to my son Alan. He filled my life with happiness and joy and I would not exchange anything in the world for his beautiful smile.

Ali M. Sadeghioon

Birmingham

October, 2014

Publications

During the course of the research presented in this thesis the following journal papers and conference proceedings were published:

Journal publications

A. M. Sadeghioon, N. Metje, D. Chapman, and C. Anthony, "SmartPipes: Smart Wireless Sensor Networks for Leak Detection in Water Pipelines," *Journal of Sensor and Actuator Networks*, vol. 3, no. 1, pp. 64–78, Feb. 2014. (Presented in Appendix D)

A. M. Sadeghioon, R. Walton, D. Chapman, N. Metje, C. Anthony, and M. Ward, "Design and Development of a Nonintrusive Pressure Measurement System for Pipeline Monitoring," *Journal of Pipeline Systems Engineering and Practice*, vol. 5, no. 3, pp. 3–6, 2014. (Presented in Appendix D)

N. Metje, D. N. Chapman, R. Walton, A. M. Sadeghioon, M. Ward, "Real time condition monitoring of buried water pipes," *Tunnelling and Underground Space Technology*, vol. 28, pp. 315–320, Mar. 2012.

Conference proceedings

R. Walton, A. M. Sadeghioon, N. Metje, D. Chapman, and M. Ward, "Smart Pipes: The Future for Proactive Asset Management," in *Proceedings of the International Conference on Pipelines and Trenchless Technology*, Beijing, China, 2011, pp. 1512–1523.

"The scientific man does not aim at an immediate result. He does not expect that his advanced ideas will be readily taken up. His work is like that of the planter, for the future. His duty is to lay the foundation for those who are to come, and point the way."

Nikola Tesla

Contents

List of Figures

List of Tables

1

INTRODUCTION

Contents

Chapter overview

This chapter provides a brief introduction to the background of smart wireless sensor networks for pipeline monitoring. In addition the motivation for the work is described and the aim and objectives of the research are identified. This is followed by a description of the layout of this thesis.

1.1 Background and motivation

Ageing infrastructures and a greater move towards sustainability have created new challenges for asset owners and operators. This has made the monitoring of critical structures such as water distribution networks crucial for the asset owners.

Transportation of vital commodities such as water, oil and gas is commonly done by means of pipeline networks. Faults in these pipes can create major financial implications and possible environmental catastrophes. During the period of 2009-2010 in England and Wales, more than 3 Giga litres of water were lost every day[1] due to faults in water pipelines (Department for Environment Food and Rural Affairs, 2011). Although the economic value of water is significantly lower than oil or gas in the UK and it is not usually harmful for the environment, the financial implications of these losses are not only limited to the value of the water that is lost but also include damage to other assets/properties and large repair costs. Additionally, in some cases pipeline failure could cause disruption to the service; which will negatively impact on the water suppliers' public image.

Technological advances and reductions in the cost of electrical components have made the monitoring of large infrastructures more feasible. Moreover, the proliferation of the Internet has opened up new applications for the "Internet of Things"; and for the Internet to serve as a backbone for infrastructure monitoring.

Currently, buried pipelines are either only monitored at key points, which can be spaced several kilometres apart, or are inspected in sections with survey based (non-permanent) techniques (i.e. ground penetrating radar). A continuous monitoring system with a higher

[1] Combined loss of distribution and supply networks.

spatial resolution would not only provide operators with a better understanding of their network, but also will have a higher reliability and a faster response to faults.

Various methods are used in order to detect and locate leaks in pipes (Liu and Kleiner, 2013; Al-Barqawi and Zayed, 2006; Misiunas, 2005). The main methods for pipe monitoring are acoustic measurements; pressure measurements; vision-based systems; Ground Penetrating Radar (GPR) based systems; fibre optic monitoring and multimodal systems.

One of the main issues in continuous infrastructure monitoring is power consumption and power availability. Most monitoring systems with an exception of passive systems (i.e. fibre optics and Radio-Frequency Identification, RFID tags) require a power supply in order to operate. The large scale of pipeline networks, their long operational life and lack of a long-term, easily accessible power source below ground, make the power supply and power consumption of continuous pipeline monitoring systems a crucial factor towards their successful implementation.

Another main challenge for pipeline monitoring is their sensing technology. The performance of the sensing technology used in a monitoring system directly affects its overall performance characteristics; such as power consumption, ease of installation, cost and reliability.

Wireless Sensor Networks (WSN) are a group of individual nodes that are capable of sensing their environment via application specific sensors, process the recorded data locally and transfer the packaged data to a central server (Akyildiz and Vuran, 2010). WSNs can be generally divided into single–hop and multi-hop networks. In the single-hop networks each node directly communicate with a designated master node (server) while in the multi-hop networks data can be relayed by other nodes multiple times before it reaches the master node

(server). The focus of this research was on the single-hop (star network) WSN for pipeline monitoring.

Any monitoring system, which is used for pipeline monitoring, is part of a larger system of pipeline networks, which contain many other sub-systems (for example logging, maintenance and operational control systems). In order for the pipeline monitoring system to be successful it needs to be designed with a holistic approach considering requirements and limitations of the overall system and other sub-systems.

The "SmartPipes" research project was jointly funded initially by UK Water Industry Research (UKWIR), Water Research Foundation (WRF, USA) and the University of Birmingham in 2006, in order to study the feasibility of a continuous smart pipeline monitoring system and its associated challenges. The second phase of this research project was also jointly funded by UKWIR and the University of Birmingham in 2010, following the success of the initial phase (Metje et al., 2011).

The second phase of the "SmartPipes" project was divided into two research projects. One of these research projects was focused on researching and developing a long-life power supply suitable for buried pipeline monitoring systems. The other aspect of the second phase of this project was focused on the research, design and development of ultra low-power wireless (long operational life) monitoring systems for pipeline monitoring and their associated sensors. This thesis presents the latter aspect of the project.

1.2 Aim and objectives

The principal aim of this research is to design and manufacture a long-term, ultra low power, continuous condition assessment monitoring system for buried water pipelines. Due to the multidisciplinary nature of the project a holistic (systems engineering) approach was chosen

in order to tackle the challenges in this research. The following objectives were identified in order to achieve this aim:

- To conduct a critical review of the literature related to current infrastructure monitoring systems, specifically underground monitoring technologies for pipeline monitoring.
- To investigate the main requirements of a long-term continuous pipeline monitoring system and to identify the limitations imposed by the environment on wireless monitoring systems for underground pipeline monitoring.
- To identify the parameters affecting the power consumption of underground wireless sensor nodes.
- To design and manufacture an ultra-low power wireless sensor node for pipeline monitoring based on commercially available components.
- To minimise the power consumption of the node through hardware and software optimisation.
- To design and develop non-invasive sensors for pipeline monitoring systems and assess their performance via laboratory tests and analytical and numerical models (finite element analysis).
- To assess the performance of the node and sensors through laboratory tests and long-term field experiments and to assess leak detection capabilities of the system in laboratory and field trials.
- To investigate the effect of soil on Radio Frequency (RF) signal propagation and comparison of existing models with results from field trials.

Therefore, the research hypothesis is that Wireless Sensor Networks (WSN) can be adapted with a holistic approach (using commercially available components) for the long-term

monitoring of buried pipelines despite the challenging conditions. In addition, it is hypothesised that RF communication through soil based on commercially available and permitted frequency bands is limited by the range of reliable communication.

1.3 Thesis layout

This thesis is composed of seven chapters, detailing the research, design and development of smart wireless sensor networks for pipeline monitoring.

A detailed and critical review of the current state of the art in pipeline monitoring is presented in Chapter 2. This chapter also includes a critical review of the current research in underground wireless sensor networks and the challenges associated with them. It concludes by highlighting the main gaps in the literature.

Chapter 3 describes the design and development of smart wireless sensor networks for pipeline monitoring. The hardware and software design iterations of the node and the efforts expended in minimising their power consumption are described in detail in this chapter.

Chapter 4 of this thesis reports on the design, theory of operation and development of a novel non-invasive relative pressure sensor. The behaviour of these sensors is described using analytical and numerical models. Additionally, the laboratory tests used for the validation and comparison of the proposed sensor with a commercial pressure sensor are presented and the results from these tests are illustrated and discussed in this chapter.

Leak detection and the localisation capabilities of the Force Sensitive Resistor (FSR) based relative pressure sensor were studied via laboratory tests and extended field trials and are described in detail in Chapter 5. This chapter also describes the methodology used in both the

field and laboratory tests. Additionally, the performance of the nodes tested during the field trials is analysed in this chapter.

Chapter 6 reports on the effect of soil on the RF transmission through soil. The methodology used for the RF attenuation field trials is described and results from these trials are presented and discussed in this chapter. A modification to method of extraction of real and imaginary parts of permittivity from TDR waveform for use in prediction of RF attenuation in soil is proposed. Results of the proposed method are compared with the existing methods and the measurement from the field trials.

Finally, the thesis is concluded in Chapter 7. This includes recommendations for future work.

2

LITERATURE REVIEW

Contents

Overview of the chapter

In this chapter a brief introduction to the structure of water pipelines is given initially and common processes of deterioration and failure are discussed. This is followed by a critical review of current pipeline condition assessment and failure detection and monitoring techniques. Wireless sensor networks and their application in infrastructure monitoring are discussed and challenges in underground wireless sensor networks are identified. Finally this chapter is concluded by identifying gaps in the knowledge in the field of wireless sensor networks for pipeline monitoring.

2.1 Pipeline systems

Water, sewerage, oil and gas are all vital parts of our every day life. Delivery and disposal of these mediums are mainly done by the means of pipeline networks. This makes pipelines one of the most important urban infrastructures. Pipeline networks are commonly large and complicated systems, which have evolved through decades. As the pipeline networks gradually develop, pipes used in these networks age. This ageing results in pipeline deterioration and eventually pipes failure. The introduction of new pipe materials tries to minimise this issue, however often more complex coupling is required for these pipes which can result in early life failures due to human errors during installation. As was mentioned in Chapter 1, pipe failures can potentially have catastrophic financial and environmental effects.

2.1.1 Water supply network structure

The main objective of any water distribution pipeline network regardless of its location or layout is to transport untreated water from its source (for example reservoirs, lakes, wells and rivers) to the treatment facility and to transport the treated water to the customers (domestic, commercial and industrial). One of the other purposes of water pipeline networks is to provide supply for fire fighting services via fire hydrants. Water pipeline networks can be divided into two main sections of transmission and distribution networks (Misiunas, 2008; Al-Barqawi and Zayed, 2006). Transmission networks are the part of the water pipeline systems that is responsible for transportation of large quantities of water between major processing or storage facilities. This part of the network usually consists of large diameter pipes (>300mm) that can stretch several kilometres (Misiunas, 2005). Distribution networks, as the name implies, are responsible for the distribution of the water to the consumers. These pipes are usually of a smaller diameter compared to the transmission networks and have more complex networks. The topology of the distribution networks depends on the topology of the cities

they serve and is composed of a mixture of branch and loop configurations. The office of Water Services (OFWAT) divides UK leakage statistics for water supply systems into distribution losses and supply losses, where distribution losses are loss of drinkable water between the treatment facility and the highway boundary and supply losses are classified as loss of water from the customers' pipe from the highway boundary to the stop tap.

2.1.2 Pipe materials and age

A variety of pipe materials have been used over time in the gradual development of pipeline networks. The material of a specific water pipe usually depends on when it was installed (Misiunas, 2005). The distribution of pipe materials used in a water network largely depends on the country and overall age of the network. Regulations and health and safety concerns also play a major role in the distribution of the pipe materials in different countries. In the UK firmer regulation on the amount of lead in pipe (Drinking Water Inspectorate, 2013) has pushed water suppliers to rehabilitate their networks in order to meet the standards. These have led to replacement or relining of some of the existing pipe materials such as lead pipes and asbestos cement pipes. Pipe material distribution data for different countries already exist in the literature (Weimer, 2001; Pelletier et al., 2003). Pipe material distribution for UK water pipelines is published by Saul et al., (2003). Overall summary of pipe material distribution in 13 different European countries is published by Rajani and Kleiner, (2004). These data are shown in Figure 2.1.

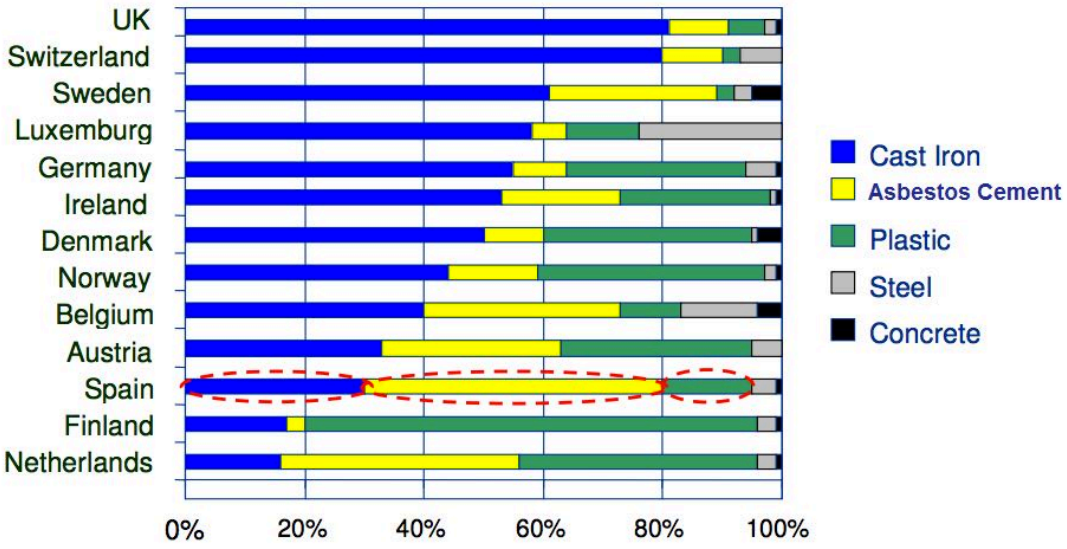

Figure 2.1 Pipe material distribution in 13 European countries (Rajani and Kleiner, 2004)

As can be seen in Figure 2.1, cast iron is the main pipe material used in water pipeline systems. However this can vary based on the age of the network and environmental factors in different countries as in Finland over 70% of water network pipes are plastic (due to the colder environment and younger network), while in the UK over 80% of pipes are metallic. The distribution presented in Figure 2.1 is changing towards a more plastic based network as currently plastic pipes are being nearly exclusively used for replacing and expanding existing water networks.

Pipeline systems like other infrastructures are subject to ageing (Rogers and Grigg, 2009). History of the first urban water networks goes back to more than five hundred years (1500) (Misiunas, 2005). As was mentioned earlier different pipe materials were introduced into pipeline networks during the last century. The average age of water pipeline networks is estimated to be approximately 50 years (Misiunas, 2005).

2.2 Pipeline deterioration process and failure

During their lifetime water pipes are exposed to harsh environmental and operational conditions. This exposure results in water pipes gradually deteriorating and eventually failing. Moreover, the ageing of the pipes negatively affects their structural condition and decreases their hydraulic capacity and performance; for example internal tuberculation in cast iron pipes can highly affect the internal diameter of the pipes and therefore affect their hydraulic capacity, while structural degradations of asbestos cement pipes can lead to reduction of their pressure rating and therefore limit their maximum operating pressure (Al-Barqawi and Zayed, 2006; Rajani and Kleiner, 2004).

Rajani and Kleiner (2004) divided the deterioration of pipes into two main categories: structural and internal deterioration. Structural deteriorations negatively affect the structural integrity of the pipe to withstand operational and environmental loads, while internal deteriorations affect the hydraulic performance and water quality (Al-Barqawi and Zayed, 2006).

The life cycle of the pipe can be divided into three main phases of “Burn in”, “In usage” and “Wear out” (Rajani and Kleiner, 2004; Rogers and Grigg, 2009; Berardi et al., 2008). Figure 2.2 illustrates the bath tub life cycle of a pipe.

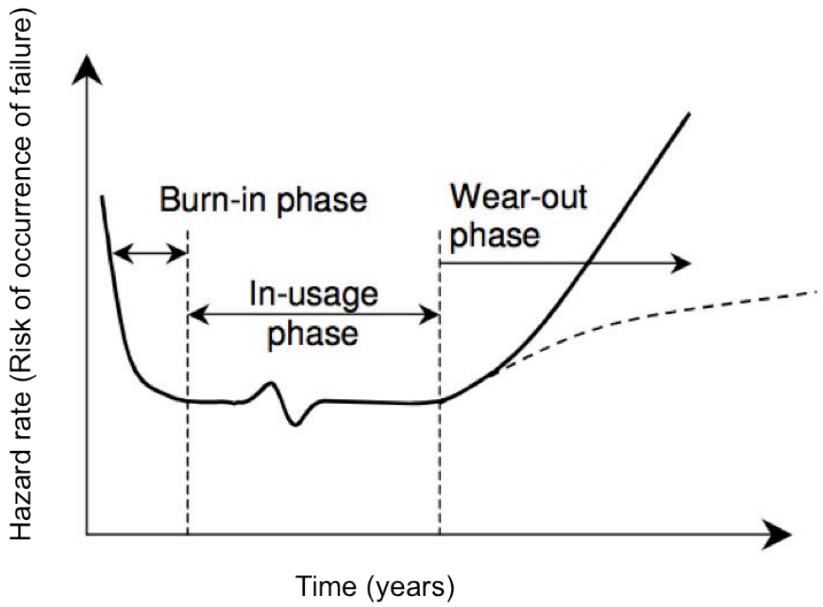

Figure 2.2 Bathtub lifecycle of a pipeline. (Adapted from Rajani and Kleiner, 2004)

The "Burn in" phase is the initial phase after installation of the pipe. In this phase failures are mainly caused by human error and other installation issues or manufacturing defects. With increase in complexity of the installation of the pipes due to new pipe materials this phase is becoming more important in the life cycle of pipes. After issues in the "Burn in" phase are resolved and the condition of the pipes are stabilised pipes enter the second phase of their life cycle which is the "In-usage" phase. Pipes enjoy a low rate of failure during this phase of their life. Failures during this phase are usually due to extreme operational/environmental conditions or external interferences. This phase is usually the longest phase of the pipes' life cycle. The length of this phase is highly dependent on the pipe material and its operational/environmental conditions. After this phase pipes enter the "Wear out" phase in which they exhibit higher failure rate due to corrosion and degradation leading to total failure of the pipe.

Pipe deterioration leading to pipe failure is usually a very gradual process. This process is divided by Rajani and Kleiner (2004) into four stages of (1)"Initiation of corrosion" (2)"crack

or hole before leak" (3)"Leak and scour begin" and (4) "Break or failure". Figure 2.3 illustrates the stages of development of pipe failure.

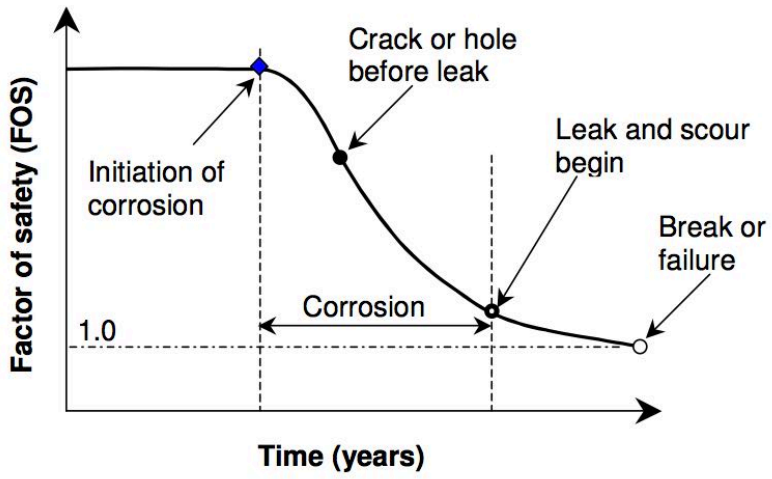

Figure 2.3 Stages of deterioration of the pipe (Rajani and Kleiner, 2004)

This classification of the deterioration is widely used in the literature (Rizzo, 2010; Misiunas, 2008). However, not all pipes follow the deterioration pattern described in Figure 2.3 and the development of the failure and the sequence in which the deterioration stages happen highly depends on the pipe material. Some pipes leak before they fail (for example ductile iron and steel pipes) while others break before they leak (more brittle material for example concrete pipes) (Sñgrov et al., 1999). Makar (2000) also shows that in grey cast iron pipes the final cracking of the pipes leading to its failure can happen in a multi-stage process with significant time between the stages. Factors affecting the deterioration process of water pipelines are divided by Kleiner and Rajani (2002) into three main categories of static, dynamic and operational factors. Static factors do not change (or can be assumed to not change) over the lifetime of the pipe (for example pipe material, geometry, and joining method). Environmental factors affecting the deterioration of the pipes are classified as dynamic factors. These factors change over the lifetime of the pipe (for example pipe age, soil moisture, soil and water temperature). Finally, operational factors are those depending on the

maintenance and operation parameters of the pipeline networks (for example use of cathodic protection, network pressure and transients). A more detailed classification and example of factors affecting the deterioration of the pipes is published in Al-Barqawi and Zayed (2006).

As was shown in Figure 2.3 the end result of the deterioration process is pipe failure. However, pipe failure is not only caused by deterioration. Causes of failure of pipes can be divided into four main categories of corrosion, excessive forces, manufacturing faults and human error (Misiunas, 2005).

In the literature corrosion is identified as the main reason for metallic pipes failure (Al-Barqawi and Zayed, 2006; Makar and Kleiner, 2000). The corrosion process of metallic pipes is highly affected by the specific material properties (corrosion resistance) of the pipe and the environment in which a pipe is laid. Aggressive soil around a pipe can significantly speed up the process of corrosion and shorten the lifetime of pipes. Other pipe materials such as cement based pipes and concrete pipes also deteriorate due to destructive chemical processes between the pipe and the surrounding soil. This is particularly dangerous in AC (asbestos cement) pipes as the weakened pipes can potentially release harmful particles into the drinking water (Al-Barqawi and Zayed, 2006). Plastic pipes are more resilient to the process of corrosion, however they can still be negatively affected by organic chemicals such as solvent and gasoline (e.g. PVC pipes) (Al-Barqawi and Zayed, 2006). Plastic pipes are relatively new therefore there is not enough research regarding degradation mechanisms which can affect them (Frank et al., 2009). Existing lifetime estimations for plastic pipes (i.e. PE pipes) are commonly based on extrapolation of empirical models developed from shorter duration of tests (Hoàng and Lowe, 2008).

Another important reason for failure of pipes is the exertion of excessive forces on them. This excessive force can be applied to the pipe via various mechanisms, for example, traffic, surrounding soil movements, third party interferences, and large temperature variations. Forces exerted on the pipes based on temperature variations are highly dependent on the pipe materials due to difference in their thermal expansion coefficients. In addition freezing conditions can exert an indirect force on the pipes via expansion of freezing water in the surrounding soil (BenSaleh et al., 2013).

Similar to any other product, pipes also suffer from flaws in production. Porosity, inclusions, micro cracks and variations in thickness are some of the manufacturing faults, which can lead to pipe failure (Misiunas, 2005). More rigorous quality control and inspection of the pipes before installation can reduce this type of pipe failure.

Human errors can affect pipelines at various stages of their life (Hurst et al., 1991). Human errors causing pipe failures can be divided into three stages of design, installation and operational errors. Errors in the design stage of the networks (incorrect rating and extreme hydraulic loadings) can significantly reduce the lifetime of the pipes. The installation phase of pipelines is affected by human errors considerably more than any other stage of pipeline life. Damage to the pipe during transportation, poor joining of pipes, and damage to the external coating of the pipes are examples of some of the common problems that can affect the pipes during the installation phase. For example this is especially important as plastic pipes usually require more complex joining methods such as electrofusion joining techniques. These techniques require a skilled operator and the joining surfaces of the plastic pipes to be free from inclusion during the joining process, which can lead to poor joining and increase of failure if not available (Bowman, 1997; Stokes, 1989).

After installation of the pipes operational human errors such as incorrect valve operations causing large pressure transients (water hammer effect) can shorten the life of the pipe or force already deteriorated pipes to fail (Schmitt et al., 2006). Moreover, the large negative pressure peaks created during these transients create a potential portal for entry of contaminants into the distribution pipes via weak fittings or joints which can pose a potential health risk for the consumers (LeChevallier et al., 2003).

Pipe failures are categorised into burst and leaks. It is very hard to identify a clear boundary between bursts and leaks and which factors can be used to categorise a failure into one of these two categories (Misiunas, 2005). Most commonly an arbitrary flow rate can be used to distinguish bursts from leaks, however this method is extremely subjective and depends on other factors such as overall hydraulic capacity of the pipe. Based on the International Water Association (IWA) guidelines (Lambert and Hirner, 2002) losses in water distribution systems are divided into three categories of background losses, reported bursts and unreported bursts. The flow rate of losses in the networks can significantly vary from a dripping tap (10 l/h) to large water main bursts (10,000 l/h) (Lambert, 1994). An arbitrary threshold of 0.129 l/s (500 l/h) is suggested by Lambert (1994) to distinguish between leaks and bursts. Due to the vagueness mentioned in distinguishing leaks from bursts, in this thesis losses which are caused by a sudden failure of pipe are classified as bursts, while existing losses and losses which grow and develop over time are classified as leaks. This method of classification is independent from the flow rate of the failure or size of the pipes and therefore can be applied more easily to the whole pipeline network.

2.2.1 Costs of failure and failure management

Failures in a pipe cause loss of the medium being transported by the pipe. This imposes a direct cost to the asset owner based on the value of that medium. However, the cost caused by

pipe failure is not only limited to the losses associated with the value of the medium the real cost of pipe failure is composed of various indirect and direct costs associated with the failure. Makar and Kleiner (2000) and Rajani and Kleiner (2004) divided the losses associated with a pipe failure in a water pipeline into three main categories of direct, indirect and social costs. Figure 2.4 illustrates these three categories and their subcategories.

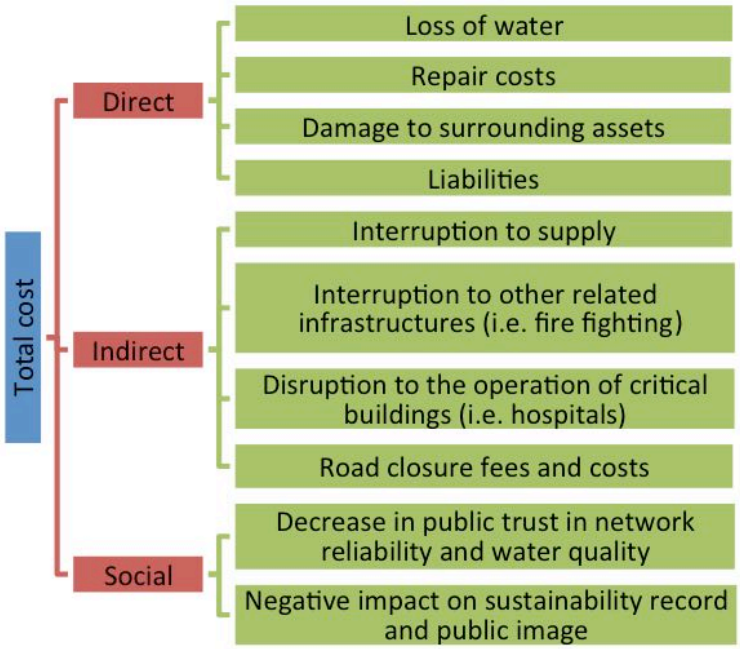

Figure 2.4 Categories of water pipe failure cost to asset owners

While it is possible to quantify direct costs in monetary terms it is more difficult to estimate indirect and social costs (Rajani and Kleiner, 2004). Although total costs of a failure depend on its severity they also increase with time (before it is fixed) (Misiunas, 2005). Figure 2.5 illustrates the increase in total pipe failure costs with time.

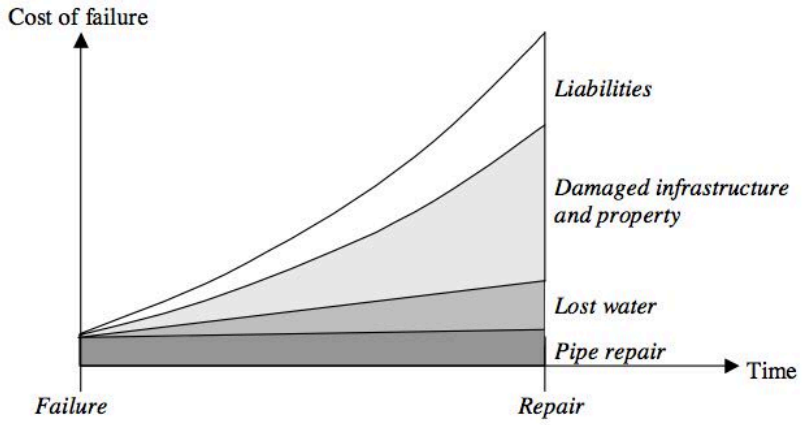

Figure 2.5 Growth of total failure costs with time (Misiunas, 2005)

As shown in Figure 2.5 repair costs will not necessarily increase with time after the failure, however other costs such as those associated with loss of water, damage to other infrastructure and liabilities increase rapidly with time. The rate of growth of these costs is determined by the severity of the failure and sensitivity of the environment and other assets close to the pipe. It can also be shown from Figure 2.5 that damage to other assets and properties would be the main component of the total cost of failure if the failure is not detected at its early stages.

Various techniques can be used to detect leaks or asses the condition of pipes. The total cost of failure management for water pipeline networks depends on the cost of the method used for condition assessment and leak detection. This can vary largely from inexpensive methods such as visual inspection by asset owner staff to expensive techniques such as fibre optic monitoring and other high-tech techniques. The cost of the failure detection system generally depends on the stage at which it can detect the failure (earlier stage detection methods are commonly more complex and therefore more expensive) (Misiunas, 2008). Figure 2.6 illustrates the total cost of leak management (leak detection costs and failure costs) for transmission and distribution pipelines as a function of time.

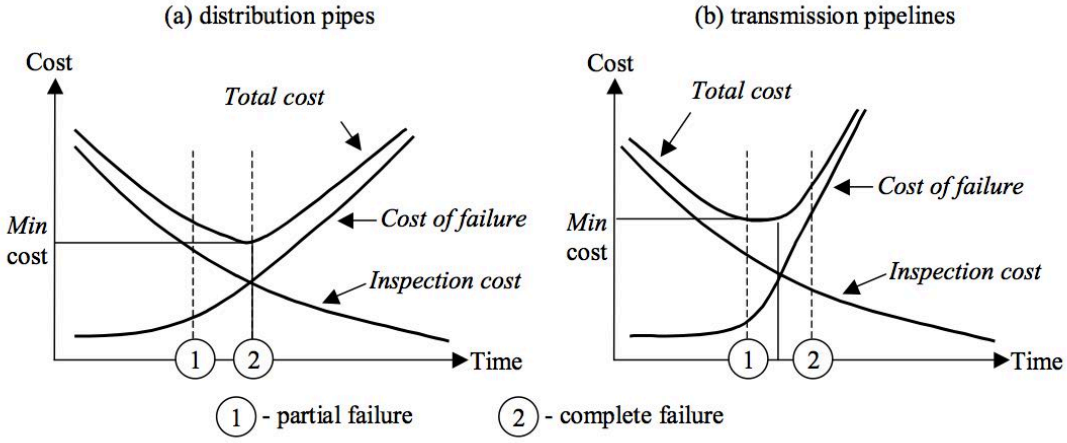

Figure 2.6 Total cost of failure management for (a) distribution and (b) transmission water pipeline as a function of time (Misiunas, 2008).

As can be illustrated by Figure 2.6 the cost of failure in transmission pipelines increases more rapidly compared to distribution pipelines due to the larger loss of water and potentially greater indirect costs. Therefore it is more economical to use more expensive leak detection and condition assessment techniques for transmission lines in order to detect failures before they reach the total failure stage, whereas in distribution pipelines these systems might not be economically justified due to the lower cost of failure. In these pipelines usually a reactive leak detection approach based on water on the surface or loss of pressure is used by asset owners. Other industries in which the medium transported by the pipe has a higher value or is hazardous (i.e. oil and gas pipelines) take a very different approach to failure monitoring. In these pipelines total failure could potentially have extremely high indirect and direct costs therefore it is more economical to detect failures at their early stages despite the higher inspection costs. Various pipeline condition assessment and monitoring techniques aim to provide cost effective solutions for detection of pipeline failures and deterioration in the water pipelines. The next section of this chapter reviews the existing techniques for pipeline condition assessment and failure monitoring in the water pipelines.

2.3 Pipeline condition assessment and failure monitoring techniques

Failure management strategies can be divided into two main categories of passive and active techniques. In passive techniques the failure is identified based on consumer complaints (low pressure and discoloured water) or reports of water on the surface, while active techniques are intended to detect the failure before it reaches the stage in which it can be detected by passive techniques (Misiunas, 2008, 2005).

Active failure management techniques are commonly referred to as Non-Destructive Testing (NDT) (Al-Barqawi and Zayed, 2006; Rajani and Kleiner, 2004). NDTs are also referred to as Non-Destructive Inspection (NDI) methods and Non-Destructive Evaluation (NDE) methods. For the purpose of this thesis the term NDE is used to refer to these methods. Active condition assessment and failure detection techniques can be further divided into two main categories of direct and indirect methods (Misiunas, 2005). Methods in the first category are based on monitoring/assessing direct parameters related to the pipeline (i.e. pressure, structural integrity) while indirect methods are based on the measurement and analysis of indicators which are indirectly related to the condition of the pipes (i.e. soil properties, historical and statistical failure data).

Passive failure detection techniques and indirect active methods are not further discussed in this thesis. Therefore, the focus of the following sections of this chapter is on a review of the state of the art active failure management techniques.

The main purpose of NDE methods is to evaluate the deterioration stage of the pipe without causing damage or affecting its properties. Different NDE techniques exist with varying degree of complexity. Detailed reviews of NDE techniques are presented in Liu and Kleiner (2013); Rajani and Kleiner (2004); Sinha et al. (2003); Sinha and Knight (2004) and Sonyok

et al., (2008). Figure 2.7 illustrates different categories of direct NDE methods and their main subcategories.

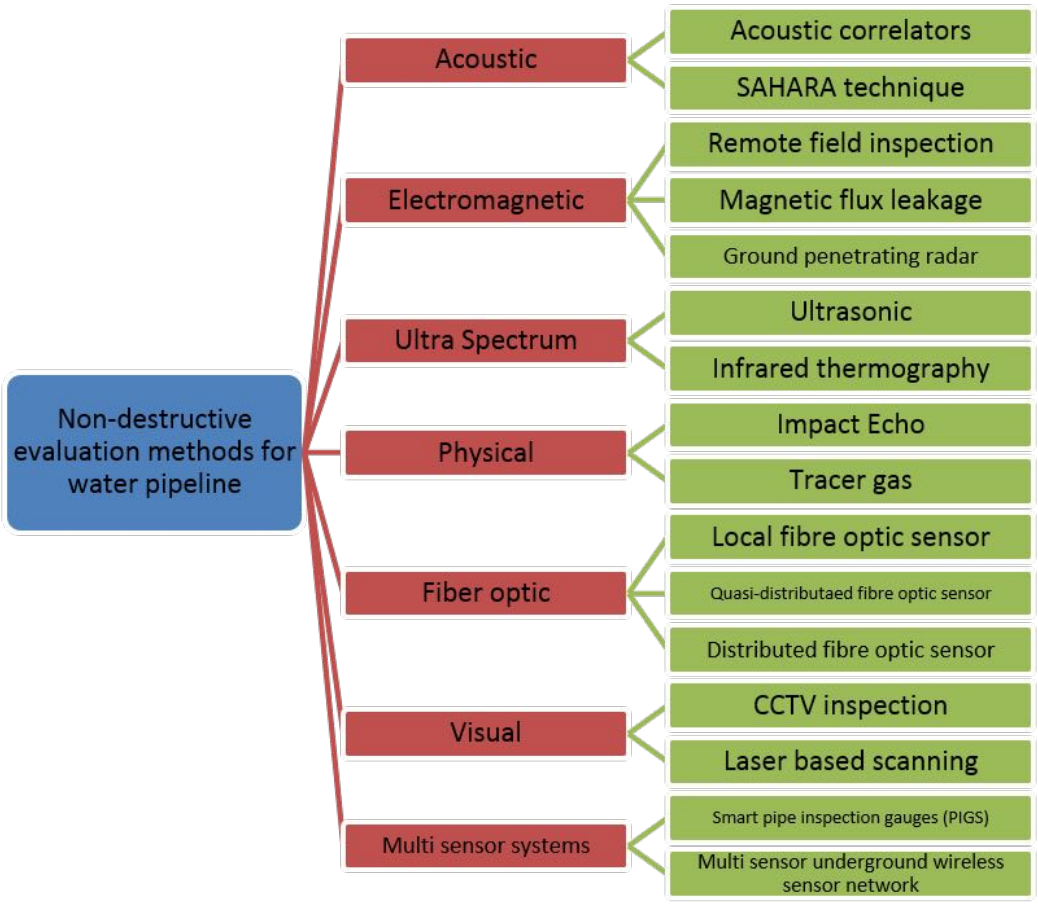

Figure 2.7 Non-destructive evaluation methods for water pipeline evaluation and monitoring (adapted from Al-Barqawi and Zayed, 2006)

As can be seen form Figure 2.7 NDE methods can be categorised into seven main categories of acoustic, electromagnetic, ultra spectrum, physical, fibre optic, visual, and multi-sensor systems. Each of these methods has its specific advantages and disadvantages that are discussed in this section. Moreover specific technologies used in some of these methods make them only usable on a certain type of pipe.

2.3.1 Acoustic based methods

Acoustic correlation is the most common technology used for failure detection and localisation in pipes. A large number of publications regarding the use of acoustic based technologies for pipeline failure detection exist in the literature (Hieu et al., 2011; Ozevin and Yalcinkaya, 2013; Gao et al., 2005; Khulief et al., 2012; Ahadi and Bakhtiar, 2010; Muggleton and Brennan, 2004; Muggleton et al., 2006). These methods are based on the detection of the acoustic emissions caused by a leak in the pipe. The frequency and magnitude of these signals depend on pipe pressure, leak diameter and type of fluid inside the pipe (Hieu et al., 2011). These signals are detected by hydrophones or accelerometers placed at fixed location along the pipe (Gao et al., 2005). The location of the leak can then be calculated by cross-correlation methods applied on the signals measured by sensors at different locations. This is based on the principle that travel time of the waves to each sensor would be different based on the distance of the sensor from the leak. Leak detection performance of acoustic systems is also affected by the type and sensitivity of the sensor (accelerometer/hydrophone) used for detection of acoustic signals. Sensors with higher sensitivity and lower noise floor will be able to detect weaker acoustic signals from smaller leaks (Gao et al., 2005). Although these systems look promising they have some disadvantages, which make them currently not suitable to be deployed as a buried wireless sensor network system. Measuring the acoustic signal requires a high sampling rate (>1KHz), which makes the system consumes more power and lasts a shorter amount of time on the limited power supply available. Moreover these systems are best suited for metallic pipes as detection of vibrations in plastic pipes could be challenging due to the higher attenuation of acoustic waves (Muggleton et al., 2006). Figure 2.8 illustrates a schematic of acoustic correlator systems.

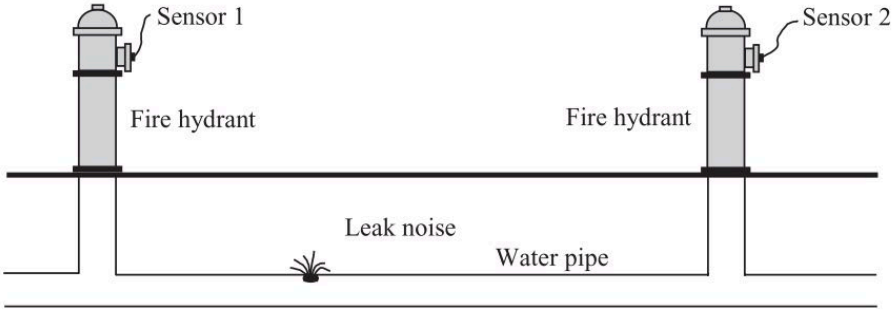

Figure 2.8 Schematic of an acoustic cross correlation leak detection system (Gao et al., 2005).

The SAHARA method described by Bond et al., (2004) is also based on the detection of acoustic emission from the leaks. However, in this system unlike the correlation-based methods, the hydrophones are not fixed at one location. In the SAHARA method the hydrophone is inserted into the pipe with an umbilical cord via a conventional 50mm tap and records the acoustic signal as it travels through the pipe. An over-ground location detection module is used to track the movement of the hydrophone in the pipe and help pinpoint the leak. The SAHARA system can also be equipped with cameras in order to provide visual feedback to the operator on the surface. Figure 2.9 illustrates the schematic of the SAHARA system and its components.

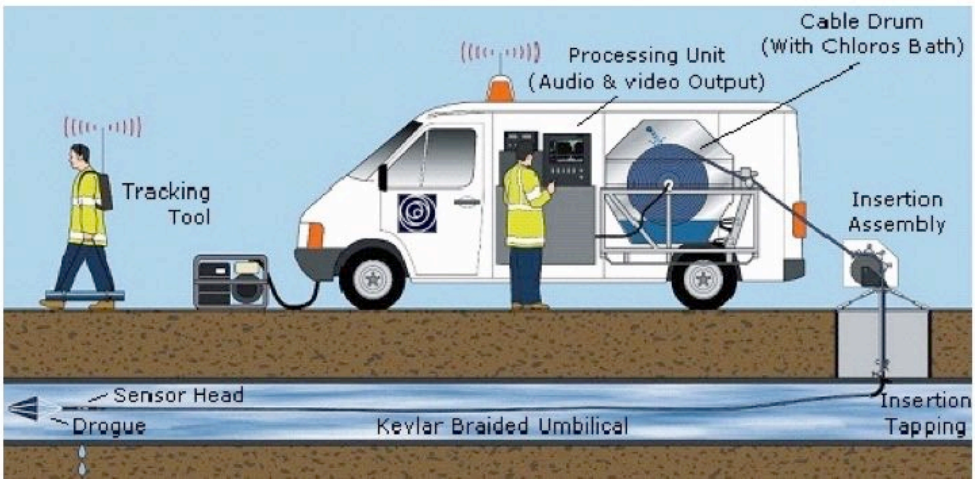

Figure 2.9 SAHARA method and its components (Bond et al., 2004).

The limitation of SAHARA method is its necessity of travel through the pipe. This is not always desirable as it can potentially jeopardise safety of the water supplies. Although it can operate in live pipes without disruption to service, the SAHARA system is limited by the diameter of the pipes in which it can effectively operate (>300mm) and is not suitable for smaller diameter water pipe. Due to the tethered nature of SAHARA, the technique is limited to 1850m of range per survey.

2.3.2 Electromagnetic based methods

Ground Penetrating Radar (GPR) is widely used for the inspection and localisation of buried assets (Hunaidi and Giamou, 1998; Misiunas, 2005; Crocco et al., 2009; Nakhkash, 2004). In the GPR method, pulses of radio frequency signals are transmitted into the ground via antennas placed on the surface. These signals are then reflected by different layers of soil, voids and other objects in the ground due to the difference in their electromagnetic properties. These reflections are then recorded by the receiver and analysed by the GPR unit on the surface. Leaks in pipes are detected by GPR via detection of voids created by leaking water in the ground or abnormalities in the measured depth of the pipe due change of the soil attenuation due to change in local water content of soil (Liu and Kleiner, 2013). Although this method has been successfully used to detect the location of pipes and leaks, its application and reliability is limited in more attenuative soils (i.e. saturated clay) or deep assets due to a reduction in penetration depth of the signals. Another drawback of GPR technology is the difficulty of interpreting the GPR measurements dictating the need for a skilled operator. GPR measurements also require another form of verification to distinguish similar assets (water and gas pipes) due to the similar GPR signature of these assets (Costello et al., 2007).

Magnetic Flux Leakage (MFL) is one of the main methods used in the detection of corrosion and defects in metallic pipes, especially oil and gas pipes. In this method the pipe wall is

magnetised using strong permanent magnets. A fault in the pipe (i.e. a corrosion pit) will cause a magnetic flux leakage at the point of defect. This can be detected by sensors inside the pipe to localise the fault. For the MFL method to work, a very good contact is required between the pipe interior and the magnets. This makes this method unsuitable for older water pipes due to their tubercular interior surface (Rajani and Kleiner, 2004). Necessity of close contact between the pipe and the magnets impose another problem for usage of the MFL method in water pipes due to the potential damage to the lining of the pipe by the contacts used in these system (Costello et al., 2007). These limitations make this method only suitable for clean steel pipes without interior lining (Costello et al., 2007; Liu and Kleiner, 2013). The principles of the MFL method are illustrated in Figure 2.10.

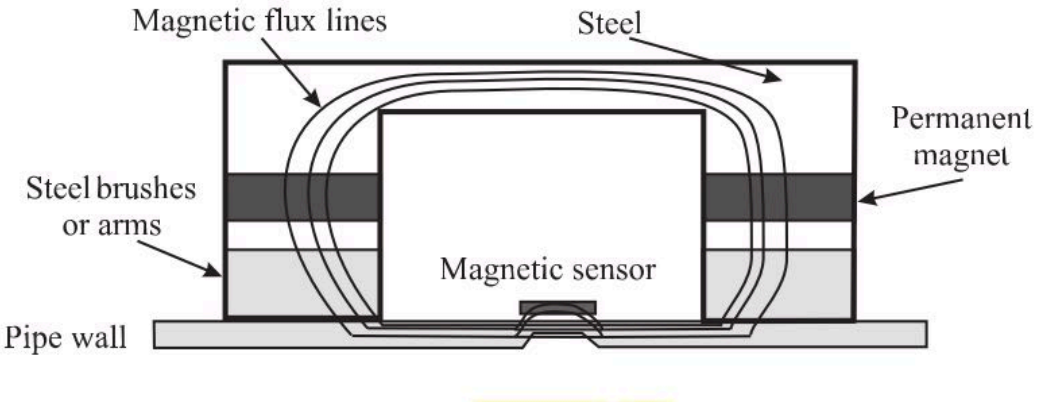

Figure 2.10 Schematic of the principal of Magnetic Flux Leakage (MFL) method (Liu and Kleiner, 2013).

The Remote Field Eddy Current (RFEC) technique presented in Jiles (1990) and Atherton (1995) is based on diffusion measurements of a low frequency electromagnetic signal at the remote field zone travelling through the pipe wall. This system consists of excitation and detection coils which are placed inside the pipe. The low frequency alternating current signal is generated by the exciter coil and is measured by the detector coil placed approximately two

pipe diameters away from the exciter coil (Atherton, 1995). The electromagnetic signal is rapidly attenuated through the direct path (inside the pipe) and travels through the pipe wall with small attenuation (Liu and Kleiner, 2013). Therefore any change in the wall thickness of the pipe shows itself as a change in the measured signal at the detector coils. Figure 2.11 illustrates a schematic describing the principles of the remote field eddy current method.

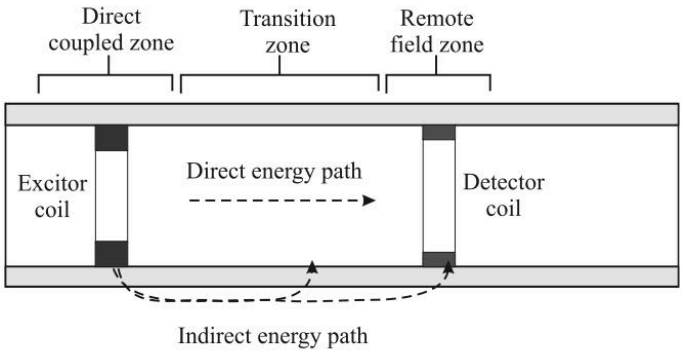

Figure 2.11 Schematic of the principles of the remote field eddy current measurement method (Liu and Kleiner, 2013).

Although in this method the sensors do not require a close contact with the pipe wall, it can only be used with ferromagnetic pipes or pipe with ferromagnetic components in them. There is also limited information in the literature assessing the reliability of this method (Liu and Kleiner, 2013).

2.3.3 Ultra spectrum based methods

In the ultrasonic testing method a beam of high frequency sound is transmitted in the medium of the pipe commonly via a piezo transducer. As the sound wave travels through different materials it is reflected and scattered based on their densities (i.e. pits, corrosions and voids). These reflections are measured and compared with a baseline measurement (Li et al., 2012). Tuberculation of metallic pipes will cause the signal to be scattered and therefore can be detected easily by this method. Ultrasonic methods are usually used in conjunction with other

methods such as smart Pipe Inspection Gauges (PIGs). Ultrasonic methods can also be classified as an acoustic method, however in ultrasonic methods the wave is induced by the monitoring system while in acoustic correlation methods the wave is induced by the leak. The ultrasonic inspection methods require access to the interior of the pipe and are mostly suited to metallic pipes due to the higher attenuation of the waves in the plastic pipes. Figure 2.12 illustrates the schematic of an ultrasonic inspection system.

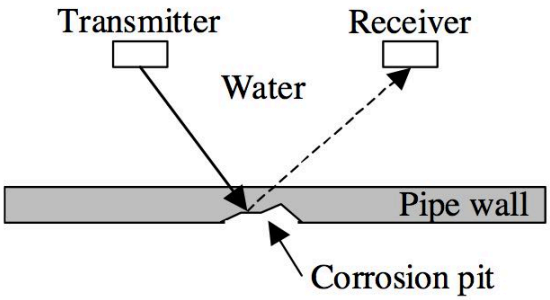

Figure 2.12 Schematic of the ultrasonic pipe inspection method (Misiunas, 2005).

Another approach to ultrasonic inspection of pipes using guided ultrasonic waves (Lamb wave) propagation and reflection is presented by Lowe et al. (1998) and more recently by Galvagni and Cawley (2012) and Jin and Eydgahi (2008). In this method a wave is induced in the pipe via transducers and travels through the pipe wall. Defects in the geometry and consistency of the pipe (rust patches) cause reflections of this wave. These reflections are then studied and analysed in order to detect defects and their locations. This method is mostly suited to metallic pipes, as the transduced waves attenuate rapidly in plastic or aged asbestos cement pipes, reducing the effective inspection range. Figure 2.13 illustrates the schematic of a guided ultrasonic wave inspection of pipes.

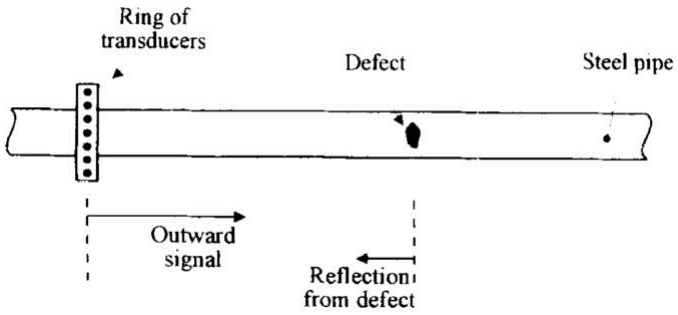

Figure 2.13 Schematic of guided ultrasonic wave inspection method (Lowe et al., 1998)

Moreover Cawley et al. (2003) identified the coherent noise due to reflections from opposite directions and propagation of multiple modes of waves as the main challenges when using medium to long range guided wave inspection. In addition, the effectiveness of these systems is lost when defects in the pipe are small and therefore the magnitude of their reflections is smaller than noise bed of the system. Multiple overlapping reflections from similar features can also limit the effectiveness of this technique (Galvagni and Cawley, 2012).

Infrared thermography is a totally non-contact inspection method used for detecting leaks in pipelines. This method is based on the detection of abnormalities in temperature of the soil around the pipe caused by the leakage of the medium being transferred by the pipe (i.e. water, oil) (Hunaidi, 2000; Costello et al., 2007). The temperature difference between the medium leaking out and the surrounding soil will cause local hot/cool spots. In these systems a sensitive thermal imaging camera is used to capture the thermal profile of the soil and detect the local abnormalities. The performance of thermography based methods highly depends on the condition (moisture content) and properties of the soil, surface material, ambient temperature, wind and solar radiation (Costello et al., 2007; Misiunas, 2005).

2.3.4 Physical methods

The impact echo pipeline inspection method is based on generating controlled impact acoustic waves (i.e. pneumatic hammer) and measuring the propagated waves via geophones attached to the pipe wall. These measurements are then analysed in the frequency domain to identify defects in the pipes (Costello et al., 2007; Rajani and Kleiner, 2004). However, for this method to perform effectively, the pipe needs to be dewatered and the internal surface of the pipes needs to be cleaned (Rajani and Kleiner, 2004).

Tracer gas leak detection of pipes is a practice in which a low density (lower than air), non-toxic and water insoluble gas is injected into an isolated section of the pipe. In the case of a defective pipe the gas will leak out from the pipe and travel upwards (due to its low density) through the ground and reach the soil surface. The marker gas can then be detected on the surface by sensitive gas detectors (Heim, 1979). High direct and indirect cost of this type of inspection makes it not widely used in the water industry (Misiunas, 2005).

2.3.5 Fibre optic based methods

Fibre optic technology has been extremely promising for large-scale civil infrastructure monitoring (López-higuera et al., 2011). A vast amount of research exists in the literature on the usage of fibre optics for tunnel, reservoir, bridge and other infrastructure monitoring (Mohamad et al., 2011; Cheung et al., 2010; Li et al., 2004; Yan and Chyan, 2010; Nikles, 2009; Myles, 2011; López-higuera et al., 2011; Metje et al., 2008). Superior performance characteristics of fibre optic monitoring have made fibre optics amongst the most suitable techniques for permanent monitoring of pipelines. The main advantages of fibre optic based systems are their passive operation (no need for local power supply), large monitoring range (few kilometres), high spatial resolution, electromagnetic interference immunity and multi-parameter sensing capabilities (Sonyok et al., 2008). Environmental parameters and

stimulations affect the geometrical (size and shape) and optical (mode conversion and refractive index) properties of fibres (Li et al., 2004). In the communication industry these effects are minimised in order to establish a clean communication between two points. However, in sensing applications these changes are used to measure the desired parameters along the fibre optic cable. Optical fibres commonly consist of a fibre core, cladding and a jacket. Fibre optic sensing systems can be generally divided into three main categories of (Li et al., 2004; Sonyok et al., 2008):

- *Local (Point) Fibre optic systems.* In these systems the desired parameters are measured at a discrete point along the fibre optic cable. These systems are usually more suited for small-scale sensing, as each sensor needs a separate channel.
- *Quasi-distributed system.* In these systems the desired parameter is measured at multiple (commonly up to 64) discrete positions along the pipe. The most common type of quasi-distributed systems is Fibre Bragg Grating (FBG) sensors. These systems have been successfully used in large-scale multipoint measurement systems (Li et al., 2004).
- *Distributed systems.* In these systems the whole fibre optic cable is used as the sensor. Therefore the desired parameter can be interrogated at any point along the pipe (within a spatial resolution of approximately 1m). Two main types of distributed fibre optic sensing systems are Raman and Brillouin optical time domain reflectometry. These systems are best suited for large scale infrastructure monitoring such as pipelines. These have been successfully used in long-distance pipeline monitoring and leak detection (Myles, 2011; Sonyok et al., 2008; Tanimola and Hill, 2009; Rajeev et al., 2013) .

In these system parameters related to the pipe (for example vibration, strain or temperature) are used in order to assess the integrity of the pipe, monitor third party interference or detect pipe failures. Moreover FBG based sensors can be used to monitor operating parameters such as pressure and flow (Li et al., 2004). The most common type of pipeline monitoring by fibre optic technology is based on detection of local temperature difference created by the leaking medium in surrounding soil (Myles, 2011).

A schematic of these three systems is illustrated in Figure 2.14.

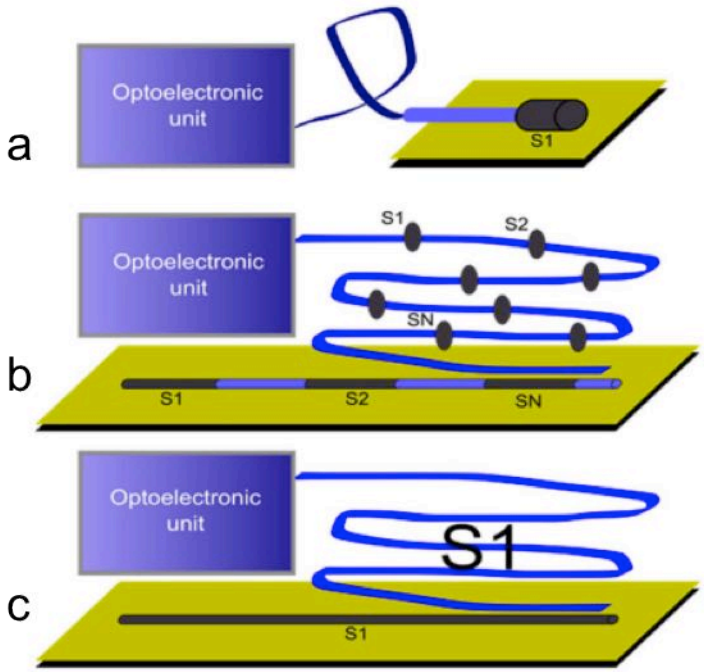

Figure 2.14 Schematic of different types of fibre optic monitoring systems. a) Local b) Quasi-distributed c) Distributed (adapted from López-Higuera et al., 2011)

Despite their good performance characteristics fibre optic monitoring of water pipelines has not been widely adopted by asset owners due to two main drawbacks of fibre optic methods. The main drawback of these systems is their inherent lack of redundancy. If for any reason a section of the pipeline is required to be replaced (due to damage or renewal) or the fibre

optics are damaged (third party interference), a large section of the fibre optic monitoring network could become non-functional or blind spots could be created in the system. Another drawback of fibre optics is their complex installation. Fibre optic networks are commonly required to be installed while the pipe is being constructed and retrofitting of them (in case of damage or for existing pipelines) can be difficult and uneconomic (Myles, 2011).

2.3.6 Visual (imaging) based methods

Closed circuit television (CCTV) is the most common visual based inspection method used in pipeline monitoring. In this method a camera travels through the pipe and records/transmits video footage of the pipe interior. Images from the camera are analysed by a skilled operator in order to detect visible defects or degeneration signs in the pipe (Misiunas et al., 2005; Liu and Kleiner, 2013). Figure 2.15 shows an example of a CCTV system used for pipeline inspections and an image of the cracked pipe captured by this method.

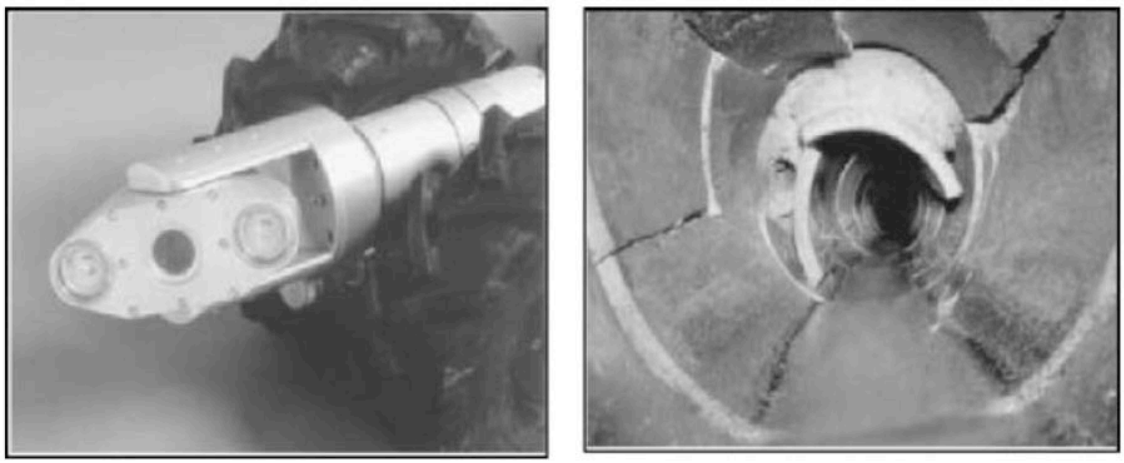

Figure 2.15 a) CCTV pipeline inspection system b) Example of interior image of a cracked pipe (via Sinha and Knight, 2004, Courtesy of Telespec Ltd).

These systems suffer from three major drawbacks. Firstly, CCTV inspection of large networks is very labour intensive and costly due to the required skilled operator and the time the survey takes (Misiunas, 2005). The second drawback of this method is its inability to detect defects or faults that do not have visual signs or are not visible in the CCTV footage due to obstructions. The third main disadvantage of these systems is their high dependency on the operator skills and consistency. Results from the interpretation of the CCTV images are commonly inconsistent due to human error (Kingajay and Jitson, 2008). The process of analysing images from the CCTV can be automated by means of computer vision and image processing algorithms to overcome the labour related issues (Costello et al., 2007; Kingajay and Jitson, 2008). However this itself introduces other issues into the system such as the need for high processing power and complex algorithms which result in an increase in cost.

Laser scanning systems (laser profilers) are based on scanning the interior of the pipes with a laser beam and analysing the results to create a highly accurate profile of the pipe interior. Unlike CCTV methods, laser profilers are capable of detecting smaller defects and are more consistent. The profile of the pipe processed by an automated algorithm can be usually viewed by the operator in real-time. Kingajay and Jitson, (2008) propose a method of combining the laser-profiling method with the CCTV inspection technique in order to increase the accuracy of fault detection by providing contour profiles of the pipe interior. Main disadvantage of this method is that it only can operate in de-watered pipes. Performance reliability of laser based systems are however not studied fully and further research is required to validate their performance (Liu and Kleiner, 2013). Figure 2.16 illustrates the proposed system by Kingajay and Jitson (2008).

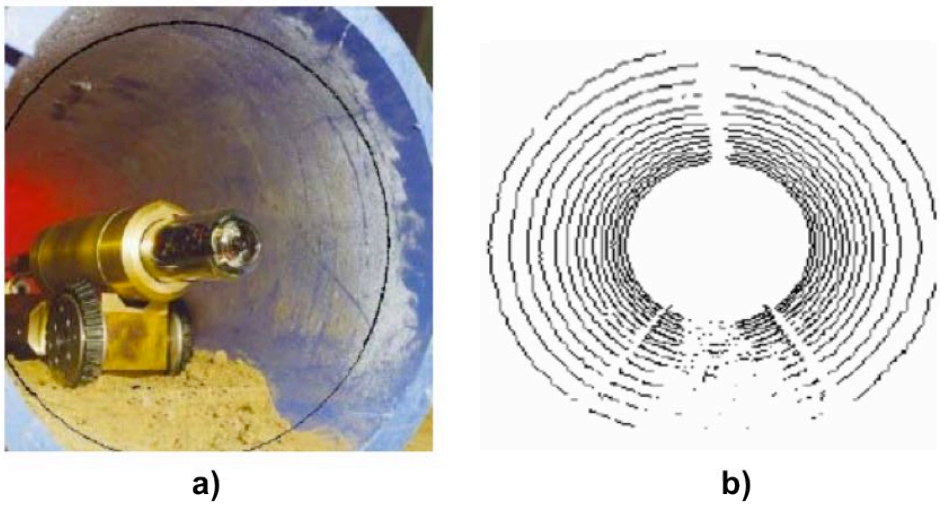

Figure 2.16 Hybrid (Laser and CCTV) based method. a) Inspection device b) sample of pipe profile output (Kingajay and Jitson, 2008).

Vision based systems also suffer from few common drawbacks. They all require access to the interior of the pipe, which is not desirable by asset owners due to risk of contamination, and most commonly they can only operate in empty pipes, which can cause interruption to service.

2.3.7 Multi-sensor systems

Smart Pipe Inspection Gauge (PIG) systems are based on instrumenting conventional PIGs in order to inspect the condition of the pipes or detect defects. Conventional PIGs are used in the water industry to clean the interior of pipes. The addition of sensors and a locating mechanism (i.e. inertial navigation) to the PIG enables it to inspect the interior of the pipe and locate faults. In this method the smart PIG is inserted into the pipe through an opening (i.e. fire hydrant) and then travels through the pipe while recording its location and inspection data. Following retrieval of the PIG these data are analysed in order to detect faults. In some cases the PIG is attached via an umbilical cord to the above ground base which analyses the data in real-time.

A successful example of a multi-sensor PIG based system is the Smart Ball™ (Pure Technologies, USA). The Smart Ball consists of multiple sensors such as accelerometers, acoustic sensors, temperature sensors and magnetometers encapsulated alongside a battery and other essential electronics in an aluminium core. The aluminium core is then covered by a foam shell in order to protect the core, facilitate the movement of the ball in the pipe and reduce the noise it creates while it travels (Fletcher and Chandrasekaran, 2008; Liu and Kleiner, 2013; Metje et al., 2011). The Smart Ball is capable of inspecting pipes with a range of a few kilometres and the detection of faults with a resolution of 1m (Liu and Kleiner, 2013). However, the drawback of this method similar to vision based methods and the SAHARA method (discussed earlier) is that it requires access to the interior of the pipes and also cannot be used in smaller diameter (<150mm) pipes.

Wireless Sensor Networks (WSN) are increasingly becoming the commonplace technology for infrastructure monitoring (Stajano et al., 2010). Advances in sensor technologies, wireless communications and electronics have significantly increased the capabilities of these systems while reducing their footprint and cost (Akyildiz et al., 2002; Deivasigamani et al., 2013; Li and Liu, 2007). Furthermore increase in the proliferation rate of the Internet has created a great opportunity for the Internet to act as a backbone for wireless sensor networks and connected infrastructures (Christin et al., 2009; Atzori et al., 2010). However, further research is required for WSN to become a robust solution for civil infrastructure monitoring. Stajano et al. (2010) provides guidelines and identify main challenges for robust implementation of WSN for infrastructure monitoring. Common wireless sensor networks comprise multiple nodes with sensors attached to them based on the different applications. These nodes read the sensors' output based on a predefined schedule or as a reaction to an event. These data are then partially processed and packaged by the node. The packaged data are then transmitted

wirelessly to a central node. According to the topology of the network, data from one node could be directly transmitted to the central node (single hop) or being relayed multiple times by other nodes (multi-hop) before it reaches the central node (Maraiya et al., 2011).

Wireless Underground Sensor Networks (WUSN) can be used in a range of applications such as precision agriculture (Balachander et al., 2013), mine monitoring (Hancke, 2012; Li and Liu, 2009), oil and gas monitoring, soil condition monitoring (Bogena et al., 2010) and pipeline monitoring (Stoianov et al., 2007). WUSN for pipeline monitoring can be divided into two subcategories of internal systems and external systems. In internal systems nodes are placed inside the pipe while in external systems the nodes are usually fixed on the pipe (i.e. at an access chamber). Various wireless sensor network systems for pipeline monitoring exist in the literature, which are reviewed in the next section.

2.4 Wireless underground sensor networks for pipeline monitoring

2.4.1 External systems

PIPENET is a fixed WSN system for pipeline monitoring. This system utilises acoustic, water level, water quality and pressure sensors (via tapping) at a high sampling rate (up to 600Hz) in order to identify, quantify and pinpoint faults in large diameter (transmission) water pipelines (Stoianov et al., 2007). In order to identify the faults data from the sensors are compared with a long-term historic base reading and correlated with other nodes (Kim, 2011). The PIPENET system uses an Intel Mote platform (as the node) to collect and analyse the data from its sensors. Figure 2.17 illustrates an overview of the PIPNET system.

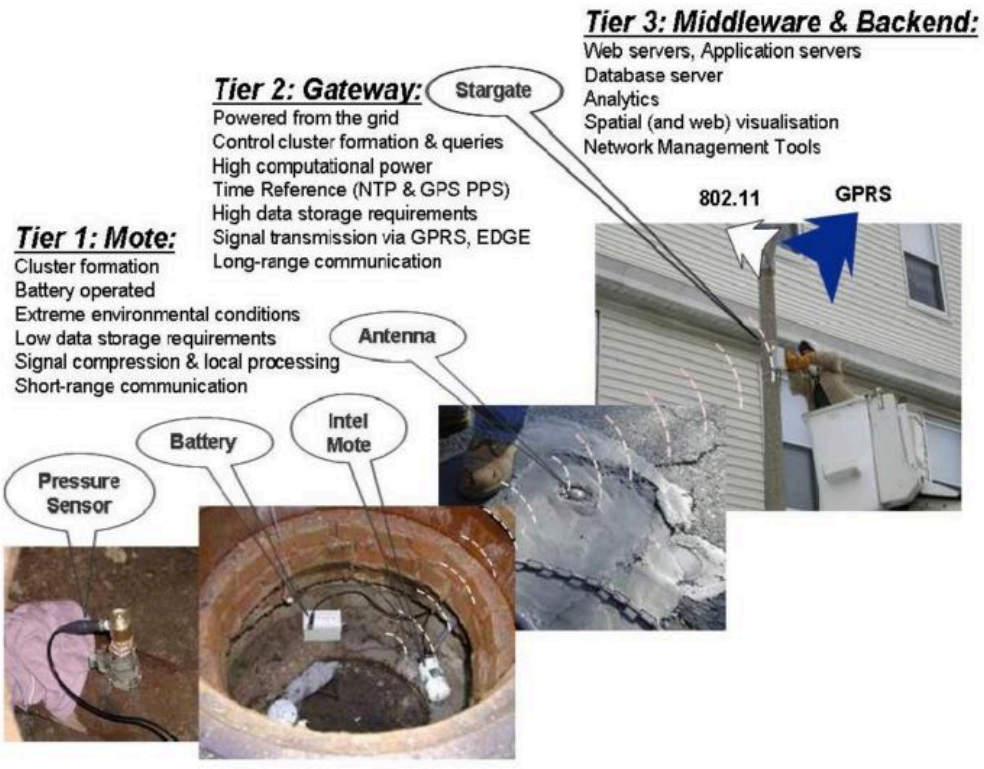

Figure 2.17 Overview of the PIPENET system (Stoianov et al., 2007).

The short battery life of 50-62 days on a 6V 12Ah battery is the main drawback of the PIPENET system (Stoianov et al., 2007) which prohibits this system to be widely used in long term (>1 year) pipeline monitoring.

The WaterWise platform manages and analyses the pressure (via direct pressure sensors), acoustic and water quality readings obtained by a network of smart nodes in order to predict the hydraulic demands and identify faults within the pipeline network. The custom designed hardware of this platform is based on an ARM Cortex M3 processor (Whittle et al., 2013). Figure 2.18 shows the WaterWise system.

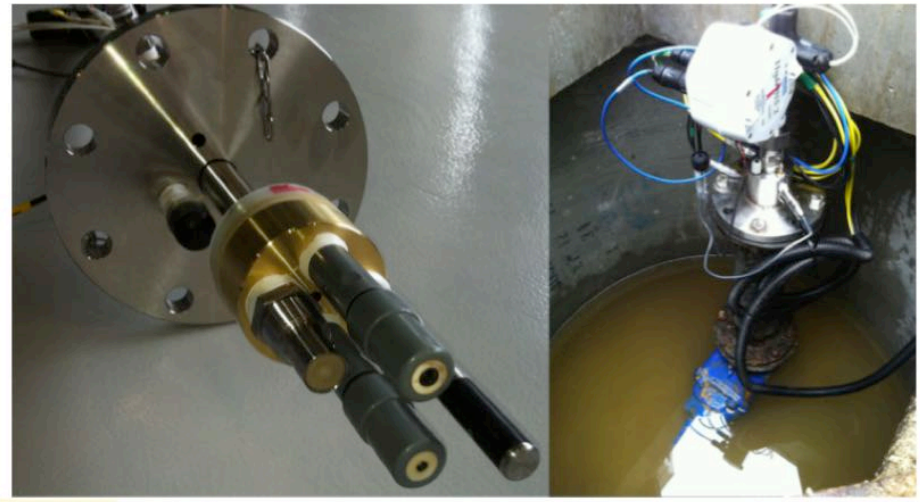

Figure 2.18 WaterWise system a) Multi parameter probe head b) installed WaterWise probe (Whittle et al., 2013).

Due to the long internode distance (500-1500m) in this platform nodes directly communicate with the central base (single hop) via 3G connections. Time synchronisation of the nodes is achieved via a GPS receiver. Similar to the PIPENET system, the WaterWise platform also suffers from high power consumption (0.036W-4.500W) and needs to be regularly recharged via an AC line or Solar panels.

PipeTect proposed by Shinozuka et al. (2010) is a WSN system for the detection and localisation of leaks by using vibration measurements (MEMS accelerometers) on the surface of the pipe. This system uses wire connections for underground communication (CAN bus) and wireless communication (ZigBee and Wi-Fi) for overground communications. The system is capable of detecting leaks in a laboratory setup however lacks field trial validation to understand the effect of the underground environment on the vibration of the pipe. The main drawback of this system is the need for wiring for the underground communications.

MISE-PIPE is a WUSN system for pipeline monitoring based on magnetic induction waveguides (Sun et al., 2011). This system aims to provide real-time leak detection and localisation for underground pipes via different types of sensors located both inside and outside of the pipe. Sensors placed inside the pipe are placed at access chambers and valves and are responsible for measuring pressure (via direct pressure sensor), flow and acoustic vibrations. These nodes have high power consumption due to their higher computation capacity compared to sensors placed outside of the pipe. The sensors which are placed outside of the pipe however are low-powered and responsible for measuring temperature, humidity and soil properties around the pipe (Sun et al., 2011). These sensors are densely deployed along the pipeline in order to provide a high spatial resolution for leak detection. Figure 2.19 illustrates the overall schematic of the MISE-PIPE system.

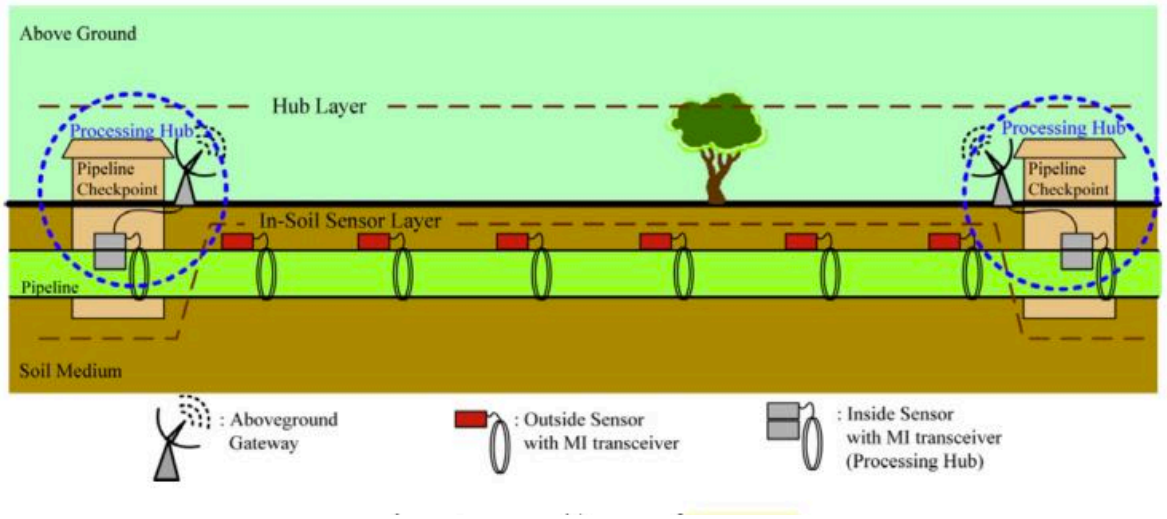

Figure 2.19 Overall schematic of the MISE-PIPE system (Sun et al., 2011). Where MI stands for magnetic induction.

Soil is a very lossy environment for electromagnetic (EM) signals. The MISE-PIPE system uses the Magnetic Induction (MI) technique to overcome this issue. Sun et al. (2011) claim that MI can provide more reliable and efficient wireless underground communication, as they

are not affected by soil properties. However this claim is only valid for non-magnetic soils. A main intrinsic drawback of magnetic waves compared to EM waves is that their intensity drops with distance significantly faster than EM waves. MISE-PIPE uses a series of passive waveguide relays in the form of relay coils along the pipe to overcome this issue and increase the transmission range (36m by using 10 relay coils). However, this significantly increases the cost of installation due to extra excavations required for the relay coils to be fitted along the pipe and makes the system only economically viable for newly laid pipes. In addition, the high-energy consumption of the inner pipe sensors limits the locations that they can be deployed.

2.4.2 Internal systems

The TriopusNet system (Lai et al., 2012) comprises nodes which are deployed into the pipe via an inlet and are carried along the pipe via the flow of water. Each node is equipped with inertial modules in order to calculate its movement and position along the pipe. When the nodes reach their predefined location they latch to the pipe via three motorised arms with suction pad at their ends (BenSaleh et al., 2013). Figure 2.20 shows the prototype of the TriopusNet node.

Figure 2.20 Prototype of the TriopusNet node (Lai et al., 2012).

When all the nodes are in their allocated place they will measure pressure and other parameters and act as a normal WSN. The TriopusNet location tracking system is adapted from the PipeProbe system (Chang et al., 2009; Lai et al., 2010) which is a mobile node system based on inertial and pressure measurements for identifying the pipeline 3D layout. A common drawback in both of these systems is their lack of accuracy of the tracking information due to errors caused by rotation, change in speed, and vibrations (Kim, 2011). Another intrinsic drawback of the TriopusNet system is that, if one of the nodes fails or needs to be replaced all the nodes downstream of it also need to be flushed due to size of the nodes (Lai et al., 2012). The TriopusNet system is a new technology and more research is required to minimise its size in order to facilitate flushing and make it possible to overcome the mentioned issues.

2.4.3 RF propagation in soil

WSN are commonly used in environments where the communication path between the nodes is not lossy (i.e air). However, WUSN nodes are buried under the surface and therefore their communication path is partially or in some cases completely through the ground. Soil is a lossy medium for electromagnetic waves (Trinchero et al., 2009) and therefore EM waves are attenuated in soil significantly more compared to air. Soil is also a complex material and many of its properties such as composition, mineralogy, density and water content directly affect its dielectric properties, which in turn affect the EM propagation and attenuation. Additionally soil is a very dynamic medium. Soil conditions such as water content can significantly change (i.e. after a rainfall). Soil composition also can vary significantly within a short space. Another complexity is that dielectric properties of soil vary based on the EM wave frequency. This complex and dynamic nature of soil makes predicting the attenuation of EM signals very complicated. Creating an efficient and reliable underground wireless communication link is one of the main challenges faced by WUSNs. Therefore, understanding the EM wave propagation in soil is essential for the development of a successful wirelesses underground sensor network for pipeline monitoring.

Different empirical models exist in the literature which predict the dielectric properties of the soil based on its composition and water content (Peplinski et al., 1995a; Mironov and Dobson, 2004; Mironov, 2004). The dielectric properties of a soil can also be measured via Time Domain Reflectometry (TDR) or Vector Network Analyser (VNA) based techniques (Logsdon, 2005; Van-Dam et al., 2005; Topp et al., 2000). Empirical and semi-empirical models exist in the literature (Akyildiz et al., 2009; Ghazanfari et al., 2011; Chaamwe et al., 2010; Bogena et al., 2009; Li et al., 2007) that aim to predict the attenuation of EM waves based on the dielectric properties of the soil. Two main models for the prediction of EM wave

attenuation in soil based on soil dielectric properties are the CRIM-Fresnel model proposed by Bogena et al. (2009) and the modified Friis model proposed by Li et al. (2007). In order to understand the propagation of EM waves in different media it is important to first understand how electromagnetic waves are propagated through free space.

EM wave propagation in free space

Friis, (1946) introduced a formula (Equation (2.1)) for calculation of the received power, $P_r(d)$ as a function of internode distance in free space for a transmitter receiver setup.

$$P_r(d) = \frac{P_t G_t G_r \lambda^2}{(4\pi)^2 d^2} \tag{2.1}$$

Where P_t is the transmitter power, G_t and G_r are the transmitter and receiver antenna gains, and d is the distance between the transmitter and receiver and λ is the wavelength of the EM wave in open space.

EM wave propagation in soil based on modified-Friis model

Akyildiz and Stuntebeck (2006) proposed a "link budget" formula based on the Friis transmission equation to act as a framework for EM wave propagation models in soil. This is given by Equation (2.2). In this model a correction factor is added to equation (2.1) in order to reflect the losses in soil medium.

$$P_r = P_t + G_r + G_t - L_0 - L_m \tag{2.2}$$

Where L_m is the path loss in soil (medium) due to material absorption and L_0 is the path loss in free space and is given by Equation (2.3).

$$L_0 = 20log\left(\frac{4\pi d}{\lambda}\right) \tag{2.3}$$

Li et al. (2007) propose a model for the calculation of path losses in soil based on the "link budget" formula presented in Equation (2.2). In this model the path loss in the medium L_m is

calculated considering three main differences between propagation of EM waves in soil compared to open space. Firstly, the EM wave propagation speed is different in soil compared to open space, which results in a different wavelength for the signal. Secondly, the attenuation of the amplitude of the signal is dependent on the frequency. Thirdly, correlation between phase velocity and signal frequency in soil causes colour scattering and delay distortion (Li et al., 2007). Based on this model the total path loss caused by the medium L_m can be divided into the attenuation losses caused by the change in wavelength L_{m1} and the attenuation losses caused by material absorption $L_\propto$ and is given by Equation (2.4):

$$L_m = L_{m1} + L_\propto \tag{2.4}$$

Attenuation losses caused by a change in wavelength L_{m1} is given by Equation (2.5)

$$L_{m1} = 20log\left(\frac{\lambda_0}{\lambda}\right) \tag{2.5}$$

Where the wavelength in free space is $\lambda_0 = \frac{c}{f}$, ($c = 3\times10^8 m/s$ and f is the signal frequency in Hz) and the wavelength of the signal in soil is $\lambda = \frac{2\pi}{\beta}$ where β is the phase shifting constant. Therefore L_{m1} is given by Equation (2.6):

$$L_{m1} = 154 - 20\log(f) + 20\log(\beta) \tag{2.6}$$

Losses due to attenuation L_α is given by Equation (2.7):

$$L_\alpha = 8.68\alpha d \tag{2.7}$$

Where α is the attenuation constant. The combined total losses in soil L_p is therefore given by Equation (2.8):

$$L_p = L_{m1} + L_\alpha + L_0 \tag{2.8}$$

Substitution of the above mentioned parameters with their equations results in Equation (2.9), which calculates the overall path loss based on Modified-Friis model for EM wave propagation in soil.

$$L_p = 6.4 + 20\log(d) + 20\log(\beta) + 8.68\alpha d \tag{2.9}$$

Where α and β are given by equations (2.10) and (2.11).

$$\alpha = \omega\sqrt{\frac{\mu\varepsilon'}{2}\left[\sqrt{1+\left(\frac{\varepsilon''}{\varepsilon'}\right)^2}-1\right]} \tag{2.10}$$

$$\beta = \omega\sqrt{\frac{\mu\varepsilon'}{2}\left[\sqrt{1+\left(\frac{\varepsilon''}{\varepsilon'}\right)^2}+1\right]} \tag{2.11}$$

Where ω is the angular frequency ($\omega = 2\pi f$), μ is the magnetic permeability and is assumed to be 1. Li et al. (2007) used Peplinski's dielectric mixing formula published by Peplinski et al. (1995b) in their research to calculate the real and imaginary parts of the complex permittivity value of soil in their paper and subsequent papers (Akyildiz et al., 2009; Vuran and Akyildiz, 2010). However, the mixing formula presented in these papers is incorrect and is based on a wrong formula initially published by Peplinski et al. (1995b) and shortly after corrected in (Peplinski et al., 1995a). For this reason comparison of the results from Akyildiz et al. (2009) and Vuran and Akyildiz (2010) are not presented in this thesis.

EM wave propagation in soil based on CRIM-Fresnel model

Bogena et al. (2009) propose a semi-empirical model based on a Complex Refractive Index Model (CRIM) to quantify signal attenuation in WUSN. Similar to the Modified-Friis model CRIM-Fresnel model is also based on the link budget formula presented in Equation (2.2). In

this model losses due to signal reflection are included in the total attenuation of signals A_{tot} (Yoon, 2013; Chaamwe et al., 2010; Bogena et al., 2009). However, the dielectric permittivity of soil is calculated based on the CRIM model, which takes into account the permittivity of soil ε_s, water ε_w and air ε_a at a specific EM wave frequency. Based on Bogena et al. (2009) the total attenuation losses A_{tot} is given by Equation (2.12).

$$A_{tot} = \alpha_c d + R_c \tag{2.12}$$

Where α_c is the attenuation due to material absorption from Dane and Topp (2002) and R_c is the attenuation due to reflection. R_c can be calculated using Equation (2.13).

$$R_c = 10log\left(\frac{2R}{1+R}\right) \tag{2.13}$$

The reflection coefficient R, with an assumption that magnetic permeability can be neglected, is calculated by Equation (2.14).

$$R = \left(\frac{1-\sqrt{\acute{\varepsilon}}}{1+\sqrt{\acute{\varepsilon}}}\right)^2 \tag{2.14}$$

The authors of Bogena et al. (2009) claim that their proposed CRIM-Fresnel model is better suited for an initial approximation of EM waves propagation in soil compared to the Modified-Friis model proposed by Li et al. (2007) due to the fact that the dielectric mixing model used by that model (Peplinski et al., 1995a) is not supported by a large data base. However, the CRIM-Fresnel model presented in Bogena et al. (2009) is not validated by field trials and its authors acknowledge that field trials are required for furthur evaluation of the model.

Comparison of existing RF propagation models in soil

Attenuation of the EM signal based on the Modified-Friis and CRIM-Fresnel models are evaluated for frequencies of 100-300Hz in order to investigate the effect of frequency on

signal attenuation in soil. Figure 2.21 illustrates the total attenuation calculated by these two models.

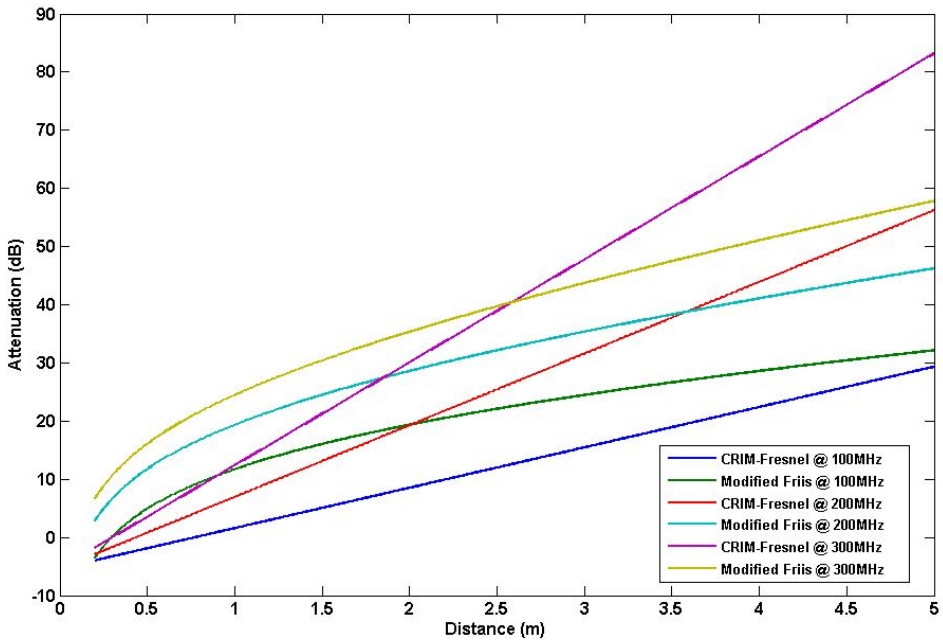

Figure 2.21 Comparison of the Modified-Friis and CRIM-Fresnel RF propagation models

As can be seen from Figure 2.21, the signal attenuation increases with an increase in frequency in both models. Therefore higher operational frequencies will have a shorter range compared to lower operational frequencies given the same input power and receiver sensitivity. This is consistent with findings from Chaamwe et al. (2010). Additionally it can be shown from Figure 2.21 that there is a significant difference between the predicted values by these models, which increase at higher frequencies.

2.5 Summary and identified gaps in knowledge

In this chapter water pipeline networks are introduced and the main causes of pipe deterioration and failure are identified and classified. Additionally the direct and indirect cost of failures for asset owners is analysed. The total cost of network management and relationship between the cost of failure and asset management are also analysed. These showed a real benefit for a low cost pipeline monitoring system that can detect failures in the network at the early stages of the failure process. State-of-the-art techniques for active pipeline failure monitoring (NDE methods) are categorised and critically reviewed. Table 2.1 presents a summary of the reviewed NDE techniques and their limitations.

Table 2.1 Comparison and limitations of NDE techniques for pipeline health assessment

Category	NDE method	Internal access	Other limitations
Acoustic	• Acoustic correlation • SAHARA	Yes	Performance is highly affected by pipe material and diameter. High power consumption.
Electromagnetic method	• Remote field inspection • Magnetic flux leakage • Ground Penetrating Radar	Yes (with the exception of GPR)	Performance characteristics and reliability of GPR highly depends on the soil type and conditions. GPR output is difficult to interpret. RFEC and MFL methods are only suited to metallic pipes.
Ultra spectrum	• Ultrasonic • Infrared thermography	Yes (with the exception of infrared thermography)	Ultrasound method is suited to metallic pipes. Infrared thermography can be affected by environmental conditions.
Physical methods	• Impact echo • Tracer gas	Yes	High costs. For IE method the pipe needs to be emptied of its content.
Fiber optic	• Local • Quasi-distributed • Distributed	No	Lack of redundancy and need for continuity.
Visual	• CCTV • Laser scanning	Yes	Requires highly skilled operator. Pipe needs to be emptied from its content.
Multi-sensor based	• Smart PIGs • Wireless underground sensor networks	Yes	PIGS are not suitable for smaller diameter pipes. Reliable communication is challenging in WUSN. Nodes power consumption limits operational life of the system.

As is shown in Table 2.1 and discussed in the previous sections of this chapter, current NDE techniques for pipeline monitoring commonly suffer from high power consumption and a requirement to access the interior of the pipe. Moreover, most of these systems have a survey-based design, which makes them unsuitable for continuous pipeline monitoring. This makes them unsuitable for long-term permanent monitoring of pipes. In addition to the comparison of NDE techniques for pipeline monitoring, published WUSN systems were reviewed. WUSN pose as a suitable platform for pipeline monitoring due to the ability to be densely deployed, multi-sensor capabilities and the continuous monitoring nature of these system. Challenges of the underground environment for these systems were also identified and described in this chapter. The reviewed WUSN for pipeline monitoring are commonly based on commercially available sensor node platforms (i.e Intel Mote). This results in the power consumption of the nodes to be too high for long-term underground deployment. Based on the review carried out in this chapter the following gasps in knowledge were identified:

- The existing NDE methods for pipeline monitoring are mainly survey-based techniques or are designed for specific type of pipes. WUSN are a suitable platform for continuous pipeline monitoring.
- The existing WUSN for pipeline monitoring are commonly suffering high power consumption and therefore have a short operational life and cannot be deployed underground for long-term pipeline monitoring. An ultra low power WSN can solve this problem and enable WUSN to be used as a long-term (>10 years) monitoring system for pipelines.
- The existing nodes for WUSN are either generic WSN nodes that are used for pipeline monitoring or are not designed for long-term (potentially permanent) underground deployment in the underground environment without the need for servicing (change of

battery or data retrieval). Moreover, these systems mostly communicate via high frequency transceivers (i.e. ZigBee and Wi-Fi) that reduce their range and reliability in underground environment.

- The internal pressure of pipelines is one of their key operating parameters. To the knowledge of the author all existing pressure sensors used in the reviewed WUSN systems for pipeline monitoring are common commercial pressure sensors, which require access to the medium in the pipe via valves or tapings. A non-intrusive pressure measurement system can greatly benefit all types of pressure based monitoring systems as well as WUSN for pipeline monitoring.
- Prediction of RF propagation in soil is critically important for the design of the WUSN. Multiple models have been published in the literature to achieve this aim, however they mainly lack field validations or performance analysis in varied soil compositions and conditions. Moreover, the performance of these models has not been compared in detail with each other and practical data.

Research carried out during this project tries to address the gaps mentioned above. Additional specific reviews are presented in each chapter were required.

3

DESIGN AND DEVELOPMENT OF WIRELESS UNDERGROUND SENSOR NETWORK FOR PIPELINE MONITORING

Contents

Overview of the chapter

This chapter reports on the design and development of an ultra low power wireless sensor network for pipeline monitoring. Following an introduction to the available pipeline monitoring sensor networks, the main challenges in the design and development of a successful Wireless Underground Sensor Network (WUSN) are identified. The general node architecture (hardware and software) of the nodes is discussed in detail. Moreover, methods of reducing the power consumption of the nodes via hardware and software design are presented in this chapter.

3.1 Introduction

As was mentioned in Chapter 2, wireless sensor networks have been used in a variety of applications (Stajano et al., 2010). The application and environment in which the sensor nodes are deployed imposes limitations and specific requirements on the sensor nodes' architecture (Sun et al., 2011). Figure 3.1 illustrates the main limitations and requirements for a WUSN for pipeline monitoring systems.

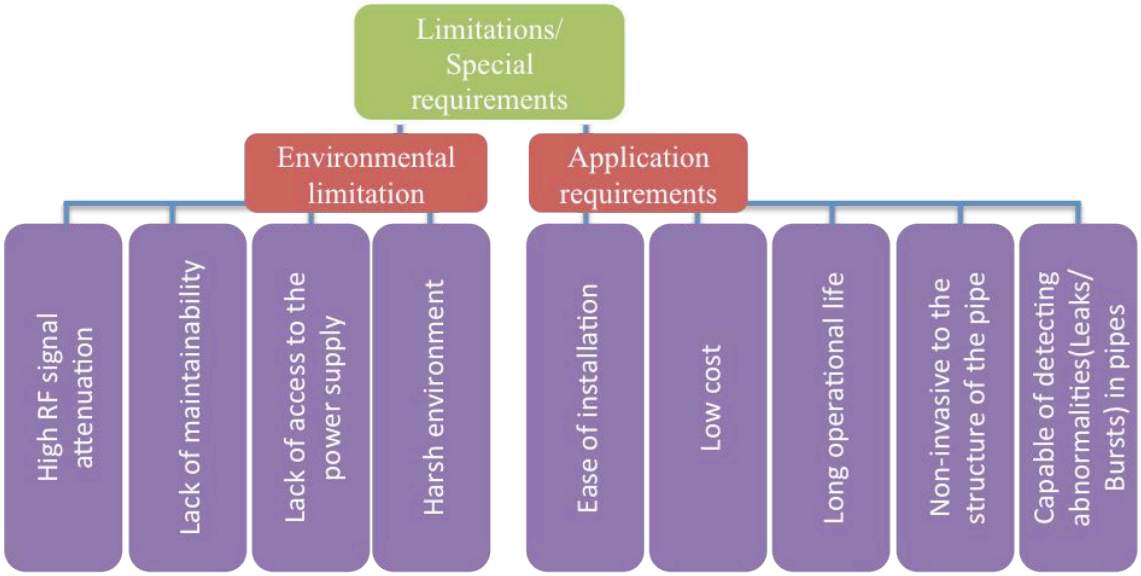

Figure 3.1 Limitations and requirements of WUSN for pipeline monitoring.

High RF signal attenuation is a challenging issue for a WUSN as the RF characteristics of soils can vary dramatically between soil types and soil conditions (for example, water content, density and composition) (Akyildiz and Stuntebeck, 2006). These effects are discussed in more detail in Chapter 6 of this thesis. High attenuation of RF signals in soil results in a shorter transmission range, which in turn affects the overall architecture and spacing of the nodes.

In pipeline monitoring, nodes are buried in the soil at the depth of the pipe. This makes them inaccessible for maintenance or replacement without re-excavation, which can be very costly.

Therefore nodes should be able to operate independently without the need for maintenance or replacement.

The above-mentioned issue of accessibility imposes another limitation on the sensor node, which is the availability of power (Akyildiz and Stuntebeck, 2006). Power sources are very limited in the underground environment and traditional power supply methods such as solar, battery (replaceable) and mains power line are not feasible. Therefore nodes should have ultra-low power consumption in order to extend their operational life on batteries or allow them to use alternative low output energy harvesters (thermal, EM harvesters).

Installing monitoring systems on existing pipelines often requires closure of roads, extensive documentation and permission, expensive excavation techniques and carries many potential risks (Misiunas, 2005). Therefore, the ease of installation is very important for Pipeline Monitoring Systems (PMS). An ideal PMS would require minimal operator skill, minimal calibration, and minimal excavation.

The overall cost of the nodes has to be minimised in order for the WUSN based PMS systems to be adopted by industry. As was previously mentioned in Chapter 2 various factors should be taken into account in order to calculate the cost-benefit of the PMS systems; for example, the value of the medium transferred, cost of repairs, government incentives.

Long operational life is one of the main requirements of the PMS. As mentioned, excavations and repairs are extremely costly; therefore a suitable PMS system should have a long operational life without the need for replacement. Furthermore, it should have a degree of tolerance to redundancy in case of an individual node failure. The operational life of the nodes is also closely related to the power consumption and power availability.

This chapter reports on the design and development of an ultra-low power node for pipeline monitoring and the research conducted into parameters affecting the power consumption of the nodes.

3.2 System structure

Wireless sensor networks can have various topologies and structure based on their application and environment. However, due to the linear nature of pipelines, the topology of a WUSN for pipeline monitoring is more limited than other applications. This limitation in topology is further reinforced by the poor RF transmission through soil, which imposes further boundaries on routing and topology of the network. Figure 3.2 illustrates the typical schematic of a wireless sensor network for pipeline monitoring.

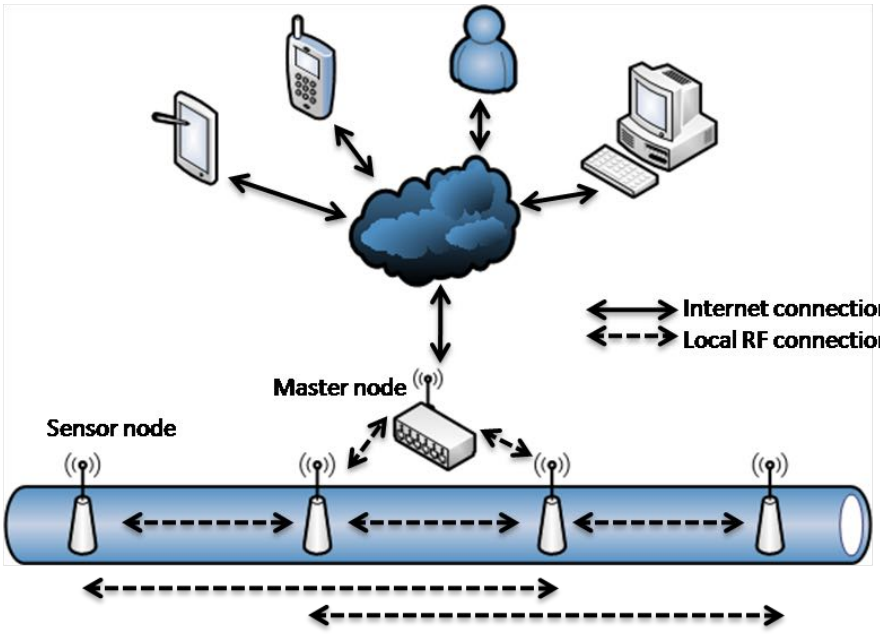

Figure 3.2 Schematic of a wireless sensor network for pipeline monitoring (Sadeghioon et al., 2014a).

The overall architecture of the WUSN for pipeline monitoring can be divided into four main levels of hierarchy:

- Sensor nodes
- Master nodes
- Cloud server
- End user

Each individual node measures multiple pipe environmental and operational parameters (for example, pipe temperature, soil temperature, pipe internal pressure and soil water content) from sensors attached to the pipe and in the pipe's surroundings. These data are then processed by the nodes and compared to the historic values at that location to check for abnormalities or indications of a leak or failure. These data are then processed and stamped with node identifier (ID) and measurement ID into compressed packages and are transmitted to the neighbouring node or the master node. The master node then further processes and time stamps the data from all of the nodes in its territory and correlates them with each other and the historic data to check for leaks or faults. This is then uploaded to the control server (cloud) via an Internet connection. The end user (i.e. asset owners) can then access these data via any Internet connected device. Figure 3.3 shows a typical data flow in a WUSN for pipeline monitoring.

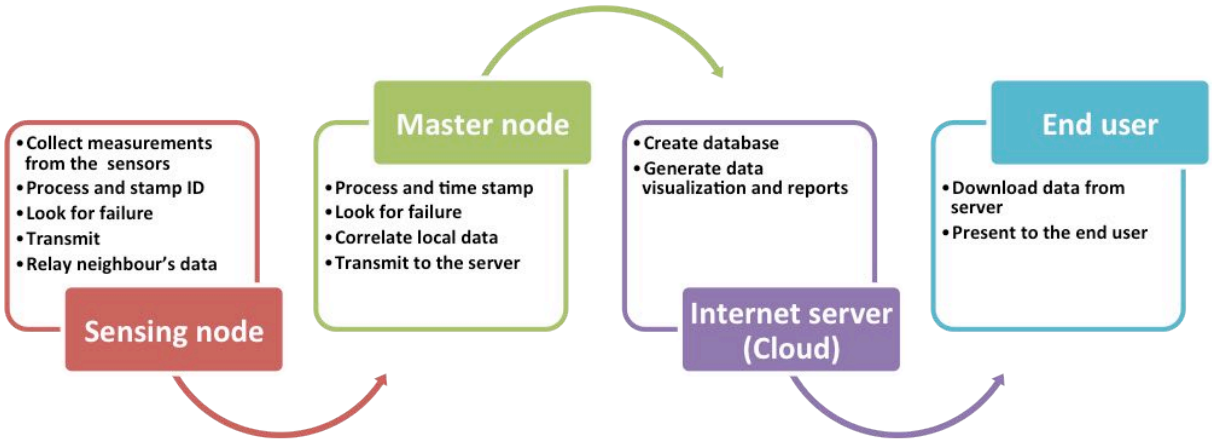

Figure 3.3 Typical data flow in a WUSN between network layers

During this project a proof of concept data management system was developed using Labview visual programming language. The developed software was capable of sorting the received data from the nodes (up to 8 nodes) based on their ID and displaying individual parameters selected by user (i.e. relative pressure) and historic values in the form of charts. In addition the data management system was capable of logging the data locally and automatically uploading the sorted data from the nodes to an Internet server (Xively™ formerly known as COSM). Figure 3.4 shows a screen shot of the developed data management software.

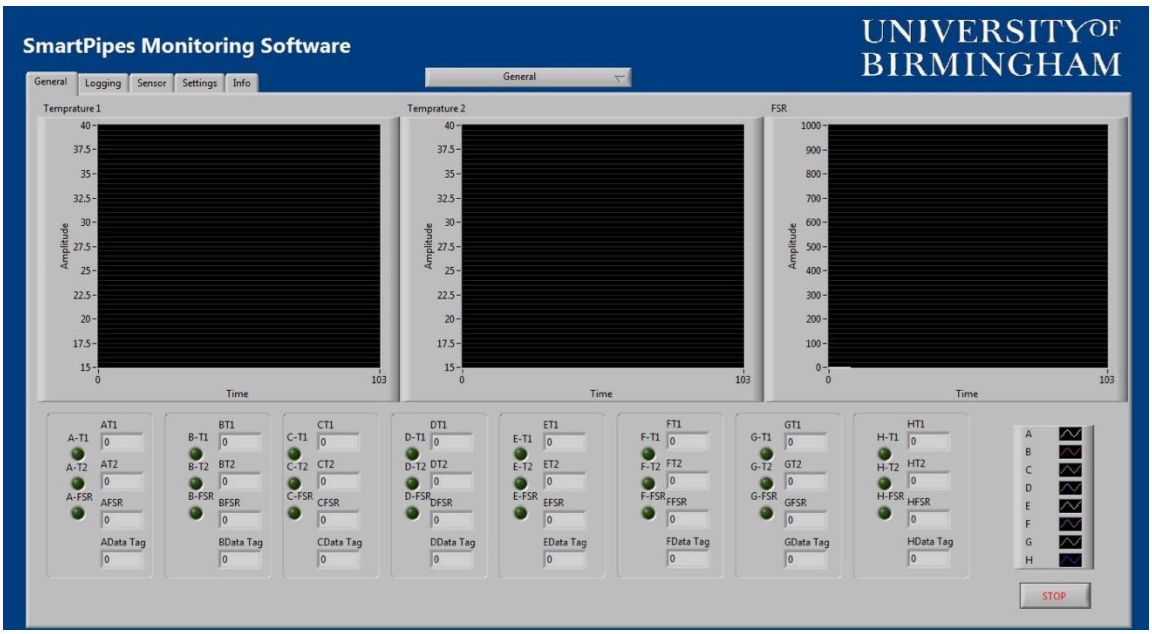

Figure 3.4 Screenshot of the developed data management software

However this software was not used for any of the field trials as it was developed later in the project and therefore is not discussed in further detail in this thesis. An overview of the design of the nodes for WUSN is described in the next section.

3.2.1 Node design overview

Having established the overall structure of WUSN, this section investigates the design of the nodes used in WUSNs. As was mentioned in Chapter 2 existing WUSNs for pipeline

monitoring commonly use generic wireless sensor node platforms (i.e.Intel Mote), which limits their operational life due to the high power consumption of these platforms. Therefore, the nodes should be specifically designed based on their intended purpose in order to successfully deploy wireless sensor networks for long-term pipe monitoring. The design of the sensor nodes can be divided into two main categorises of hardware design and software (firmware) design. The main factors affecting the design of the nodes are hardware constraints, fault tolerance, scalability, overall cost, environment and power consumption. These constraints can affect the design of both the hardware and software of the nodes.

The hardware of a WUSN node can be divided into four main subsystems: Microcontroller Unit (MCU), transceiver, power management and signal conditioning (Figure 3.5). Each of these subsystems is responsible for a specific task in the operation of the node.

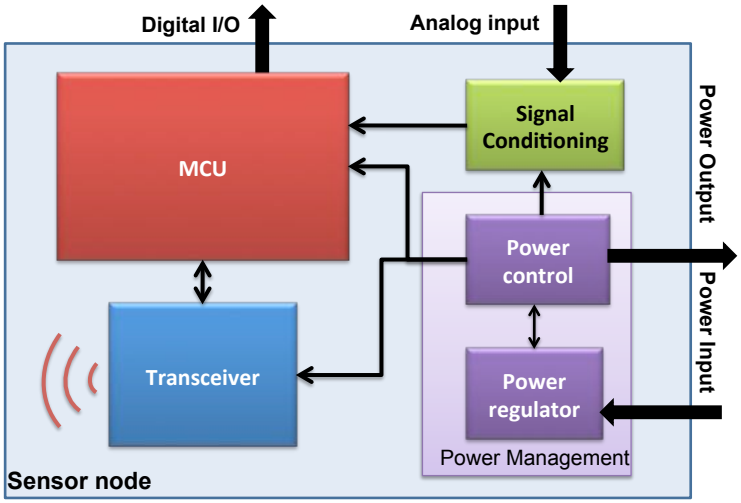

Figure 3.5 General schematic of the node and its subsystems (Sadeghioon et al., 2014a).

The MCU subsystem is mainly responsible for gathering the data from the sensors, processing them into a usable form, running the leak detection algorithms and buffering them into the transceiver. This unit is usually composed of an ultra-low power microcontroller and its required circuitry. The MCU subsystem is also responsible for time keeping. An internal

timer (watchdog timer) or a real time clock (RTC) can be used for time keeping. The design of this subsystem can considerably affect the overall performance of the node.

A transceiver subsystem is responsible for connecting the node to the other nodes/master node. The operational characteristics (for example, RF frequency, RF output power and power consumption) of the transceiver are highly dependent on the application of the node (i.e. lower frequency for highly attenuating environments) .

Various types of power supply or energy harvester systems can be used to power the nodes and the power management circuitry is responsible for conditioning and managing the supplied power, in order to provide a usable power supply for different components of the board. The design of the power management system plays a major role in determining the power efficiency of the node as the majority of the losses happen during power conversion.

Depending on the application of the WSN's nodes, various types of sensors (MEMS accelerometers, temperature sensors, pressure sensors) can be connected to them. The output of these sensors can be in the form of digital output, voltage, change in resistance, etc. In order to interface these outputs with the input of the microcontroller, usually a form of conditioning (for example, amplification, bridge and step change) is required. The signal conditioning subsystem is responsible for this task. An efficient and robust design of this subsystem is crucial for obtaining high quality data from the sensors.

In addition to the above mentioned aspects of the hardware and its design, the size of the node is also important, as the nodes should be small enough to be easily deployed on the pipes without a need for large excavation.

WUSNs are composed of a large number of individual nodes. These nodes can potentially fail due to hardware or software faults. These faults could be caused by various factors, such as individual component failure, software glitches, degradation due to the harsh environment or external damage caused by third parties. Fault tolerance of the sensor network is defined as the capability of remaining functional without any major disruption caused by node failure (Akyildiz and Vuran, 2010). Dense node deployment and higher standard components with a lower failure rate can potentially increase the fault tolerance of a WSN; however, they cause other problems, such as increase in cost of manufacturing and deployment. Other methods, such as systematic recovery algorithms, can be used to maintain the overall fault tolerance of the WSN (Akyildiz and Vuran, 2010). The desired fault tolerance of a network greatly depends on the criticality of the application, acceptable cost of manufacturing and deployment, and ease of deployment. In pipeline monitoring, the cost of dense deployment of the nodes on current pipes is high and infeasible. Therefore a suitable WUSN for pipeline monitoring should achieve high fault tolerance by improved node design and component selection. This is less critical for new pipes installation using conventional trenching techniques, as the nodes can be densely deployed without incurring major extra installation costs.

Pipeline systems such as water distribution systems can extend to thousands of kilometres. This creates a scalability issue for the monitoring of these pipes using WUSN. These networks should be able to handle all the information generated by the nodes effectively and efficiently. This imposes certain constraints on the network and data management design of the WUSN.

As mentioned earlier in this chapter, low overall cost is one of the main requirements for any pipeline monitoring system. The overall cost can be divided into three main parts: manufacturing cost, deployment cost, and maintenance cost. Manufacturing costs are directly related to the hardware design and component selection. Although using high performance components can be beneficial in terms of fault tolerance and system performance, they could significantly increase the production cost of the nodes and make dense deployment of the system economically not feasible. On the other hand, using higher performance components could reduce the failure rates and therefore reduce the maintenance costs. This creates a need for careful hardware design of the nodes in order to minimise the overall cost of the network system. In pipeline monitoring, the deployment cost of the PMS on existing pipes is a major part of the overall cost of the PMS. Pipes are usually buried and deploying the PMS at the pipe level can be very costly; therefore the system should be designed with deployment in mind to reduce the overall cost. This can be achieved by designing the installation of the nodes to be carried out via keyhole vacuum excavation techniques without a need for tappings in the pipes.

The environment of the nodes also greatly affects the design of the nodes. In underground pipeline monitoring, the environment of the nodes can be harsh and therefore the design and packaging of the nodes needs to be robust in order to survive for the desired lifetime. The underground environment also greatly affects the RF transmission of the nodes and they should be designed specifically for the underground environment in order to operate correctly.

As mentioned, power consumption is one of the main challenges of any WSN. Power consumption is even more critical for wireless sensor networks in underground pipeline monitoring to due lack of access to the nodes. Various aspects of hardware and software

design are involved in reducing the power consumption. A power consumption goal of 10μW for one transmission per 8 hours was chosen for the purpose of this research based on an average theoretical lifetime of >50 years on 2 AA batteries (although it should be noted that the current shelf life of the batteries is significantly shorter than 50 years). Efforts to minimise the power consumption of the developed node through hardware and software design are further discussed in detail in the next section of this chapter.

3.2.2 Power consumption

Energy resources for wireless sensor networks are usually very limited and in some cases non-replenishable. This makes the power consumption efficiency of the nodes extremely critical in determining their operational life and therefore suitability for infrastructure monitoring. In particular low power consumption is crucial for WUSNs in pipeline monitoring.

In multi-hop sensor networks, application level nodes can be divided into data generators and data routers (Akyildiz and Vuran, 2010). Data generators are solely responsible for data collection from the sensors at defined time intervals (or in the case of an interruption) and transmission of these data to the neighbouring/master node. In addition to the responsibilities of the data generators (data collection and transmission), data routers are also responsible for relaying the data from the neighbouring nodes forward to the next node/master node. This is crucial for WUSNs as the transmission range of the nodes is relatively short (approx. 3-5m). A complete understanding of the operation of the nodes and the power consumption of different components at different steps during the duty cycle of the node is required in order to be able to minimise the power consumption. A typical routine for a node in infrastructure monitoring can be divided into four or five modes (depending on their role in the network):

measurement, processing, receiving, transmission and sleep. During each of these modes certain components of the node are active, which makes the power consumption of these modes different from each other. Moreover, the duration of each mode is different and is dependent on design factors such as measurement frequency and processing speed. These modes and the major tasks undertaken at each mode are illustrated in Figure 3.6.

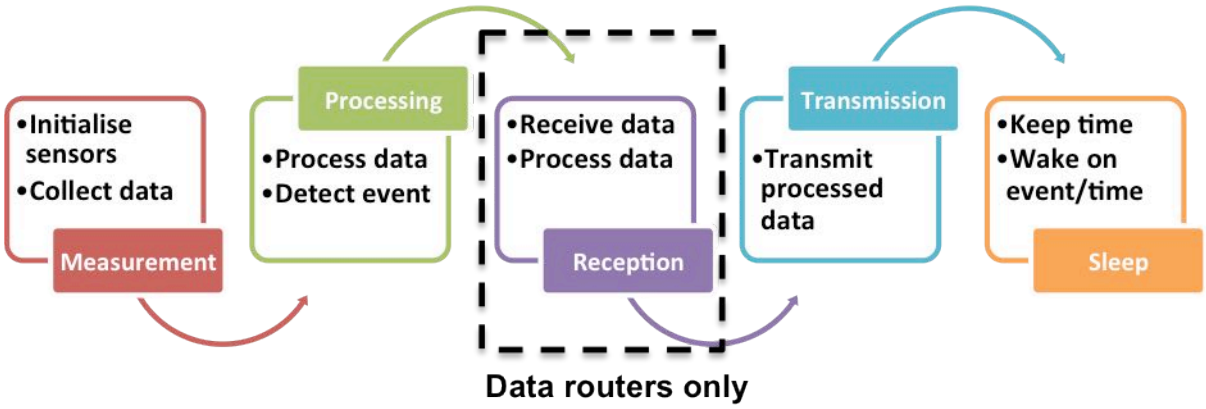

Figure 3.6 WUSN operation modes and the major tasks undertaken at each mode.

During the measurement period the MCU turns the sensors on, initialises them and reads their output, based on the output type via ADC/Digital communication. During this mode these values are stored as variables in the volatile memory of the MCU. The power consumption of this mode is mainly dependent on the power consumption of the sensors, settling time of the sensors and processing speed. Therefore, the power consumption of this mode can be reduced by choosing faster sensors with lower power consumption and optimising the MCU processing speed via firmware. The processing speed of the MCU should be optimised for the application, as higher processing speed will reduce the duration of the processing; however this will increase the power consumption of the MCU. During the processing stage, the MCU analyses the data from the sensors and compares it to the historic data. The processing speed is the main parameter affecting the power consumption and as mentioned, it should be optimised in order to achieve the lowest power consumption at this stage. The voltage at

which the MCU core is operating is also crucial in determining the power consumption of the MCU. The effect of operating voltage is further discussed in Section 3.3.4 of this chapter. The reception mode only exists in the data router nodes at this stage; the MCU turns on the receiver at a synchronised time and waits for data from the other nodes (based on the routing protocol). These data are then processed if necessary and stored in the volatile memory of the MCU. The power consumption at this stage is highly dependent on the power consumption of the transceiver in receive (RX) mode and the duration of time that the transmitter needs to be on. This duration is affected by time synchronisation accuracy, length of packets, bandwidth, start-up time of the transceiver and internal transfer speed (between the MCU and transceiver). In the transmission mode the MCU turns on the transmitter (in the case of the data generator) and transfers the processed data to the buffer of the transceiver; these data packets are then transmitted by the transceiver. Data router nodes append the data generated locally to the relayed data; therefore these will have a longer message length. The length of the message is proportional to the number of sensors/required data and number of relayed messages. Factors affecting the power consumption are similar to those of the reception mode. During the sleep mode the MCU turns off all the unnecessary components and internal modules of the node and solely performs the critical tasks required for the operation of the node. After entering the sleep mode, the MCU starts a timer in order to keep the time and wakes again based on the predefined synchronised duration or interrupts (which can be caused by sudden events). The power consumption in this mode is dependent on the time keeping method, the power consumption of the MCU during the sleep mode and the length of the sleep period. The length of the sleep period is determined by the measurement frequency. The power consumption of the node during sleep is very low compared to the other modes of operation; however, in pipeline monitoring nodes will spend most of their time in sleep mode

as the data is commonly only measured every 15 minutes and transmitted daily. Therefore, the total energy consumed during sleep can be significantly higher than the energy consumed during the other modes combined. This makes the measurement frequency a very important factor in overall power consumption of the node. Table 3.1 summarises factors affecting the power consumption of the node during each operational mode.

Table 3.1 Main factors affecting the power consumption during different operational modes of each node.

Operation mode	Factors affecting the power consumption
Measurement	• Sensors' consumption • Sensors' settling time • Processing speed
Processing	• Core voltage • Processing speed
Reception	• Transceiver power consumption in RX mode • Synchronisation accuracy • Number of hops • Length of message • Bandwidth
Transmission	• Transceiver power consumption in TX mode • Bandwidth • Length of message • Buffering speed
Sleep	• MCU power consumption during sleep • Length of sleep period (measurement frequency)

The average power consumption of the node P_{Av} depends on the power consumption and duration of all of the operational modes of the node. This can be calculated using Equation (3.1). All units are in seconds and Watts.

$$P_{Av} = \frac{(T_m \times P_m) + (T_{tx} \times P_{tx}) + ((T_{total} - T_{tx} - T_m) \times P_{sleep})}{T_{total}} \quad (3.1)$$

Where T_m is the duration of measurements and processing, P_m is the power consumption of the node during measurement and processing, T_{tx} is the duration for which the transmitter is

on, P_{tx} is the power consumption of the node during transmission mode, P_{sleep} is the power consumption of the node during sleep mode and T_{total} is the transmission interval.

As mentioned earlier, the measurement frequency plays a major role in determining the overall power consumption of the unit. As the measurement frequency decreases, the percentage of the time in which the node spends in sleep mode increases and therefore the overall average power consumption decreases, until the point that the average power consumption is mainly determined by the power consumption of the nodes in sleep mode. Figure 3.7 illustrates the theoretical average power consumption of a node based on the measurement frequency.

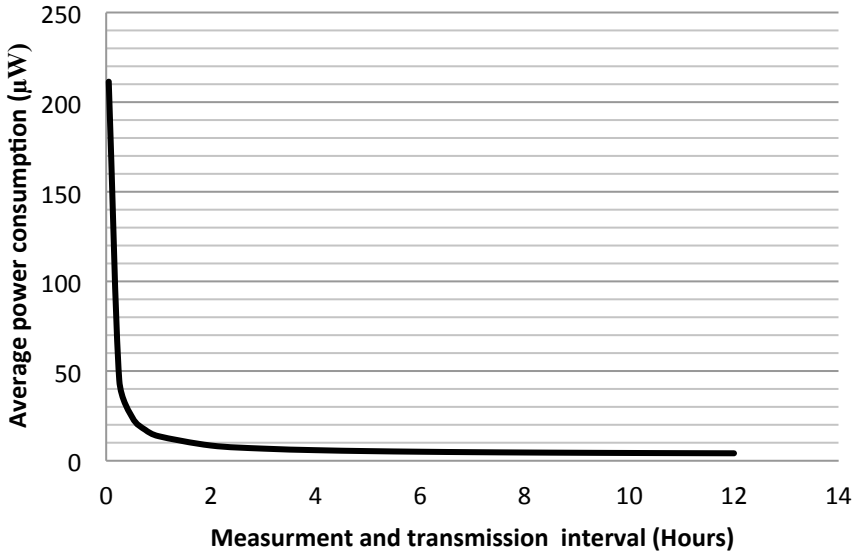

Figure 3.7 Theoretical power consumption of the node based on measurement frequency Based on the assumed power consumption during sleep of 3.3µW and operational power consumption of 75mW (operational duration of 500ms).

As can be clearly seen from Figure 3.7, the measurement and transmission frequency greatly affect the overall power consumption of the node. This effect is especially significant at small measurement intervals (<1 hour). In this region an increase in the measurement and transmission internal results in a sharp decline in power consumption. Moreover it can be

seen from this figure that the effect of measurement and transmission frequency on power consumption is significantly reduced at longer measurement intervals. In these regions the average power consumption is mainly based on the power consumption of the node during sleep mode. In pipelines, faults usually develop slowly; this enables the pipeline monitoring system to operate at lower measurement frequencies. If more frequent measurements are required, the node can measure at a different rate to the transmission rate. This will increase the sampling frequency without affecting the power consumption significantly. In this measurement regime the node will take measurements at a more frequent rate than its transmission rate, store the data in its memory and transmit all the information simultaneously. This provides a major saving in power consumption of the node, compared to transmitting at the same time as the measurement is taken. However, this will also increase the message length at the time of transmission, which will increase the transmission duration and increase power consumption. Equation (3.1) can be modified to incorporate the effect of this regime on power consumption. Equation (3.2) can be used for calculating the average power consumption of the node based on different transmission and measurement rates.

$$P_{Av} = \frac{(T_m \times P_m \times n) + ((T_{tx} + n \times T_b) \times P_{tx}) + ((T_{total} - (T_{tx} + n \times T_b) - (T_m \times n)) \times P_{sleep})}{T_{total}} \qquad (3.2)$$

Where T_b is the extra time burden on the transmitter caused by each measurement and *n* is the number of measurements being taken between each transmission intervals, which can be calculated by Equation (3.3), where T_{mg} is the measurement interval.

$$n = \frac{T_{total}}{T_{mg}} - 1 \qquad (3.3)$$

The measurement frequency and transmission interval are determined in the firmware of the node and need to be set based on the application requirement. Figure 3.8 illustrates the effect

of the measurement frequency on power consumption based on Equation (3.2) for different transmission intervals.

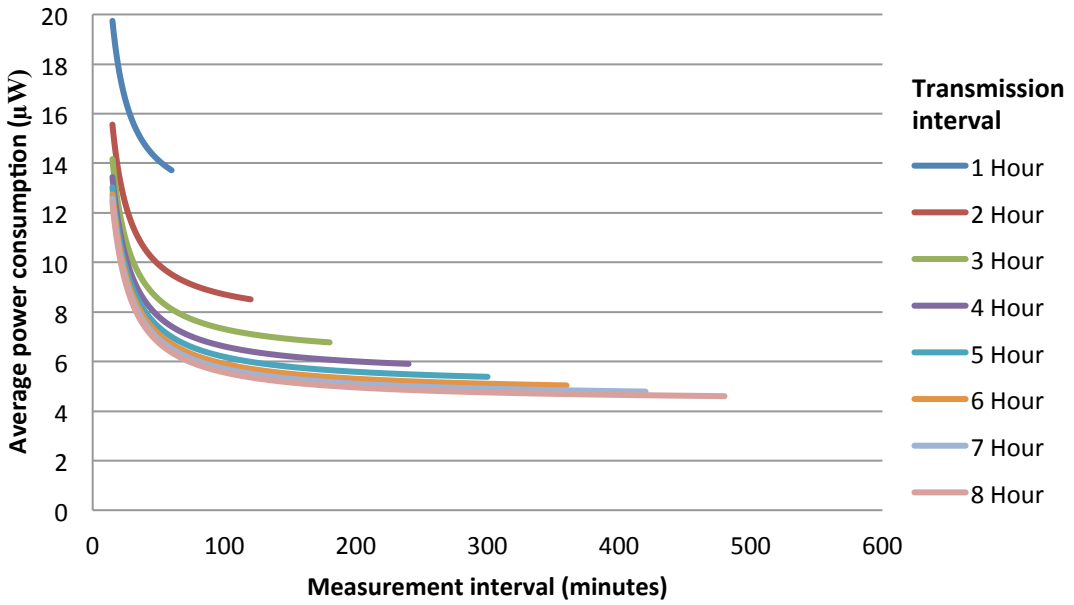

Figure 3.8 Effect of measurement interval on average power consumption

As can be seen from this figure, the effect of the measurement interval on power consumption is very similar to the effect of the transmission interval. The overall power consumption of the node is greatly affected by shorter transmission interval and is less affected by longer intervals (>2hours). It can also be seen from this figure that higher measurement frequencies are achievable without affecting the power consumption by increasing the transmission interval. The node consumes approximately 14µW at a transmission interval of 1 hour and measurement interval of 52 minutes, but by increasing the transmission interval to 2 hours the measurement interval can be decreased significantly to 19 minutes. The choice of measurement and transmission interval is highly affected by the application in which the nodes are deployed (for example, power availability and criticality.). In this research a transmission interval of 8 hours with a measurement interval of 30 minutes is selected for

pipeline monitoring, due to the mentioned scarcity of power and slow changing nature of the pipes.

In addition to understanding the effect of measurement and transmission intervals on the average power consumption of the node, it is also important to analyse and compare the power consumption of the node at each of its operational modes during one cycle. It is also important to analyse the total energy consumed by the node at each mode. This will assist in identifying the big consumers (components) and the modes with the highest energy consumption. Figure 3.9a, illustrates the power consumption of the node during each mode, while Figure 3.9b illustrates the total energy consumed by the node during each mode for one full cycle (2 hour transmission interval).

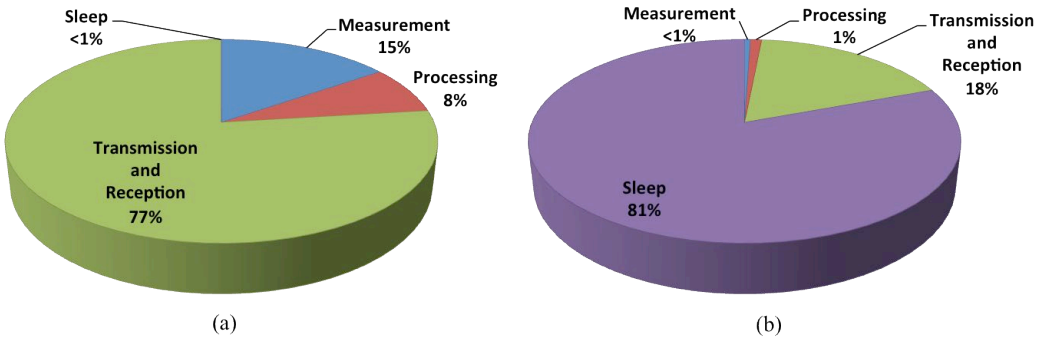

Figure 3.9 (a) Power consumption of the node during each mode, (b) Total energy consumed by the node during each mode for one full cycle (2 hour transmission interval).

As can be seen from this Figure 3.9a, The "Transmission and Reception" mode has the highest power consumption compared to the other modes of operation and the "Sleep" mode has the lowest power consumption (<1%). However, as it is shown in Figure 3.9b, the "Sleep" mode consumes the highest energy for a full cycle. This is due to the fact that the nodes spend most of their time in the "Sleep" mode compared to the other operational modes. For the purpose of increasing efficiency and decreasing power consumption of the node, the overall

energy consumption of the nodes should be considered. The overall energy consumed by the nodes can be minimised by reducing the duration and decreasing the power consumption of the node during each mode. As mentioned previously, this can be done via the hardware and software design of the nodes. This is discussed further in the following sections in this chapter.

3.2.3 Hardware design

During this research an ultra-low power wireless sensor node was designed specifically for monitoring a water distribution pipeline. Throughout the design process of the node, all of the mentioned requirements and limitations were taken into account in order to produce a suitable system for this application. The design and development of the node went through four iterations, with each iteration improving the performance characteristics of the node. The main objective of the design was:

- Ultra-low power consumption (<10μW)
- Good RF performance (min 0dBm) and flexibility in operational frequency
- Adequate connectivity (for interfacing sensors)
- Low cost
- Small size

Table 3.2 shows the main limitations and improvements of each of the iterations of the node. Versions 0.5 and 1.0 of the node are described briefly in the following sections of this chapter, as they were not used in field trials. However, the design and development of versions 1.5 and 2.0 are described in detail as these were used extensively during the research.

Table 3.2 Comparison of the limitations and improvements made for each of the iterations of the node

	Version 0.5	Version 1.0	Version 1.5	Version 2.0
Main Objective	Proof of concept	PCB based and more tailored to the application	Smaller size and lower RF frequency	Field ready node
Limitations	• High power consumption • Not reliable • High RF frequency • High operating voltage	• High RF frequency • Low number of input/output terminals • Size • Poor RF performance	• Not ruggedized • Poor analogue performance • Rigid management	• Average analogue performance • Difficult assembly
Improvements over previous version	N/A	• Significantly lower power consumption • More reliable PCB based circuit	• Lower RF frequency range • Smaller dimensions • Better RF performance	• External antenna connector • Lower power consumption • Flexible power management • Improved analogue performance • Increased reliability

Version 0.5

This was an initial prototype and was used as a proof of concept to help establish the required processing performance and connectivity requirements of the node. This node was solely used for laboratory tests. The design of this node was based on the mbed platform, which is a development board based on NXP LPC1768 (Cortex-M3 core) microcontroller. A 2.4 GHz transceiver module (RFD21733) was used as the transceiver of the node (for a photo of this version of the node see Appendix A). Table 3.3 shows the specification of version 0.5 of the node.

Table 3.3 Specification of version 0.5 of the node

Specification	
Microcontroller	NXP LPC1768
Speed	96 MHz (32-bit)
Ram	32 KB
Program memory	512 KB
A/D ports	6
A/D resolution	12 bit
Interface	USB, 2×SPI, 2×I2C, 3×UART, CAN
Transceiver	RFD21733
RF frequency	2.4 GHz
RF output power	0dBm
Antenna/Antenna gain	SMD, 2.5 dBi
Input voltage/ MCU voltage	4.5-9V/3.3V
Average power consumption	300 mW

The power consumption of this module was significantly higher than the target of 10µW due to the high power consumption of the mbed module and lack of deep sleep mode in the firmware. In addition, the program memory and Ram were both higher than the requirements of the node for conducting the basic functions mentioned in previous sections. The transceiver module of this node was solely tested in open air and found to be suitable for the purpose of the nodes. However, based on the literature, lower frequencies of transmission were preferred (Chaamwe et al., 2010). The inability of the mbed to operate in voltage ranges lower than 4.5V was another limitation of this node. The power consumption of the node is greatly affected by the voltage at which it operates; this makes lower voltage circuitry more favourable in designing the node. However, the operating voltage of individual components, such as the microcontroller, sensors and transceiver, limits the minimum voltage at which the nodes can operate. The subsequent version of the node was designed and developed based on findings from this version of the node and is discussed in the following section.

Version 1.0

Version 1.0 of the node was the first design that was developed on a PCB. This version of the node was a major step change from the previous version in various aspects of performance and specification (for a photo of this version of the node see Appendix A). This version was designed based on the requirements of a node for monitoring pipelines, which were mentioned earlier in this chapter. Minimising the sleep power consumption of the node was one of the main objectives for the design of this node. As mentioned earlier, the microcontroller of the node plays a major role in the overall power consumption and performance of the node. Table 3.4 shows the specification of version 1.0 of the node.

Table 3.4 Specifications of version 1.0 of the node

Specification	
Microcontroller	Microchip 16LF1933 (XLP)
Speed	32 MHz (8-bit)
Ram	256 Bytes
Program memory	7 KB
A/D ports[2]	4
A/D resolution	10 bit
Interface	2×SPI, 2×I2C, 1×UART
Transceiver	RFD21733
RF frequency	2.4 GHz
RF output power	0dBm
Antenna/Antenna gain	SMD, 2.5 dBi
Input voltage/MCU voltage	3.3-6V/3.3V
Average power consumption	87.4 µW

[2] This is the number of A/D channels which are accessible based on the design of the node and does not reflect the total number of the A/D channels of the microcontroller

In this version of the node a low power 8-bit Microchip MCU was used for its low power consumption during active and sleep mode. This MCU features Microchip nanoWatt XLP technology. This enables the MCU unit to have very low power consumption (<1μA @1.8V) during sleep mode with an active watchdog timer. As was mentioned earlier in this chapter, during the sleep mode, due to its very low duty cycle required for pipeline monitoring, the MCU cuts the power to all the unnecessary components (transceiver and sensors) in order to conserve energy. In this version of the node a MOSFET switching circuitry was used to control the power to the transceiver module.

Another source of loss of energy is the power conversion circuitry. As the node spends most of its time in sleep mode it is crucial that the power management circuitry of the node has low quiescent current. In this version of the node a low quiescent current CMOS low dropout (LDO) voltage regulator was used in order to regulate the voltage from the power supply to a fixed 3.3V for the MCU and other components. The limitations of this version of the node were its size, reliability, fixed RF frequency, fixed power management regime and low number of Input/output terminals. These issues are addressed in the next iteration of the node, which is described in the following section of this chapter.

Version 1.5

Limitations of the previous version (Ver.1.0) of the node, such as relatively high power consumption, high fixed RF transmission frequency and low number of I/O, prevented it from being deployed for initial trials at the University of Birmingham (described in Chapter 4). Version 1.5 of the node was designed to improve on these limitations. This version of the node was designed based on a single layer PCB. However components were placed on both sides of the board in order to reduce its dimensions. Additionally, using a mixture of surface

mounted and through-hole components drastically reduced the physical dimensions of the node. Reduction in size, made the ruggedized packaging of the nodes easier and in turn made them more suitable for the initial trials. The PCB of this version of the node was fabricated using the wet etching technique. Figure 3.10 illustrates the development stages of node version 1.5 and the completed node.

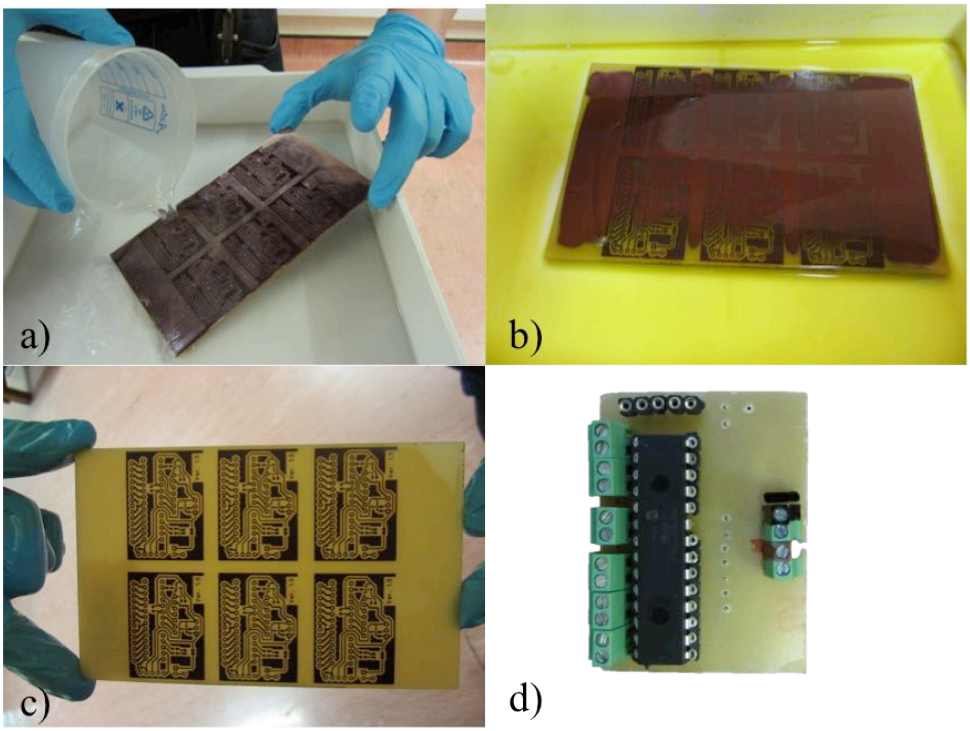

Figure 3.10 Node version 1.5's development stages a) photoresist development b) copper etching c) photo resist removal d) finished node

The transceiver used in the previous versions of the node had limitations such as high transmission frequency, low RF power, lack of connectivity to an external antenna and narrow operating voltage. For version 1.5 of the node a new family of transceiver module (ER400TRS and ER900TRS) was selected to address some of these limitations. The main features in choosing the new transceiver were availability of the module in multiple frequency ranges and good RF performance. The possibility of attaching an external antenna (max 50Ω load) was also another improvement compared to the previous version of the node. This

capability significantly improved the RF performance of the node and made it feasible to be used in initial trials, which are discussed in later chapters. Table 3.5 illustrates the specifications of version 1.5 of the node.

Table 3.5 Specification of version 1.5 of the node

Specification	
Microcontroller	Microchip 16LF1933 (XLP)
Speed	32 MHz (8-bit)
Ram	256 Bytes
Program memory	7 KB
A/D ports[3]	6
A/D resolution	10 bit
Interface	2×SPI, 2×I2C, 1×UART
Transceiver	ER400TRS-02/ER900TRS-02
RF frequency	433-4 MHz/868-9 MHz
RF output power	+10dBm/0dBm
Antenna/Antenna gain	External/ 2.5 dBi
Input voltage/MCU voltage	3.6-6V
Average power consumption	42 µW

Another improvement in the design of this version of the node was an increase in the number of I/O ports. This improvement allowed multiple sensors to be attached to the node (temperature sensors and pressure sensors). Additionally, the power consumption of this version of the node was significantly reduced (≈50% less than in the previous version), due to lower power consumption of parts, ability to turn external components completely off and firmware optimisation, which is described in detail in Section 3.34.

[3] This is the number of A/D channels which are accessible based on the design of the node and does not reflect the total number of the A/D channels of the microcontroller.

Despite all the improvements in this version of the node during initial trials some limitations were found to still persist, which meant there was a need for a further version of the node to address them. The main limitations of this version of the node were power consumption, limited input voltage range and reliability for the field trials. Version 2.0 of the node was designed and developed to address these issues and is discussed in detail in the next section of this chapter.

Version 2.0

This was the final version of the node developed during this research. The main objective during the design process of this version of the node was to develop a node that was capable of being deployed in the field trials. Table 3.6 illustrates the specification of this version of the node.

Table 3.6 Specification of version 2.0 of the node

Specification	
Microcontroller	Microchip 16LF1827 (XLP)
Speed	32 MHz (8-bit)
Ram	384 Bytes
Program memory	7 KB
A/D ports[4]	6
A/D resolution	10 bit
Interface	2×SPI, 2×I2C, 1×UART
Transceiver	ER400TRS-02/ER900TRS-02
RF frequency	433-4 MHz/868-9 MHz
RF output power	+10dBm/0dBm
Antenna/Antenna gain	External/ 2.5 dBi
Input voltage/MCU voltage	1.8-16V
Average power consumption	2.2 µW

[4] This is the number of A/D channels which are accessible based on the design of the node and does not reflect the total number of the A/D channels of the microcontroller.

One of the issues of the previous node was the lack of a robust antenna connector. In the design of this version of the node, an SMA antenna connector was added to the node to address this issue. This enabled the node to connect to various types of antenna (50Ω load) in order to improve its RF performance and range. In addition, this enabled the antenna to be placed at a different location to the node (for example at the ground surface).

The analogue performance and noise-related issues were another limitation of the previous versions of the node. A ground plane was included in the design of this version to reduce the noise due to cross talk and interference. In addition to reduction in noise, ground planes facilitated routing of the PCB by providing immediate access to the ground terminal and eliminating the need for complicated routing for the ground pins of the components.

Programming the MCU of the nodes required access to five of the MCU pins[5]; in the previous version of the node these pins were connected to a straight pin header, which allowed the programmer to be directly connected to the node. This proved to be adequate for the purpose of the laboratory trials. However, the exposed nature of the pin header and lack of rigidity in this method of connection made it unsuitable for this version of the node, which was focused on field trials and reliability. Therefore, a mini USB port was adopted to connect the programmer to the MCU of the node. This allowed the programmer to be easily connected to the node and is significantly more reliable than the open pin header connectors.

It was apparent from initial experiments on the previous version of the node that in order for it to be suitable for field trials, the PCB of the node needed to be more reliable and rugged. Therefore, the manufacturing process of this version of the PCB was outsourced to a commercial PCB manufacturing facility. (The researcher carried out all other stages of the

[5] MCLR,V_{DD},$V_{SS,}$

design, development and assembly of the node.) This made more complex routing and layering (4 layered PCB) feasible for this version of the node; which in turn allowed the node to have more features and components without affecting its footprint. The PCBs of this version of the node also have a protective layer over the conductive traces (solder mask), which made the nodes more reliable and suitable for field trials by providing more resistance towards corrosions environmental damage. Figure 3.11 illustrates the version 2.0 of the node.

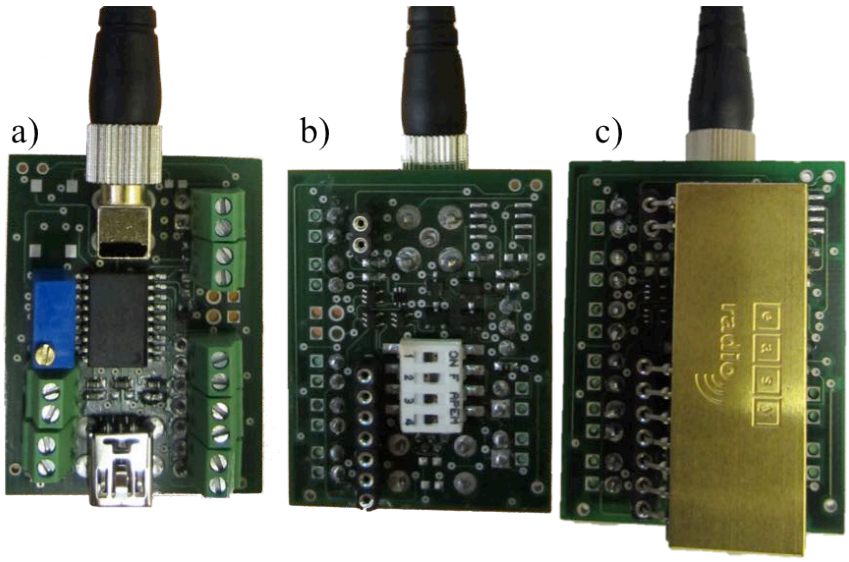

Figure 3.11 Different views of version 2.0 of the node. a) front, b) back without transceiver, c) back with transceiver

The main change in the design of this version of the node compared to previous versions was the design of the power management module. In previous versions of the node a fixed LDO was used to regulate the input power from the source (i.e. battery). The total power consumption of the node is directly related to the operating voltage of the MCU and other components of the node. For this version of the node a multi-step power regulator module was designed and used. The power regulator of this version has four subsystems; each of the subsystems was capable of a range of input voltage and a single/dual fixed output voltage. A switch on the back of the node allowed the selection of each of these subsystems based on the application and available power source. Figure 3.12 illustrates the schematic of the power

management module of this version of the node. The flexibility of the power management module in this version of the node allowed it to be adapted to various power supplies in order to maintain high efficiency.

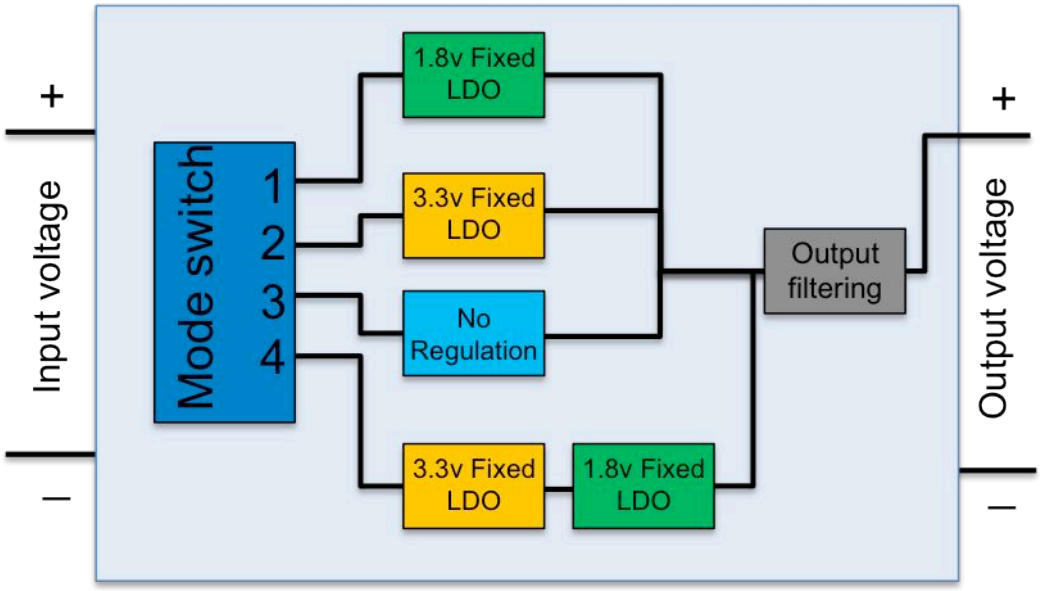

Figure 3.12 Schematic of the power regulator module for version 2.0 of the node

Mode 1 of the power regulator module was designed to be connected to input voltages between 2.0-5.5V. In this mode the regulatory circuit was composed of a 1.8V LDO voltage regulator and basic ripple smoothing circuitry. In this mode the MCU of the node operated at 1.8V, which enabled the node to have low power consumption during the sleep mode. The minimum operating voltage of the sensors and the transceiver of the node was higher (3.3V); therefore in this mode they will not be able to operate from the voltage supplied by the regulator. Therefore, the power for the transceiver and other sensors was supplied directly by the power source (i.e. battery). Mode 1 was mostly suited to low voltage power supplies (3.3-5V), for example Li-Ion batteries and solar cells.

The design of mode 2 of the power regulator was similar to mode 1 with a different set voltage output. In this mode the node was capable of accepting input voltages of 3.3-16.0V.

The output voltage of the regulator was fixed at 3.3V and all the components of the node were powered via the output of the regulator. This version was mostly suited to power supplies with a higher input voltage (5.5-16.0V), for example piezoelectric harvesters.

In mode 3 of the power management module the power was directly supplied via the power input terminals. In this mode the node only performed passive smoothing (shunt capacitors) on the input power supply to make it more stable. This mode allowed the power management to be carried out externally and was mostly suited to power supplies with integrated power managements or special power management requirement, for example, thin film batteries.

Mode 4 of the power regulator was designed to provide two constant voltage supplies of 1.8V and 3.3V. This enabled the MCU to operate at its lowest operating voltage while providing a stable output voltage for the sensors and transceiver. In this mode the input supply could be in the range of 2.5-16.0V. This enabled the node to operate with higher voltage power supplies while maintaining low power consumption during sleep. A drawback of this mode compared with mode 1 was an increase in the total power consumption of the node due to an increase in quiescent consumption of the additional LDO used in this mode.

3.2.4 Firmware design

Hardware components of the node greatly affect overall power consumption and performance; however, another main component of the nodes' design that can greatly improve the performance is their firmware. The firmware of the nodes is the program that is stored in the MCU. It contains a set of instructions to control different components of the nodes and process the data gathered by the node. During this research the firmware of the nodes, with an exception of node version 0.5, were compiled by MikroC Pro compiler

(MikroElektronika, Belgrade), which is a dedicated C compiler for the PIC microcontroller family. The firmware of node version 0.5 was developed using an online C compiler, which is specifically designed for mbed processors.

The design of the firmware of the nodes was highly dependent on the specification of the hardware components and their performance. Digital sensors communicate with the node via different digital protocols, for example I2C, UART, SPI and one wire serial. Therefore, the firmware of the node will change based on the types of the sensors which are connected to the node. The MCU of the node and its capabilities also greatly affect how the firmware is designed and developed. Processing power, sleep instructions and communication speed are the main MCU parameters which affect the firmware design and performance. These are further discussed in the later parts of this chapter.

As was shown in Figure 3.6 the node goes through each of the main operational modes and performs the tasks required at each mode linearly and then repeats the cycle. The firmware of the node is responsible for the order and duration of each of the operations. A detailed description of each of the steps carried out by the firmware of the node is as follows:

1. When the node is initially powered, the clock frequency, I/O settings, A/D settings and interrupts are set up based on the firmware requirements.
2. Global variables and counters used in the program are defined and initialised.
3. A sequence of 5 blinks is performed on the green heartbeat LED to indicate the correct initialisation of critical parameters.
4. Temperature and pressure sensors connected to the node are powered up via a MOSFET.
5. Settling time is allowed for the sensors to reach a stable state.

6. Measurements from the sensors are taken by the MCU based on the communication type between the node and sensor (Analogue/Digital).
7. All sensors are powered down to conserve energy.
8. Data conversion and calibration is carried out on the data from the sensors in order to transform the sensors' raw output into a usable form.
9. The results are compared with the adaptive thresholds for each parameter and flags are set if necessary.
10. The results and flags are packaged together with the node's unique identifier and transmission identifier.
11. The UART module of the MCU is initialised.
12. The transceiver module is powered on.
13. A short delay is allowed for the transceiver and the UART module to stabilise.
14. The transceiver stays in listening mode for a set period of time waiting for data from other nodes (only applicable for data router nodes).
15. The received data is processed and if required (in case of major flags) is packaged with local data (only applicable for data router nodes).
16. The packaged data is transferred to the buffer of the transceiver.
17. Data is transmitted by the transceiver.
18. The transceiver is powered down completely to conserve energy.
19. A Watch Dog Timer (WDT) registry is set for the desired period of time and the timer counter is cleared.
20. All unnecessary internal modules of the MCU are disabled.
21. Sleep instructions are performed in order to put the MCU in deep sleep with a WDT wake up.

22. The MCU is woken up from deep sleep by the WDT.
23. The timer counter is checked; if the correct sleep time is reached the program goes to step 4, if not, the counter is increased and the program goes to step 21.

Reduction in overall "ON" time and the accuracy of timings in order to maintain synchronization with other nodes are the two main challenges in the design of the firmware for WUSN. There are also other challenges in the design of the firmware of the nodes, for example, efficient data processing algorithms and data security; however they are out of the scope of this research. A study into the parameters affecting the duration of "ON" time and the steps taken to minimise them, a comparison of different timing methods for node synchronisation and the design, development of the proposed timing method are described in the next section of this chapter.

Sleep power consumption and timing

As mentioned previously, nodes spend most of their time in the "Sleep" mode. Therefore the energy consumed at this mode is a large proportion of the total energy consumed by the node and reduction in sleep power can greatly affect the overall power consumption of the node. The main factors affecting the power consumption during the sleep mode are the method of timing and the voltage of the power supply.

The timing accuracy of the nodes is one of the main challenges in the design of the firmware. In order for the whole network to be able to communicate efficiently a timing mechanism is required to synchronise all, or a section of, the nodes in the network together. This allows the node to wake up from sleep at a certain time and wait for the transmission from its neighbouring node. Various methods can be used for synchronization of the nodes (Akyildiz and Vuran, 2010). The main methods used for time synchronisation between the nodes are:

real-time clock, “Wake on Radio”, RC timing circuits, GPS, MSF radio signal and internal timers. These methods have very different properties, which makes them suitable or unsuitable for a specific application, and are discussed below.

Real-time clocks (RTC) are an accurate timing method used in many time-sensitive applications. In this method extra timer circuitry is responsible for absolute time keeping. The node is activated from deep sleep on the occurrence of the predefined alarm produced by the RTC. Some MCU units contain an internal real-time clock, which removes the need for external circuitry. However, RTCs are most commonly in a separate integrated circuit (IC) form factor. In addition to the requirement of extra circuitry, usage of RTCs will increase the power consumption of the node during sleep as all the RTC circuitry needs to be active in order to keep time.

“Wake on radio” is another method of synchronisation and timing used in WSN (Akyildiz and Vuran, 2010). In this method the nodes enter the sleep mode and will wake up upon receiving a signal via its transceiver. Unlike the RTC method “Wake on radio” based nodes do not need extra circuitry. However, in order for the transceiver to be able to receive the signal and wake up the rest of the system from sleep, it needs to be in a semi-active mode (powered but not transmitting). This results in a significant increase in power consumption during the sleep period compared to other methods.

A resistor capacitor (RC) circuit can be used to control the timing of the sleep period and provide an interrupt for the MCU to wake it up from sleep (Microchip Technology Inc., 2009). In this method the duration required for the capacitor to charge/discharge is used for relative timing (timing restarts every cycle) of the sleep period. This duration is mainly determined by the resistivity and capacity values of the circuit. Circuitry for this method

solely contains passive components (resistors and capacitors) and therefore can potentially have very low power requirements. However, inaccuracies in capacitance and resistivity values of the parts (commonly 1-10% part to part variation) can lead to large inaccuracies in timing.

A GPS time stamp can be used in order to synchronise wireless sensor nodes with high accuracy (Elson and Römer, 2003). However for the node to be able to receive the GPS signal they need to be equipped with GPS modules and have a separate GPS antenna. These requirements can significantly increase the power consumption and the cost of the nodes. Moreover GPS time synchronisation is mainly suited for terrestrial WSN due to signal reception issue in covered areas.

MSF time synchronisation method is based on a highly accurate, low frequency (60 kHz) time signal that is broadcasted throughout the UK and large sections of northern and Western Europe. Similar to GPS time synchronisation, in this method nodes require a special receiver module in order to be able to lock their timer to the broadcasted signal (Ikram et al., 2010; Chen et al., 2011). Due to lower carrier frequency of the MSF signals they penetrate into buildings and covered areas easier than GPS signals.

Internal timers can potentially be used for the purpose of timing and synchronisation in WSNs (Microchip Technology Inc., 2009). Microcontrollers commonly have multiple internal timers running at different frequencies. These timers are mainly used within the firmware of the MCU to control time related tasks (for example pulse generation/detection, delay timing and baud rate control). The accuracy of these timers greatly depends on the MCU's manufacturing specifications and the operational conditions of the MCU (for example temperature and voltage stability). A Watchdog timer (WDT) is a type of timer that is mainly used for fault

detection (also known as Computer Operating Properly, COP timer) in microcontroller-based systems. WDTs are commonly controlled by two separate registers (configuration and counter value). The configuration register is used for setting the timer duration and turning the WDT ON/OFF. The counter register holds the value of the counter and resets every time the WDT is cleared or the maximum value is reached. When a WDT is used for fault detection within the system, the MCU regularly resets the WDT before it reaches its maximum value. A WDT generates a system reset if a fault happens in the system and the MCU is not capable of resetting the WDT before it reaches its maximum value. This will ensure that software-related problems (freezes and timing issues) are solved automatically. This feature is extremely important in applications where the system is not easily accessed and therefore cannot be reset manually. The WDT feature of an MCU usually has a lower power requirement compared to other internal timers and can run during the sleep mode. In this research a method of relative timing based on an internal Watchdog timer of the MCU is proposed for WUSNs. A Watchdog timer can be configured to control the duration of the sleep period. In this method the duration of the WDT is initially set to a short period (for example 1s) for the “Active” period of the node and is later cleared and set to the desired duration of the sleep period just before the node enters the sleep mode. This results in the WDT operating as a fault detection timer during the “Active” period and as a sleep timer during the sleep period. During the sleep period, the MCU will not be able to clear the WDT counter register and therefore the WDT will generate a reset signal at the end of its predefined duration. This reset signal, however, will only bring the MCU out of sleep mode and not completely reset the MCU. This will allow the firmware to continue its normal operation from before the point that it had entered the sleep period. Although some of the MCUs feature extended Watchdog timers, the maximum duration of these timers are commonly shorter (approximately 4 minutes) than the

required sleep period for a WUSN (15 minutes). Creating a counter and loop in the firmware and re-entering the "Sleep mode" until the desired duration of sleep is reached can solve this issue. This method can provide adequate accuracy for a single-hop network, as the incoming data is time stamped by the mother node at the time of logging.

Another factor which greatly affects the power consumption of the node during the sleep period is the supply voltage. The sleep power consumption of version 2.0 of the node at different supply voltages was measured in order to understand the relationship between the supply voltages and the sleep power consumption. Due to the extremely low currents during the sleep mode a precision desktop multi-meter was used to measure the power consumption of the node. Figure 3.13 illustrates the effect of the supply voltage during the sleep period.

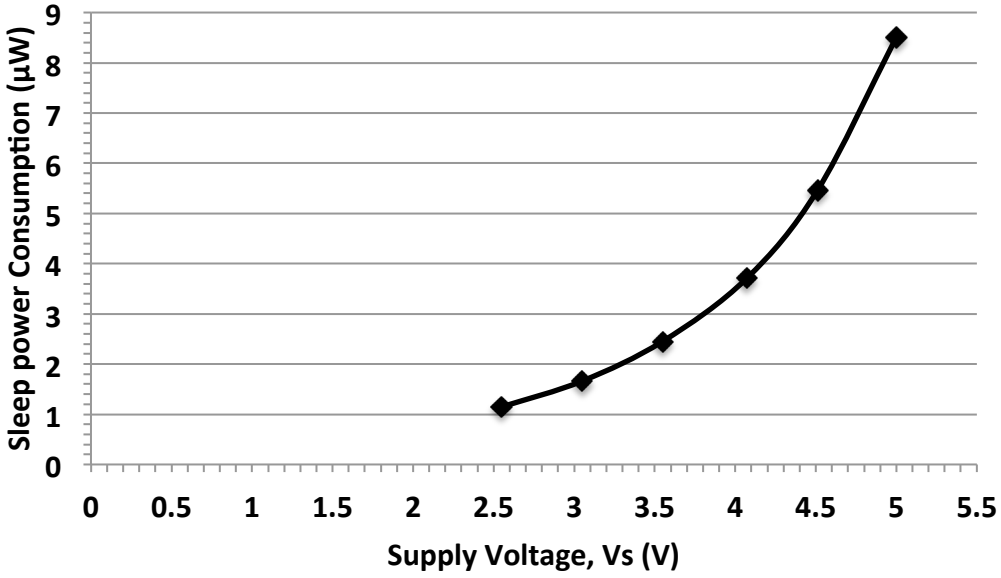

Figure 3.13 Effect of supply voltage on power consumption during sleep for version 2.0 of the node

As can be seen from this figure, power consumption of the node during the sleep period is highly dependent on the voltage of the power supply to the node. Doubling the supply voltage

from 2.5V to 5.0V will result in more than a seven times increase in the power consumption of the node. The sleep power consumption is independent from the operating frequency as the MCU is always operating at the lowest possible clock frequency (32KHz) during the deep sleep mode.

Power consumption saving through "ON" duration reduction

The duration of each of the firmware steps is dependent on: the processing power of the MCU, the settling time required for individual components, the internal communication speed between different modules and sensors, and the size of the data that is being processed and transmitted (which is also related to the number of sensors/readings). Although an increase in the processing speed of the MCU will result in a shorter processing time, it will also increase the instantaneous power consumption of the node. Similarly higher internal communication speed requires higher processing speed, which will in turn increase the instantaneous power consumption while reducing the time of that step. For the nodes to be able to operate efficiently a balance between these parameters is required. In this research, the effects of and relationships between these parameters on the performance of the node were carefully studied in order to determine efficient settings for the intended application of the nodes.

Version 2.0 of the node is used in this research in order to measure the instantaneous power consumption and duration of each step of the firmware. In order to solely focus on the effect of the firmware on power consumption, mode 3 of the node was used during the measurement of power consumption of the nodes at different firmware settings. This is due to the fact that each of the modes of the power regulation had its own quiescent power consumption and efficiency, which was independent of the power consumption of the node (affected by the firmware). The node was powered by a regulated adjustable power supply, V_S through a low

value (4Ω) resistor, R. Voltage across this resistor, V_R was measured and stored by a "Labjack U6 PRO" data acquisition device (10KHz and 20KHz sampling rate). Figure 3.14 illustrates a schematic of the test circuit used for measuring the power consumption of the nodes.

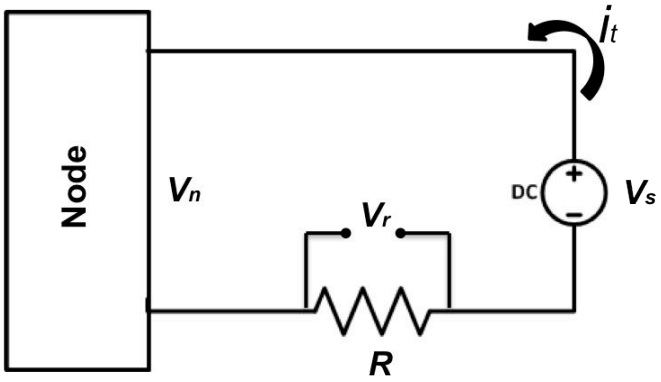

Figure 3.14 Schematic of the circuit used for power consumption measurements

The total current of the circuit i_t can then be calculated by $\frac{V_R}{R}$. The supply voltage at the node V_n can be calculated by $V_n = V_S - V_R$. The expected current of the circuit is small, consequently; it can be assumed that $V_R \ll V_S$ and therefore, $V_n \cong V_S$. Based on this assumption, the power consumption of the node P_n can be given by Equation (3.4).

$$P_n \cong \frac{V_R}{R} \times V_S \tag{3.4}$$

Equation 3.1 shows that the power consumption of the node is directly related to the supply voltage. Figure 3.15 illustrates the power consumption profile of the node (operating at $V_S = 3.5V$) during one transmission cycle.

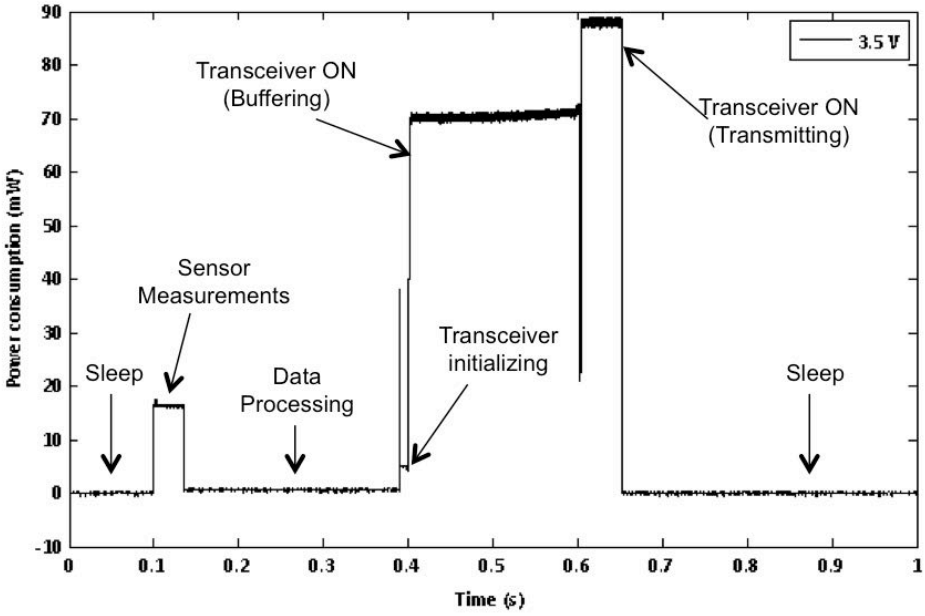

Figure 3.15 Power consumption profile of the node during one cycle (operating at 3.5V & 0.5MHz)

It can be seen in Figure 3.15 that the main steps of the firmware are clearly visible in the power consumption profile of the node. Moreover, the power consumption profile of the node helps to identify the most power hungry steps of the firmware. From this figure it can be seen that the transceiver buffering stage of the firmware consumes the most amount of energy compared to other stages of the firmware during the "ON" mode. This is greatly affected by the internal transfer speed and operational frequency of the node.

Operational frequency of the MCU greatly affects the duration of the processing related stages. An increase in this frequency will result in shorter processing times and shorter steps. However, it will also increase the instantaneous power consumption of that step. In addition, an increase in frequency will allow higher transfer speeds between the MCU and the transceiver; which consequently reduces the duration of buffering (step 16 of the firmware). The power consumption of the node was measured at six different MCU frequencies, settings of 0.5, 1, 2, 4, 8, 16 MHz. The baud rate of the node at each MCU frequency setting was set

to the maximum stable baud rate that was achievable by the node. Table 3.7 shows the maximum baud rate at each frequency settings.

Table 3.7 Internal baud rate setting at each MCU frequency step

Test group	MCU frequency MHz	Max. stable baud rate
1	0.5	2400 bps
2	1	4800 bps
3	2	9600 bps
4	4	19200 bps
5	8	38400 bps
6	16	38400 bps[6]

At each frequency mode the node power supply was varied from 2.5-5.0V in 0.5V steps in order to investigate the effect of the supply voltage on the power consumption. Figure 3.16 illustrates the effect of the voltage (V_s) on the power consumption profile of the node (MCU operating at 0.5 MHz).

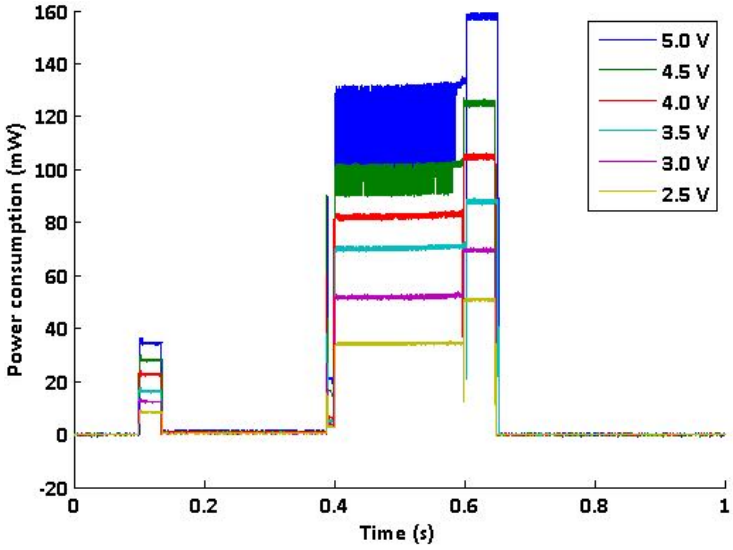

Figure 3.16 Comparison of the power consumption profile of the node at different operating voltages

[6] The maximum baud rate achievable at this frequency is limited by the maximum baud rate of the transceiver (38400 bps)

it can be seen from Figure 3.16 that the increase in supply voltage affected the power consumption of each step of the firmware differently (during the “ON” period). An increase in the supply voltage of the node mainly affects the power consumption of the stages related to the transceiver (initialisation, buffering and transmission) and the sensor measurement stage. This is mainly due to an increase in power consumption of the individual components (sensors and transceiver module). The supply voltage to the node largely affects the power consumption of the node during the sleep period. However, this is not visible from Figure 3.16 due to the big difference in the amplitude of the power consumption during “ON” and “Sleep” periods.

For the purposes of this research the total energy consumed during one transmission cycle (with an overall duration of one second) is used in order to compare the effects of different factors on the power consumption of the nodes. This is obtained by calculating the area under the power profile of the node during one cycle. Figure 3.17 illustrates the relationship between total energy consumed at each cycle and the supply voltage to the node.

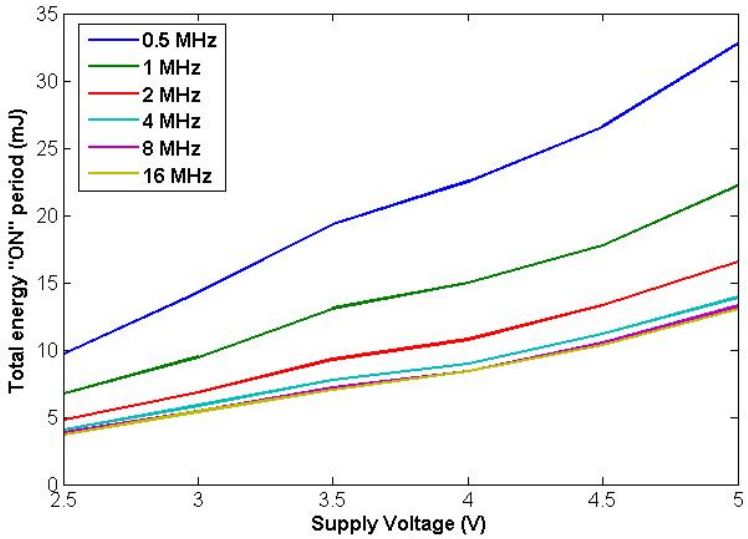

Figure 3.17 Total energy consumed during "ON" period vs. supply voltage at different operating frequencies

Figure 3.17 shows that supply voltage has a moderate effect on the total energy consumed by the node during the "ON" period. However, this effect is less significant than the effect shown in Figure 3.13 (sleep power consumption). In addition, the energy consumed by the node during the "ON" period is affected more by the supply voltage at lower operational frequencies compared to higher frequencies. This is because an increase in V_s will mainly increase the power consumption of the node during transmission and the measurement related steps of the firmware. However, the duration of these steps reduces as the operational frequency increases. Figure 3.18 illustrates the effect of the operation frequency on the power consumption profile of the node (V_s=3V).

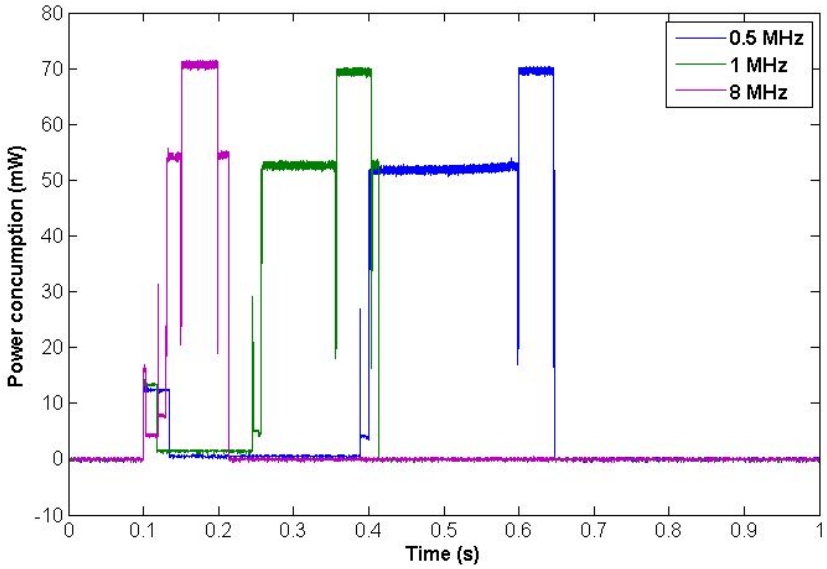

Figure 3.18 Effect of operating frequency on the power profile of the node

Figure 3.18 shows that the total "ON" period duration of the node is significantly decreased as the operating frequency increases; this is due to faster processing capabilities of the MCU and a higher internal baud rate between the MCU and the transceiver. It can also be shown from Figure 3.18 that the instantaneous power consumption of the node during each step is marginally increased. This is mainly due to greater power requirements by the MCU at a

higher processing speed. The duration of the processing related stages of the firmware (sensor measurement, data processing) are greatly affected by the operational frequency of the node. The duration of the buffering stage of the firmware (step 16) is also indirectly affected by the operating frequency of the MCU; as the processing speed increases the maximum stable baud rate achievable between the MCU and the transceiver increases, which will reduce the required buffering time. This significantly affected the overall energy consumption of the node as this stage of the firmware has the second highest amplitude of instantaneous power consumption. In contrast to other steps (during the "ON" period) of the firmware, the duration of step 17 of the firmware (transmission of data through air) is fixed (approximately 50ms). This is due to the fact that this duration is only dependent on the over the air baud rate of the transceiver module (determined by manufacturer) and the length of the transmitted message (fixed in all tests). Figure 3.19 illustrates the relationship between the MCU frequency and the duration of the "ON" period.

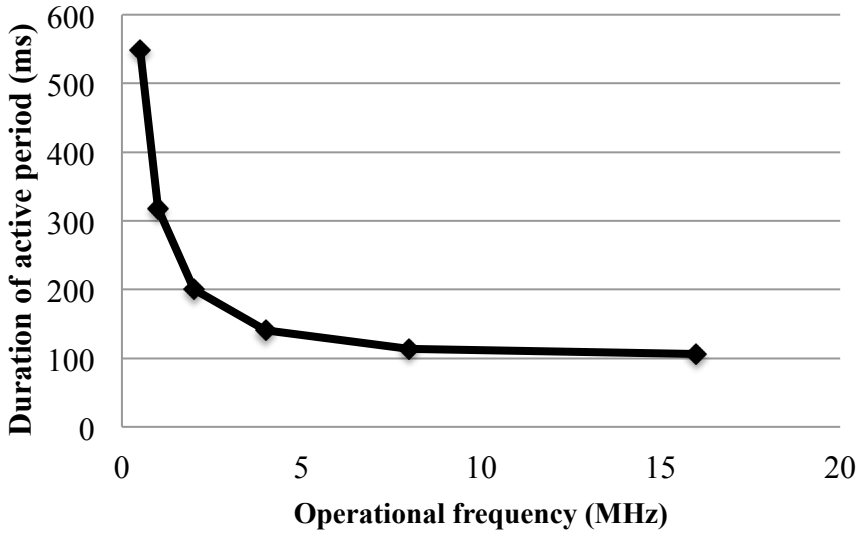

Figure 3.19 Active period duration vs. operational frequency

Figure 3.19 shows the total duration of the "ON" period is greatly affected by the operational frequency in the range of 0.5-4.0MHz. However, an increase in the MCU frequency beyond 4.0MHz has a smaller effect on the duration of the "ON" period compared to lower frequency MCU ranges. This is due to the fact that as the MCU frequency increases, the fixed length steps of the firmware become the dominant proportion of the overall active duration.

Figure 3.20 illustrates the relationship between the total energy consumed during one test cycle and the MCU frequency at various supply voltages.

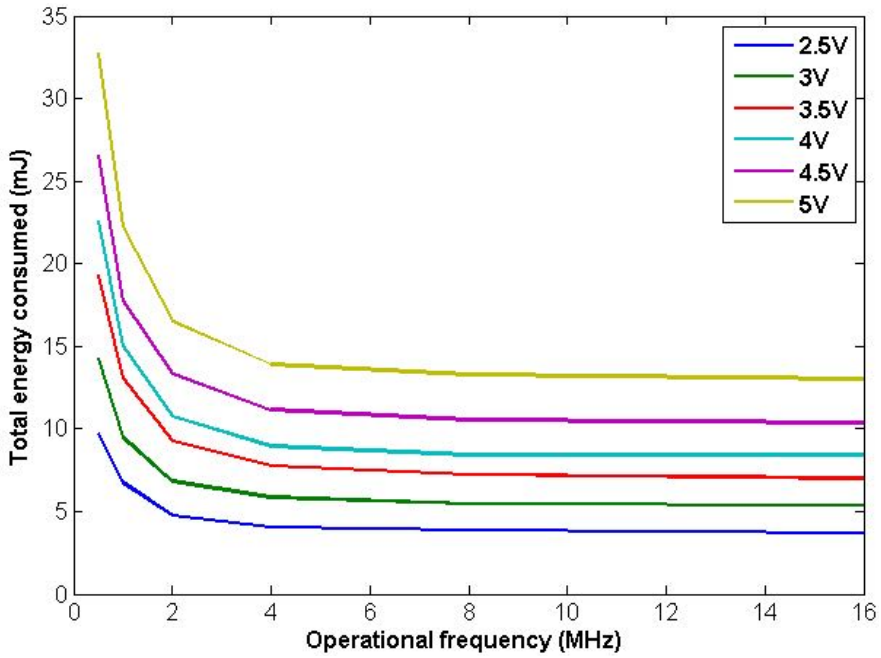

Figure 3.20 Total energy consumed during "ON" period vs. operational frequency of the node at different supply voltages.

Figure 3.20 shows that the total energy consumed by the node drops rapidly as the operational frequency of the node increases from 0.5MHz-4.0MHz. This is due to the reduction in duration of the buffering and other stages of the firmware. Energy savings from these reductions are a large percentage of the overall energy consumed and therefore have a great effect on the total energy reduction. It can also be seen from this figure that the effect of operational frequency on the total energy consumed is significantly reduced in a higher

frequency range (4-16MHz). As mentioned previously, this is due to the fact that the total energy consumed is dominated by the “fixed length” steps of the firmware (stabilisation delays and transmission), and the energy savings based on the reduction in duration of other stages are a small percentage of the total energy consumed. The energy saving is especially small from 8Mhz-16MHz due to the fact that the internal baud rate between the MCU and the transceiver is limited at 38400 bps (at 8Mhz) and cannot be increased any further at 16MHz to reduce the buffering time.

Figure 3.21 visualises the combined effect of operational frequency and supply voltage on the “ON” period energy consumption of the node. This helps to fully understand the effect of supply voltage and operational frequency and identify the most efficient firmware parameters for the node.

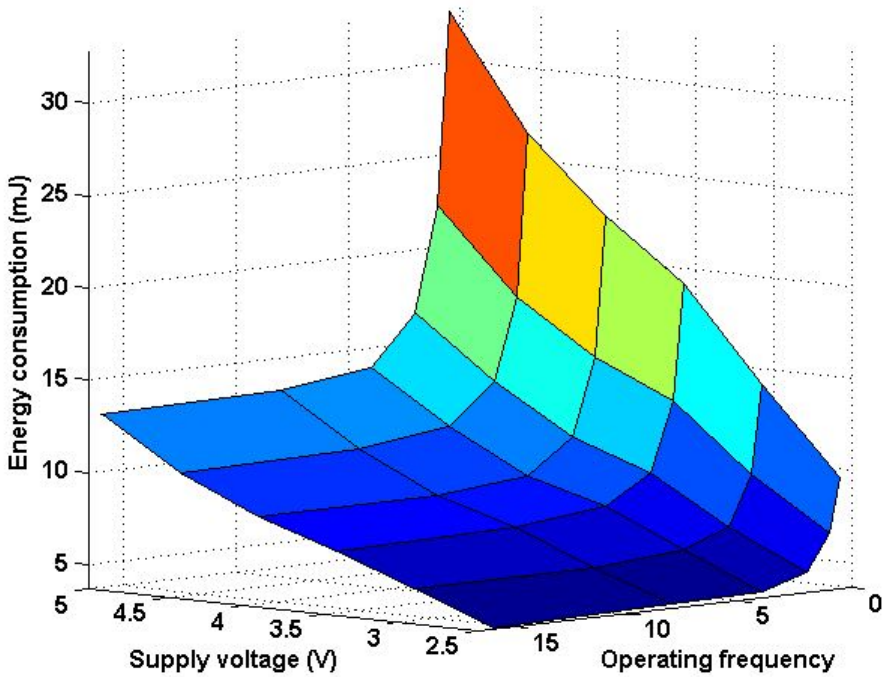

Figure 3.21 Relationship between supply voltage, operating frequency and energy consumed during the "ON" period.

Figure 3.21 shows that the active energy consumption can be reduced by lowering the supply voltage and increasing the operational frequency of the node. The node consumes approximately 3.7mJ during the active mode at a supply voltage of 2.5V and operating frequency of 16Mhz. This is significantly lower than the maximum energy consumption of the node (32.8mJ) and further shows the importance of the firmware on the overall power consumption of the node.

The power consumption of the node based on the results from these tests can be calculated for different measurement and transmission intervals. Figure 3.22 shows the average power consumption of the node at different measurement and transmission intervals (Vs=2.5 and MCU frequency at 16MHz).

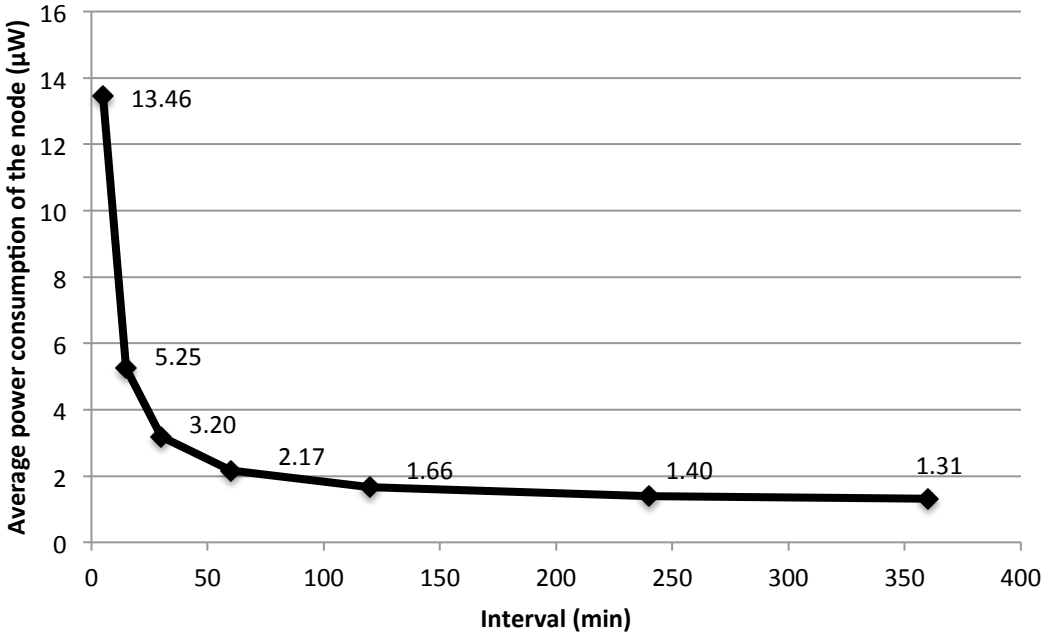

Figure 3.22 Actual average power consumption of node version 2.0 based on measurement interval

Figure 3.22 shows the achieved average power consumption of the node is significantly lower than the objective of the research (10µW for 360 minutes interval). The node on average

consumes 5.25 μW for one measurement with a transmission every 15 minutes (a common time interval used in the water industry) and consumes only 1.31 μW for a transmission and measurement at 360 minutes interval. This ultra-low power consumption allows it to theoretically operate for over 100 years on the energy stored in two AA batteries[7]. This creates opportunities for new energy harvesting methods, which were conventionally not powerful enough for WUSNs to be feasible.

3.3 Summary

In this chapter the structure of the WUSN is described and the limitations that are imposed on them due their environment (underground) were identified. The most desirable specification for a successful WUSN for pipeline monitoring, based on these limitations and their final application, is identified as:

- Ease of installation
- Low cost
- Long operational life (low power consumption)
- Non-invasive to the structure of the pipe

Low power consumption is the critical requirement of a WUSN for pipeline monitoring (Akyildiz and Stuntebeck, 2006; Akyildiz and Vuran, 2010). In order to fulfil this requirement, the hardware and software of the node has gone through four iterations. The process for designing and developing a WUSN for pipeline monitoring and the key features of each version of the node has been explained in this chapter.

The sleep mode was identified as the main consumer of the total energy amongst different modes of the node. Using XLP microchip MCUs and a flexible power management system

[7] Typical battery capacity of 2000mAh and 1.5V

significantly reduced the sleep power consumption of the node. The effect of the supply voltage and operating frequency of the node on the overall power consumption was analysed. Results from these tests further validated the importance of firmware design and operational parameters on the power consumption of the node. These results showed that an increase in the operational frequency of the MCU will result in a reduction of the ON duration and consequently a reduction in overall power consumption. The final version of the developed node (version 2.0 with the latest firmware) for a WUSN had an extremely low average power consumption of 5.25 μW for one measurement and transmission every 15 minutes and 1.31 μW for one measurement and transmission every six hours. This allows the node to have a long operational life on limited power sources or to be able to continuously operate continuously by harvesting energy from the pipe, the medium inside the pipe or the surrounding of the pipe. Ye and Soga (2012) present various methods of harvesting energy from water distribution systems.

The next chapter of this thesis describes the design and development of sensors for pipeline monitoring based on the requirements of a WUSN. Additionally, the design and development of the data management systems for the collection and processing of the data are also described in the next chapter.

4

DESIGN AND DEVELOPMENT OF NON-INTRUSIVE SENSORS FOR PIPELINE MONITORING

Contents

Overview of the chapter

This chapter reports on the design and development of a non-intrusive pressure measurement system based on Force Sensitive Resistors (FSR). The theory of the FSR-based pressure measurement system is described and analysed using both analytical and numerical techniques. Moreover, a Finite Element Analysis (FEA) of the sensor assembly is presented and compared with the analytical technique. The proposed sensing system is also compared with a commercial pressure sensor in order to validate its performance. The feasibility of using temperature sensors in pipeline monitoring is also studied by conduction of laboratory trials.

4.1 Introduction

Numerous parameters can be measured in order to monitor the structural and operational integrity of pipeline networks; such as pressure, soil water content, temperature, strain and corrosion. As mentioned previously, easy and non-intrusive installation (to the pipe) and adequate accuracy are the main characteristics of a suitable sensor for pipeline monitoring. In addition, due to the inaccessibility of the buried pipeline the sensors should have a long operational lifetime, similar to that of the pipe itself. The pipe internal pressure is one of the main parameters in pipeline monitoring, as any fault in the pipeline such as leaks, bursts or blockages will affect the internal pressure of the pipe (Misiunas, 2005). Various methods can be used to measure the internal pressure of a pipe; however, most of these methods require access to the medium inside the pipe via a valve (Misiunas, 2005; BenSaleh et al., 2013). This poses major limitations in the deployment of these pressure sensors, as they are more difficult to install and can potentially affect the structural integrity of the pipe. Pressure data can be used to provide useful information for leak detection in pipeline monitoring. An ideal pressure sensor for pipeline monitoring should have the following characteristics:

- Be capable of measuring the pipes' internal pressure fluctuation
- Be easy to install (without need for complex tools or skills) and manufacture
- Be non-intrusive to the structure of the pipe.

In addition to the above-mentioned characteristics, a suitable pressure sensor should also be able to easily integrate with existing data loggers and sensor nodes. To achieve this, the output signal from the sensor should be in one of the common forms (analogue / standard digital) of sensor signals.

Following the above-mentioned characteristics, a novel non-intrusive relative pressure sensor assembly for pipeline monitoring was designed and developed. The theory of the operation, analysis and validation of the sensor are described in the following sections of this chapter. In addition, the feasibility of temperature measurement for assessing pipeline operational parameters (for example flow rate) and environmental parameters (surrounding temperature and pipe wall temperature) is studied and analysed in this chapter.

4.2 Theory of operation of relative pressure sensor assembly

The medium inside the pipe is often pressurised in order to provide a higher hydraulic head to transport the liquid across the network and ensure no foreign ingress into the pipe, which might contaminate the liquid inside. This will cause all pipes to expand to some extent, depending on the structural properties of the pipe. Moreover, any change in flow through obstruction, failure or pressure management will cause the pipe to expand or contract. Although this expansion or contraction is normally small it can be measured and used in order to monitor the pressure changes inside the pipe. Pressurised pipes can be modelled as thin walled pressure vessels with open ends. Hoop (circumferential) stress in the pressurised pipe when modelled as a thin walled cylinder can be calculated using Equation (4.1):

$$\sigma_H = \frac{P.r_0}{t_0} \tag{4.1}$$

Where σ_H is the Hoop stress; P is the internal pressure; r_0 is the initial radius of the pipe and t_0 is the initial pipe thickness. The corresponding Hoop strain ε_H can then be calculated by Equation (4.2), where E is the Young's modulus of the pipe material.

$$\varepsilon_H = \frac{\sigma_H}{E} = \frac{P.r_0}{t_0.E} \tag{4.2}$$

Since ε_H is the change in circumference (δ_C) divided by the initial circumference (C), the change in circumference, δ_C and radius, δ_r, can be found by Equations (4.3) and (4.4).

$$\delta_C = C.\varepsilon_H = 2\pi r_0 \frac{P.r_0}{t_0.E} \tag{4.3}$$

$$\delta_r = \frac{P.r_0^2}{t_0.E} \tag{4.4}$$

From Equation (4.4) it can be shown that $\frac{r_0^2}{t_0.E}$ is constant and therefore a change in pressure causes a linear change in radius. By attaching a restraining clip around the pipe this change in radius can be converted to contact pressure which then can be measured by a force sensor (i.e. Force Sensitive Resistor, FSR). The force sensor is attached to the pipe with a high strength stainless steel clip (i.e. Jubilee clip). The pressure inside the pipe causes it to expand and induces a contact force between the pipe and the clip. Figure 4.1 shows a schematic of the sensor arrangement when attached to the pipe.

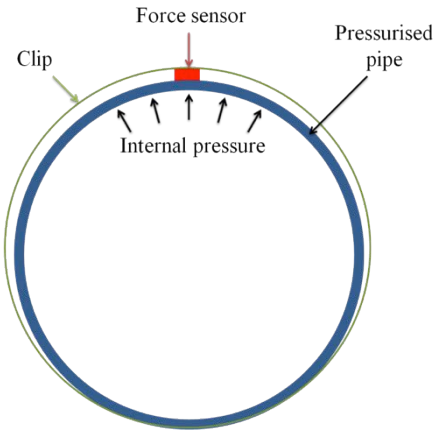

Figure 4.1 Schematic of the pressure sensor assembly

This contact pressure can be modelled as two concentric pressurised shells with open ends. Since the clip and the pipe are in contact, the radial expansion of the pipe and the clip are equal. Equations (4.5) and (4.6) can be used to calculate the contact pressure of two concentric pipes (clip and pipe).

$$\frac{(P - P_c).r_P^2}{t_P.E_P} = \frac{P_c.r_j^2}{t_j.E_j} \tag{4.5}$$

$$\mathrm{P_C} = \frac{P.r_p^2.E_j.t_j}{(r_p^2.E_j.t_j) + (r_j^2.E_p.t_p)} \tag{4.6}$$

Where P_C is the contact pressure between the pipe and the clip; r_j and r_p are the radii of the clip and the pipe; E_j and E_P are the respective material's Young's modulii of elasticity of the clip and pipe and t_j and t_p are the thickness of the clip and pipe respectively.

This contact pressure translates to a contact force on the force sensor sensor. This contact force F_C can be calculated using Equation (4.7); where A_S is the sensing area of the sensor and K is a constant between 0 and 1, which indicates the ratio of the total contact pressure that is applied to the sensor.

$$F_c = K.P_C.A_S \tag{4.7}$$

The force sensor can be installed when there is no pressure inside the pipe and an initial contact force can be applied to the sensor by tightening the clip. At this stage, the output signal of the force sensor can be measured and used as a reference for further measurements.

A variety of methods can be used to measure the pipe strain or contact force between the pipe and clip mentioned in Equation (4.7). An ideal sensor for this application should have the following characteristics:

- Large dynamic range
- High sensitivity
- High signal to noise ratio
- Minimal signal conditioning requirement
- Easy to install
- Low cost

Strain gauges are the most common type of sensor used in strain measurements. However these sensors require special installation (glued to the pipe) and complex signal conditioning circuits. This makes them not suitable for the purpose of pipeline monitoring. In order to overcome these issues other alternatives for measurement of strain or the contact force caused by expansion of the pipe were investigated. Interlink FSR® 402 was selected for the purpose

of this research based on its ease of installation, minimal signal conditioning circuitry, low cost price and larger sensing area, compared to the alternative options.

Basic FSR sensor construction can be described as two membranes that are separated by a spacer ring creating an air gap (Interlink Electronics, 2010). One of the membranes is coated with FSR ink. The other membrane has two separate electrical tracks printed on it; as the FSR sensor is compressed these tracks come in contact with the FSR ink. The FSR ink creates a short between the two tracks with a resistance based on the force applied (Interlink Electronics, 2010). Figure 4.2 illustrates the schematic of the construction of the FSR sensor.

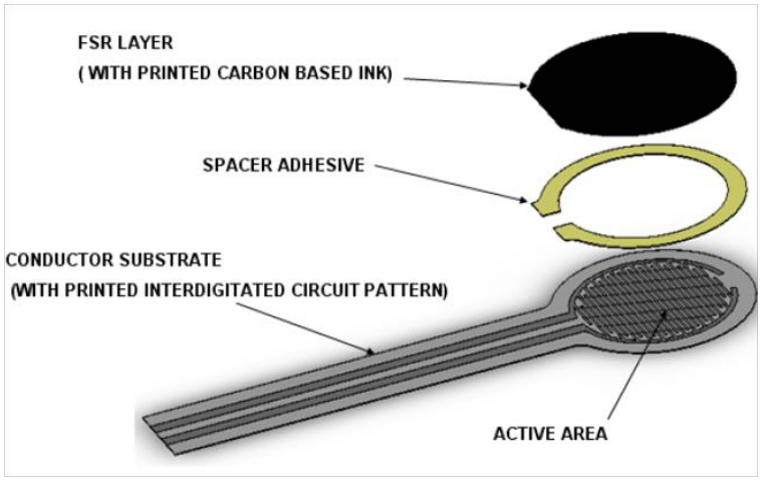

Figure 4.2 Schematic of the FSR construction (Interlink Electronics, 2010)

In order to understand the construction of the FSR, a sample sensor was delaminated to study each layer separately. The main layer, which is responsible for the sensing characteristics of the sensor, is the FSR layer, which is coated with carbon based ink (FSR ink). Surface Electron Microscopy (SEM) was used to study the structure of this layer. Figure 4.3 illustrates an SEM image of the FSR layer with 250 times magnification.

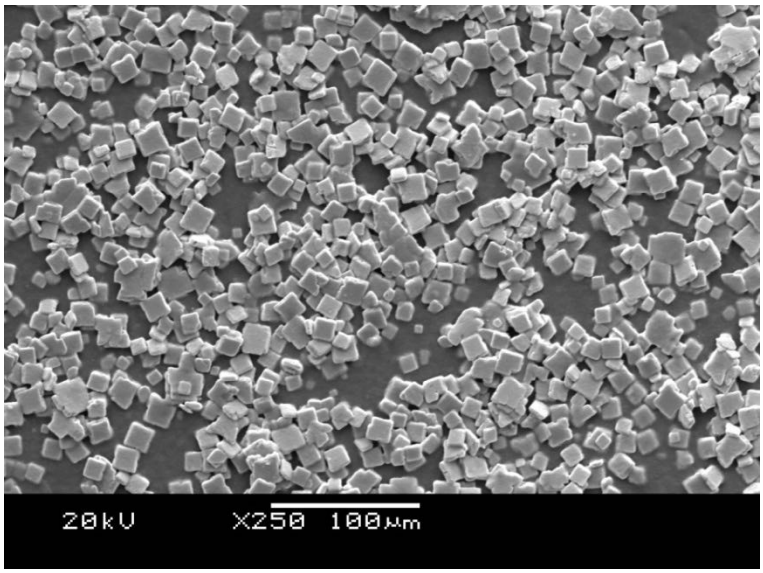

Figure 4.3 SEM image of the FSR layer

As can be seen from Figure 4.3 the surface of the FSR layer is covered by small conductive particles, which as the sensor is compressed, come into contact with the conductor comb, which in turn creates a connection between the terminals of the FSR. As the pressure on the comb's membrane increases, more of these cubes come into contact with the combs, reducing the resistance between the terminals of the FSR.

A simple voltage divider circuit can be used to convert the change in resistance of the FSR, (due to pressure change), into a change in voltage (analogue signal). This can be easily measured by the WSN node or data acquisition device. This voltage can be related to a absolute internal pressure of the pipe, by calibration with respect to a direct reference pressure sensor. However the aim of the proposed pressure sensor is to determine relative pressure changes and thus there is no need to convert the output of the sensor to absolute pressure values. Figure 4.4 illustrates the schematic of the signal conditioning circuitry used in the proposed relative FSR based pressure sensor assembly.

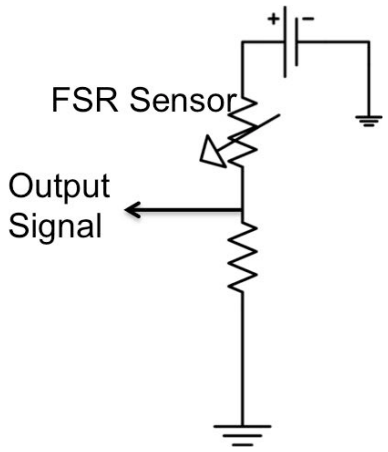

Figure 4.4 Schematic of the signal conditioning circuit used in FSR based pressure sensor assembly (Sadeghioon et al., 2014b).

This simple passive signal conditioning allows the sensor to operate at a very low power consumption (due to lack of active components). Power consumption of the FSR sensors and their signal conditioning circuit depends on the supply voltage and the overall resistance of the circuit. Moreover, continuous response nature of the FSR sensors and their passive output conditioning circuit allows the sensors to be sampled at high resolution and sampling rates (limited by the acquisition device).

4.3 Sensor assembly analysis

The working domain of the sensor assembly can be calculated from Equations (4.6) and (4.7). It is crucial to analyse this domain carefully in order to fully understand the response of the sensor assembly in different operational conditions (i.e. different pipe materials and clips) and identify the most suitable design parameters for the sensor assembly (clip material and thickness) for each specific parameter.

4.3.1 Analytical modelling of pressure sensor assembly

A MATLAB script was used to calculate the resultant force on the FSR sensor for different pipe dimensions at 1kPa of internal pressure for two different pipe materials based on Equation (4.7). The resultant force for the MDPE ($Ep = 1GPa$) and the cast iron pipe (E_j=$100GPa$) are respectively illustrated in Figure 4.5(a) and Figure 4.5(b). The dimensions and material properties of the clips are assumed to be constant ($t_j = 1mm$, $E_j = 190GPa$).

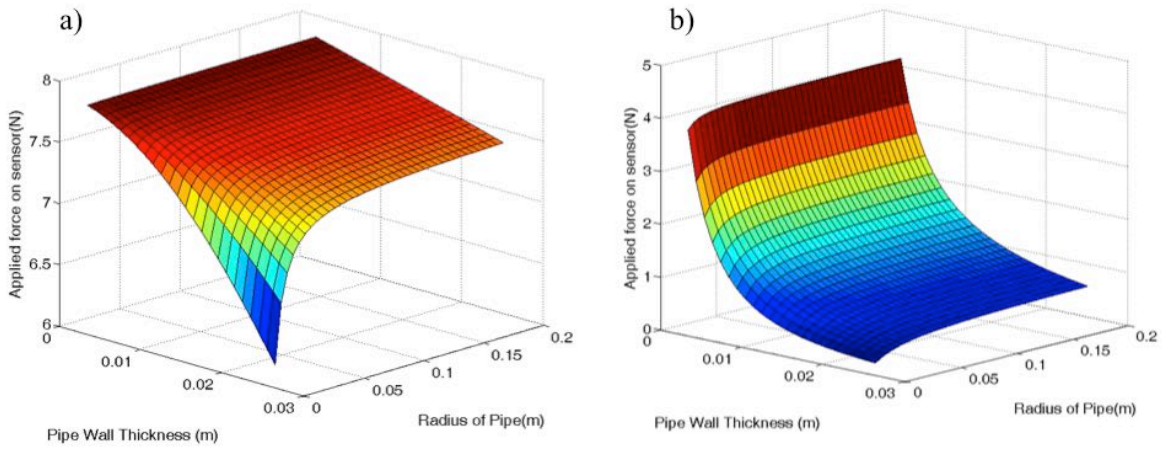

Figure 4.5 Calculated resultant forces on the FSR based on 1kPa of internal pressure for different pipe dimensions and materials a) MDPE pipe b) cast iron pipe

As was shown in Figure 4.5 the resultant force on the FSR sensor is significantly higher in the MDPE pipe than in the cast iron pipe. This is due to fact that the Young's modulus of the MDPE is lower than the cast iron pipe, which results in the plastic pipe expanding more compared to the metallic pipe and causing higher contact pressure between the pipe and the clip at each internal pressure. It can also be seen that the profile of the resultant contact force on the FSR at different pipe dimensions is different in MDPE compared to cast iron. In cast iron pipes the resultant contact force drops rapidly with the increase in the pipe wall's thickness as the pipe becomes stiffer. However an increase in the pipe wall's thickness has a

significantly smaller effect on the resultant contact force in MDPE pipes (except at very small pipe radii), compared to cast iron pipes. Additionally it can be seen from Figure 4.5 that the radius of the pipe has a bigger effect on the resultant force in MDPE pipes compared to cast iron pipes. The model illustrated in Figure 4.5, based on Equation (4.7), indicates that the proposed sensor is more suitable for indirect relative pressure measurement in plastic pipes compared to metallic pipes, if the clip material and dimensions are the same. Design parameters (dimensions and material) of the clip of a FSR based sensor assembly can be modified to overcome this limitation and increase the resultant contact force on the FSR on metallic pipes. Thickness of the clip and the Young's moduli of the material used in the clip, are the two parameters that can be modified to increase the contact force on metallic pipes. A change in the geometry of the clip is a more feasible option compared to a change of the clip material, as materials with very high Young's moduli can be significantly more expensive to source and harder to manufacture. Figure 4.6 illustrates the effect of the clip thickness on the contact force between the pipe and the clip for different pipe dimensions (cast iron pipe).

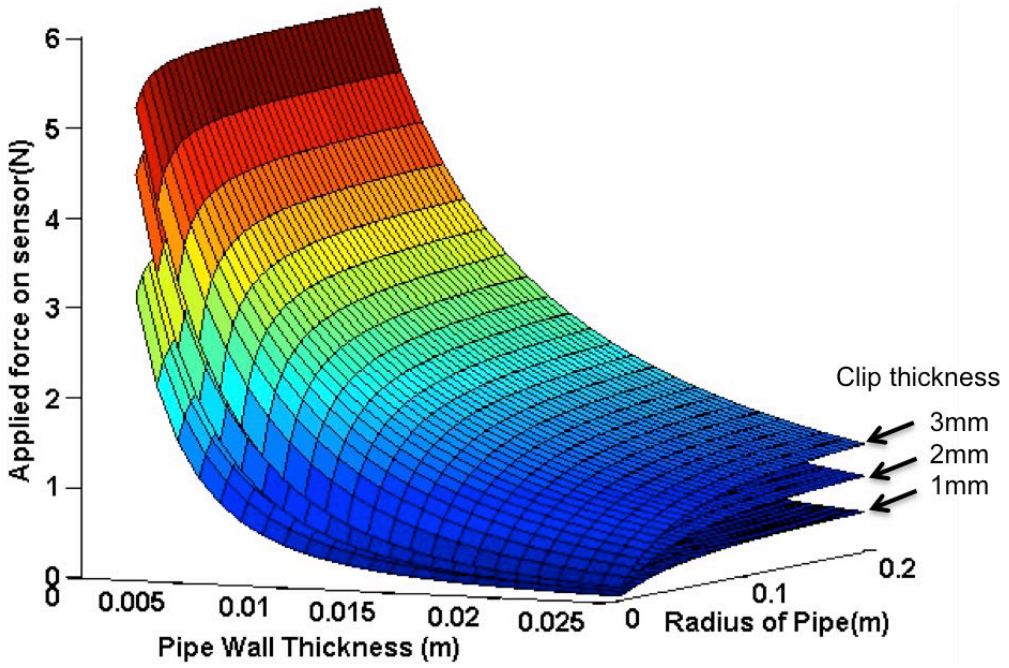

Figure 4.6 Effect of clip thickness on the contact force

As can be seen from Figure 4.6, an increase in the thickness of the clip results in an increase in the contact force between the pipe and the clip. This effect combined with an increase in the Young's modules of the clip, can be used to increase the usability of the FSR relative pressure measurements in pipes. However this relationship is not linear and follows the Equations (4.5) and (4.6).

4.3.2 Finite element analysis of the pressure assembly

A finite element analysis (FEA) is carried out on the sensor node assembly in order to further validate the response of the proposed sensing method in different conditions and the analytical model. SolidWorks simulation package is used for the purpose of finite element analysis in this research. Results from the FEA study were also compared with the results from the MATLAB script for further validation of the MATLAB model. In these studies, the width of the pipe and clip was assumed to be 200mm. This is due to inaccuracies of the FEA model in calculation of the contact pressure at the edges of the clip. Therefore the clip is

assumed to have the same width as the pipe in order to minimise the effect of errors in calculation of contact pressure at the edges of the clip on the overall average contact pressure between the pipe and the clip. The pipe and the clip are assumed to be fixed at one side (restricting lateral and axial movement of the clip in relation to pipe). This will also create an error in the calculated contact pressure at the edge of the pipe (where it is assumed to be fixed). However, this effect is assumed negligible, as the area that it affects is significantly smaller than the total area of the contact pressure. Moreover the boundary between the pipe and the clip is assumed to be "non penetrable". The contact pressure is calculated by averaging the contact pressure of all of mesh elements on the internal surface of the clip. The mesh size was set to maximum "finest" setting, which resulted in 44706 mesh elements (4 points Jacobean). These assumptions have been made to simplify the FEA study in order to reduce computational requirements of the model and create a comparable model to the model used in the MATLAB script. Figure 4.7 illustrates the FEA model and its study parameters used in this study.

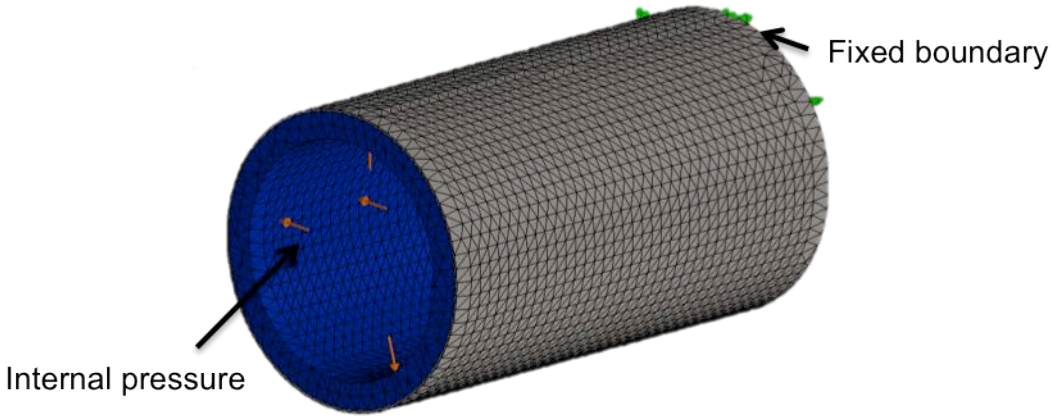

Figure 4.7 The meshed FEA model and its boundary conditions

A mesh analysis was also carried out on the FEA model to independently validate its results. During this analysis the mesh size used in the FEA model was changed from "Coarse" to "Fine" setting (20.86-5.21mm) and the results from the contact pressure at each mesh setting were recorded. A convergence in these results can be used to validate the stability of the FEA model and to identify the minimum number of mesh elements (maximum element size) required. Figure 4.8 illustrates the results from the mesh analysis (at 0.1 MPa pressure).

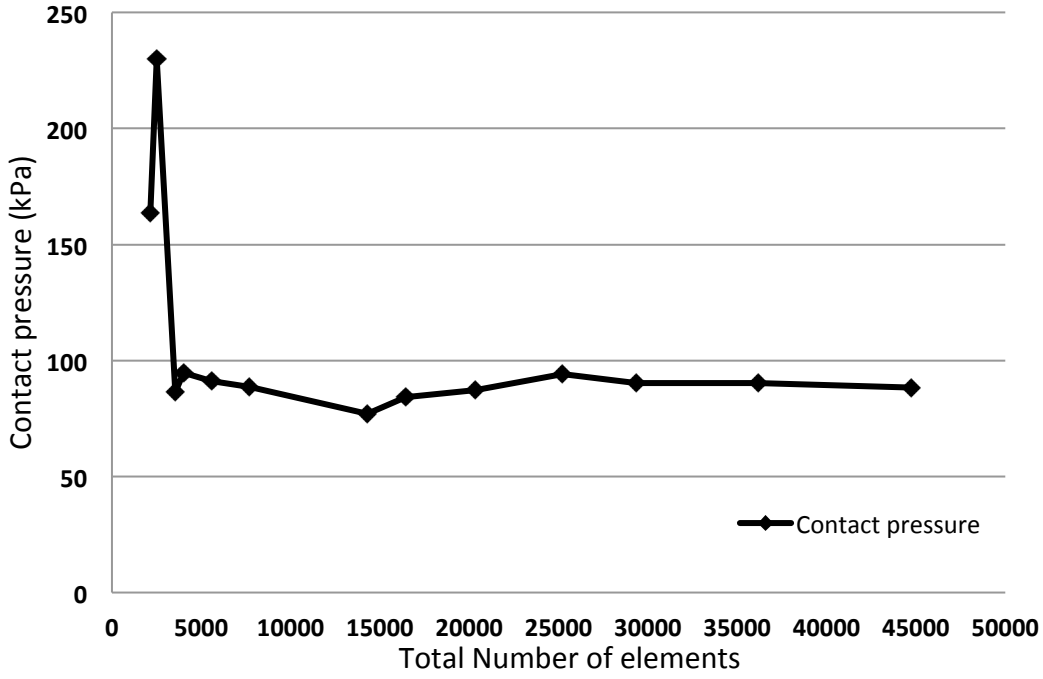

Figure 4.8 Effect of mesh size on the resultant contact pressure between the clip and the pipe.

As can be shown from Figure 4.8, results from the mesh analysis showed a good convergence in the results from the FEA analysis which validates the FEA model.

In order to further investigate the performance of the analytical analysis presented in Equation (4.6) the results from this equation were compared with the FEA analysis (using "fine" mesh settings). In this study the contact pressure was calculated for a HDPE ($Ep = 1GPa$) plastic pipe with 90mm diameter and 10mm wall thickness at pressures in the range of 0.1-1.0 MPa

(in 0.1 MPa steps). The jubilee clip is assumed to be a simple collar made from stainless steel $E_j = 100GPa$ with a thickness of 1mm. A comparison of the results from the MATLAB model and the FEA is presented in Figure 4.9.

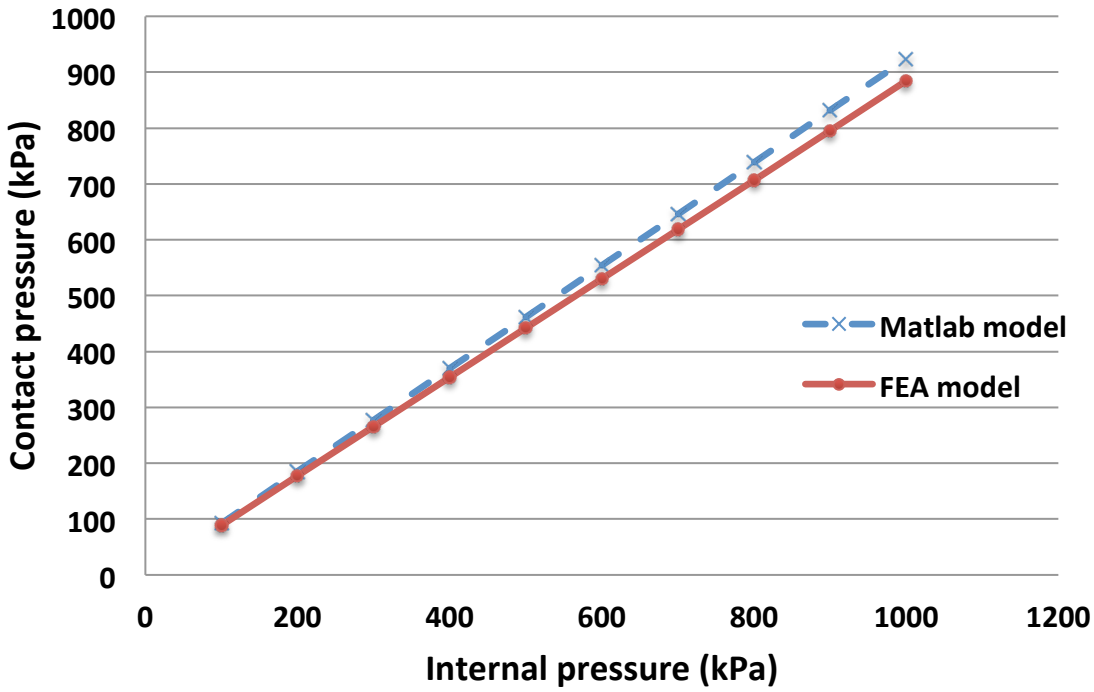

Figure 4.9 Comparison of the analytical model and FEA model

As can be shown from Figure 4.9 the MATLAB model correlates closely with the FEA model. The results of this study showed a constant error of 4.29% between the contact pressure calculated by the FEA model and Equation (4.6). This further verifies the use of Equation (4.6) for approximate calculation of the contact pressure for the FSR sensor assembly at different geometrical and operational parameters.

4.4 Comparison and validation tests and results

In order to further validate the proposed sensor assembly, its response was compared with a direct commercial pressure sensor. Both the static and dynamic responses of the FSR based

pressure sensor were tested and a correlation study was carried out on the results to validate the usability of the proposed sensor for indirect relative pressure measurements.

In these tests a section of a PVCU pipe (150mm diameter) was used to test the response of the pressure sensor assembly. Both ends of the pipe were flanged off and two inlet/outlet valves were attached to the end plates. The pipe was pressurised up to 0.4 MPa (4 bar) via one of the valves using compressed air. The commercial direct pressure sensor (Impress sensors and systems, UK) was attached to the other valve in order to measure the pressure inside the pipe. The FSR sensor assembly was attached via a stainless steel jubilee clip to the pipe. A LabJack U3 data acquisition device was used to record the data from both of the sensors at a sampling rate of 100Hz. During the tests the internal pressure of the pipe was cycled between 0-0.3 MPa (0-3 bar). Figure 4.1 illustrates a photo of the test setup.

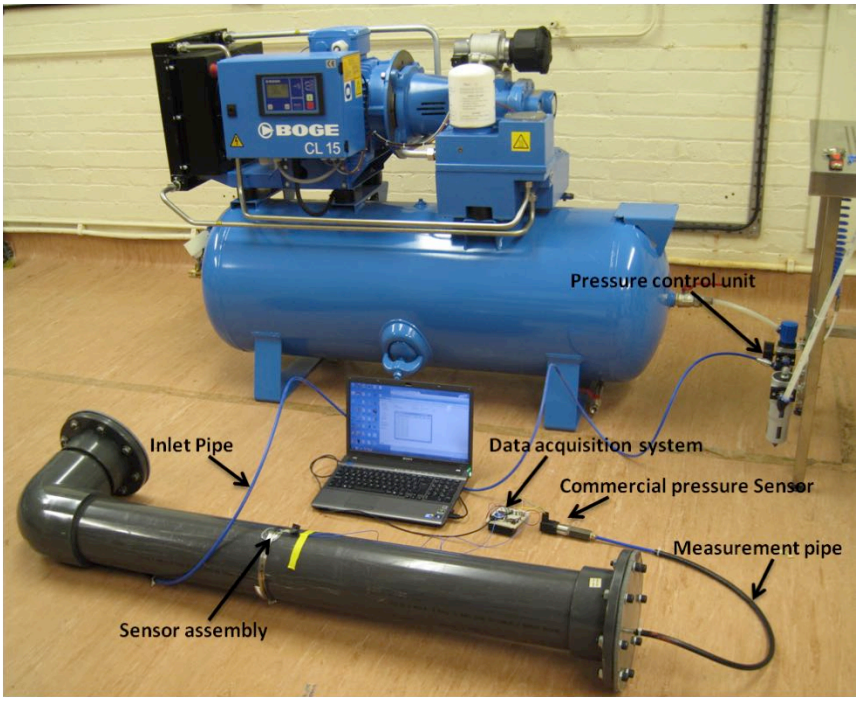

Figure 4.10 Experimental setup of comparison test between FSR based and direct pressure sensor (Sadeghioon et al., 2014b)

Focuses of the static tests were mainly on linearity and sensitivity of the FSR sensor in comparison with the direct pressure sensor. During these tests pressure in the pipe was gradually increased (via a pressure controlled valve connected to a compressor) in multiple steps in order to remove the effect of the rate of pressure change on the results. Data from both of the sensors were measured (after pressure was stabilised) at each of these steps for further analysis.

Dynamic comparison tests were carried out in order to analyse the effects of rate of pressure change on the response of the FSR based pressure sensor and investigate hysteresis, repeatability and rate dependence error of the FSR based relative pressure sensor. During these tests the pipe was pressurised by fully opening the inlet valve (pressure controlled) which was connected to a pressure controlled compressor; this resulted in rapid pressurisation of the pipe up to the predefined pressure of 0.3 MPa. When the maximum pressure was achieved the outlet valve was gradually opened to release the internal pressure of the pipe. This resulted in a lower rate of pressure change during the de-pressurisation compared to the pressurisation step. This cycle was repeated multiple times to ensure repeatability.

The output from the direct pressure sensor during static tests is plotted against the output of the FSR based pressure sensor in Figure 4.11 and a first degree polynomial was fitted to these data, to measure the linearity and performance of the FSR based pressure sensor.

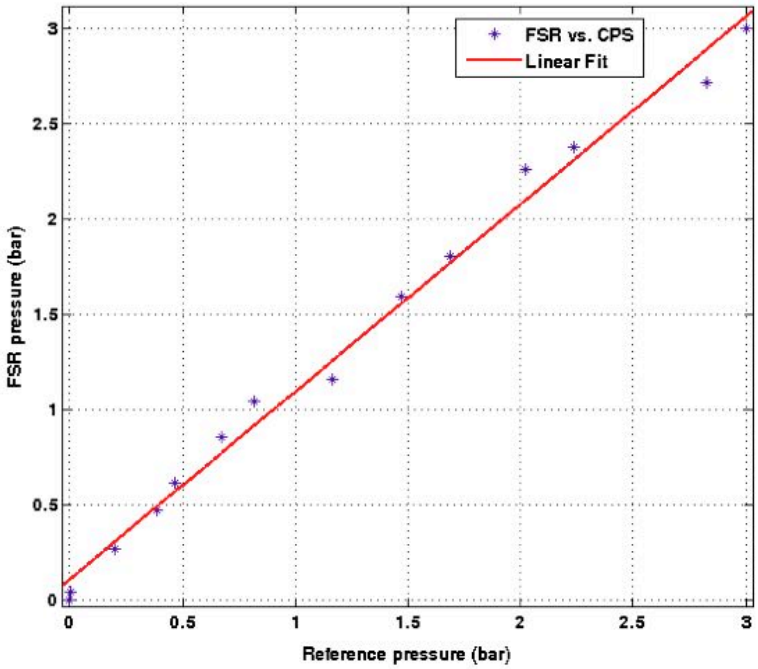

Figure 4.11 FSR based pressure sensor versus direct commercial reference pressure sensor (CPS) during static tests (Sadeghioon et al., 2014b)

It can be shown from Figure 4.11 that the FSR based pressure sensor closely correlates with the data from the reference direct pressure sensor. Additionally the R^2 value of the linear fit showed a highly acceptable linear fit (R^2=*0.9905*). The ratio of applied contact pressure, K (Equation 4.7) is estimated by calculation of the total contact pressure using Equation (4.6) and comparison of the output with the response of the FSR sensor at each step of internal pressure. These calculations showed that the ratio of applied contact pressure was stable (K=0.845±0.073) over the range of tested internal pressures. The value of K and the stability of it can be used to analyse the performance of the clip mechanism. Values of K closer to 1 indicate that the majority of the total contact pressure is applied to the sensor, which shows a better fit between the clip and pipe. This can be achieved by using an attaching mechanism with adequate tensile strength and flexibility to form a uniform contact (without gaps) between the pipe wall and the clip. In addition stability of the value of K in a pressure range

shows that the fit between the pipe and clip is stable and also can be used as means of testing the repeatability of installation.

For the dynamic tests, the output of the FSR based pressure sensor is plotted against the direct reference pressure sensor in Figure 4.12 for both stages of pressurisation and de-pressurisation.

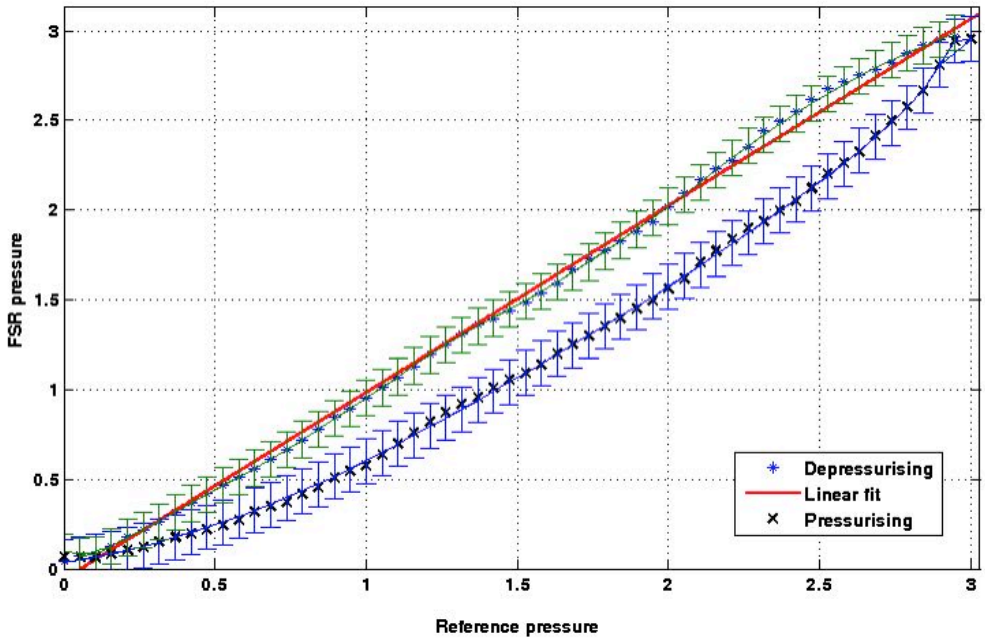

Figure 4.12 FSR pressure sensor output versus direct reference pressure sensor during dynamic tests (Sadeghioon et al., 2014b)

It can be seen from Figure 4.12 that the linearity of the FSR based pressure sensor is greatly affected by the rate of change of the internal pressure of the pipe. As can be shown from Figure 4.12 the output of the FSR sensor was less linear during the pressurisation stage compared to the de-pressurisation stage. This is due to the higher rate of pressure change during this stage. Although results from this study show that the linearity and error of the of the FSR based pressure sensor is rate dependent, this will not affect the end usability of these sensors for pipeline monitoring as the pressure changes in the systems are not usually

extremely rapid (excluding pressure transients). It can also be seen from Figure 4.12 and Figure 4.11 that the FSR sensors exhibited a total system error of approximately 10kPa when compared to the commercial pressure sensor. This error is intrinsic to the FSR sensor structure and the measurement equipment and defines the minimum detectable change in the internal pressure. It is important that this error is taken into account in applications where the sensor assembly is required to measure the absolute value of the change in the pressure. In these applications the minimum detectable change in the pressure is defined by the total system error. Therefore, the range of change in the pressure should be larger than this error in order for the measurements to be reliable.

The time domain response of the FSR based pressure sensor was also compared with the direct pressure sensor to study the correlation between these two methods. Figure 4.13 illustrates the normalised response of the FSR pressure sensor and direct reference pressure sensor during three cycles.

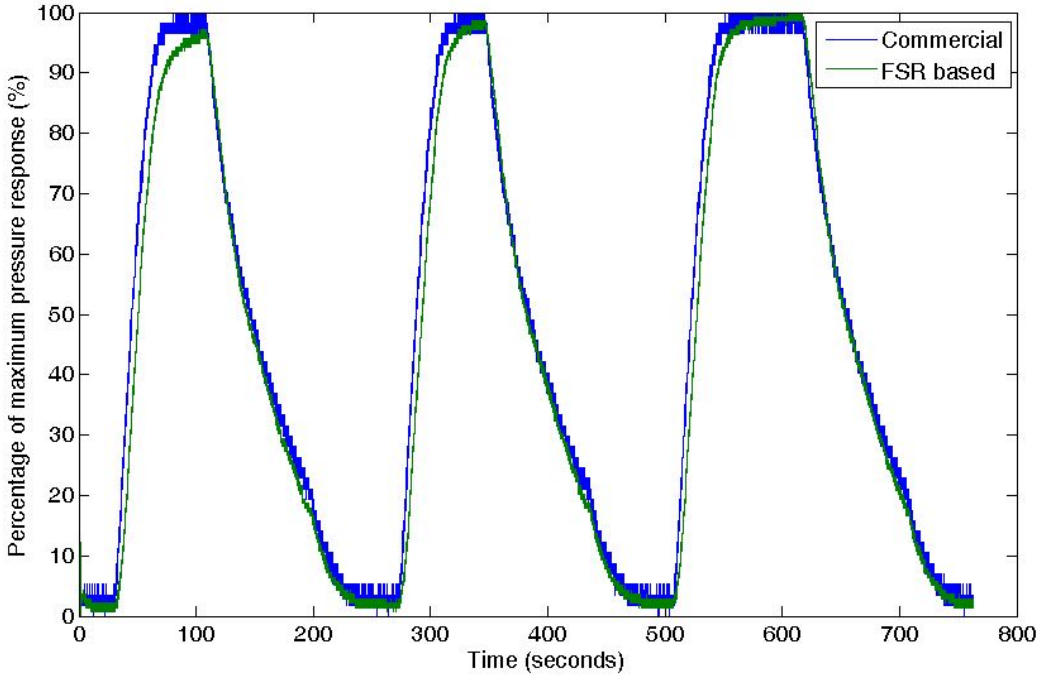

Figure 4.13 Time domain normalised response of the FSR based sensor compared with the direct reference sensor (Sadeghioon et al., 2014b)

As can be shown from Figure 4.13 the output of the FSR based sensor highly correlated with the reference direct pressure sensor. A statistical correlation study was also carried out on the data. Results from this study showed a correlation factor of 0.9928, which also indicates a high correlation between the two sensors. The rate dependency of the FSR based pressure sensor at high pressure change rates is also shown in Figure 4.13, as the FSR based sensor has a small delay to reach the maximum value compared to the reference sensor during the pressurisation stage. This is caused the rate dependence error in the output of the FSR sensor. The rate dependent error is assumed to be caused by the mechanical structure of the sensor assembly and the interaction between the pipe and the clip as the pipe expands (i.e. friction and slippage between the pipe wall and inner surface of the clip). However, further study is required to fully understand the source of this error. As was mentioned in Chapter 3, values from sensors in pipeline monitoring are commonly measured every 15 minutes. Therefore this

issue will not jeopardise the application of FSR based pressure sensors for pipeline monitoring.

The sensitivity of the FSR sensor assembly (mV/bar) is an important aspect in analysing its usability for pressure monitoring. Sensitivity of the overall assembly is dependent on the geometrical and material properties of the pipe and the clipping mechanism. The supply voltage to the voltage divider circuitry used for measuring the FSR sensor also linearly affects the over sensitivity of the sensor assembly. Therefore the sensitivity of the FSR based pressure sensor should be calculated specifically based on the operational parameters of the application in which it is been used. For the test setup, which was mentioned previously, the sensitivity of the FSR sensor was 115mV/bar (based on a supply voltage of 5V).

The resolution of the FSR based pressure assembly is dependent on the measurement equipment used for measuring the output of the FSR, as the FSR sensor itself has a continuous response to force. As an example, using a 12 bit A/D convertor with an input range of 0-5V will result in a sensitivity of approximately 0.01bar, while using a 16 bit convertor can increase the resolution to approximately 0.0007 bar for this specific example.

Although the FSR sensors are not required to be precisely calibrated during the installation, care should be should be taken when they are installed on existing pipes to avoid foreign materials (i.e. grit and lumps of soil) being trapped between the clip and the pipe. Existence of such foreign objects between the clip and the pipe can result in poor contact between the clip and pipe, which can reduce the ratio of the total contact pressure (k) that is applied on the FSR sensors. In addition, these particles can potentially cause inconsistency in the results and cause unexplained changes (i.e. when they collapse or move) in the measured relative pressure. Therefore, prior to the installation of the sensor assembly on existing pipes the

surface of the pipe should be cleaned and after the installation the sensor assembly should be inspected to confirm that no particle is trapped between the clip and the pipe, in order to ensure repeatability and consistency of the results.

The location in which the sensor assembly is installed can also affect its performance. For example, concrete walls of a chamber that the pipe passes through and connection flanges can potentially limit the expansion of the pipe at their proximity, which will affect the performance of the sensors. The level of confinement caused by these can also change as the external loadings change or with ageing (for example creep of repair clamps with time) Therefore, installation of the sensor assembly at the proximity (<200mm) of these confinements should be avoided where possible.

4.5 Temperature sensors for pipeline monitoring

Temperature is one of the key parameters of any physical system. Variations in environmental temperature can potentially affect the performance of the pipe material and joints in the long term. An example of this is an increase in the number of leaks/bursts during the cold seasons of the year in water supply pipelines (Kleiner and Rajani, 2002). Moreover, the temperature of the pipe varies based on the temperature of the medium it carries and its flow rate. A faster flow rate will reduce the residence time of the medium in the pipe and in turn reduce warming up/cooling down of the pipe (dependent on the temperature difference between the medium around the pipe and inside the pipe). The wide application of temperature sensors in various fields has led to these sensors being readily commercially available in a wide range of specifications and variations. For the purpose of this research, an analogue output temperature

sensor (LM-35) with typical accuracy of 0.5°C was used for temperature monitoring of the pipe and its surroundings.

This sensor can easily be connected to any of the versions of the node through the A/D ports. Initial laboratory trials were carried out to study the feasibility of the temperature monitoring of pipes. In these tests two temperature sensors were attached to the version 1.5 of the node to measure the temperature of the pipe wall and the environment around the main cold water supply pipe to the Mechanical/Civil Engineering building at the University of Birmingham. This pipe is easily accessible as it is passing through a maintenance room of the building. These tests were designed to investigate the functionality of the sensors and to investigate the effect of the flow rate on the temperature difference between the pipe and its surrounding. One of the temperature sensors was placed on to the pipe (under a thermal insulator layer) in order to measure the temperature of the pipe wall and the other temperature sensor was placed 200mm away from the pipe in order to measure the temperature of the room. The node was powered by four batteries (size C). Sensors were measured every 34 seconds and data were transmitted wirelessly to a laptop placed in a separate room in proximity of the node (approximately 40m away from the node), where they were time stamped and logged on a laptop. Figure 4.14 illustrates a photo of the node and temperature sensors attached to the pipe.

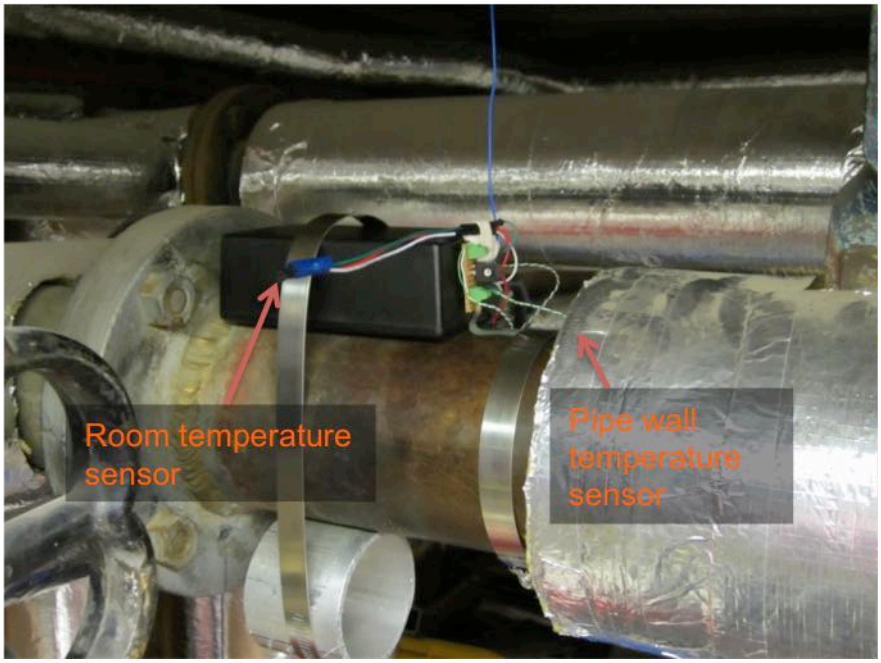

Figure 4.14 Temperature sensor trials on the cold water supply to the Mechanical/Civil engineering building at the University of Birmingham

A FSR based pressure sensor was also installed on the pipe during this test. However, due to the geometrical parameters of the pipe and lack of pressure variation in the pipe, no fluctuation in relative pressure was measured. Figure 4.15 illustrates the temperatures of the pipe and its surroundings for a duration of seven days.

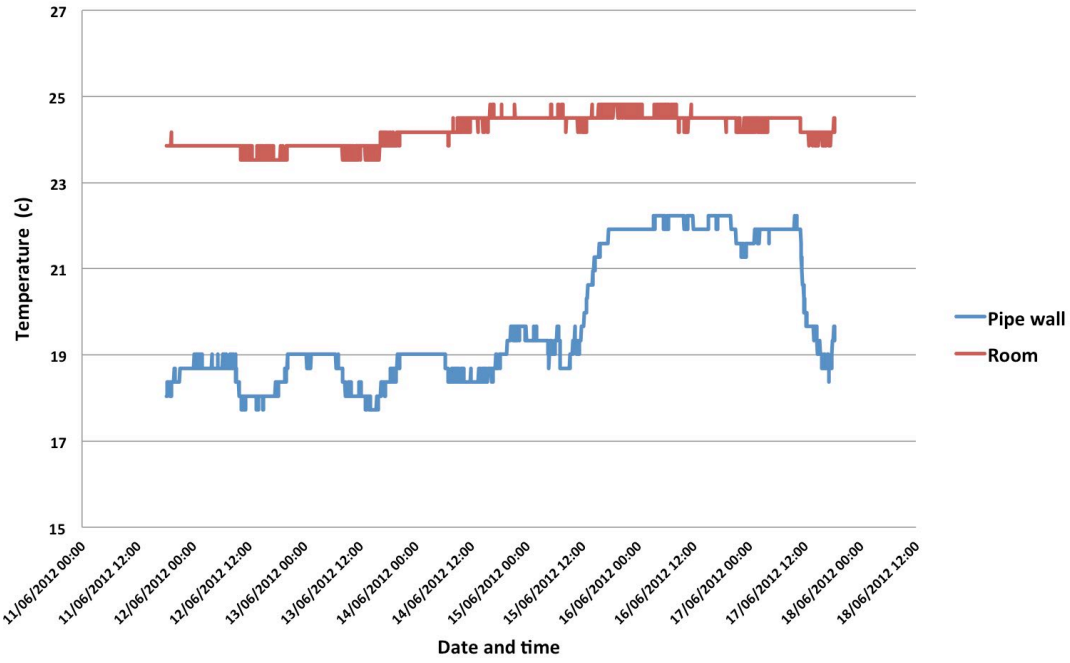

Figure 4.15 Temperature readings of water supply pipe wall and its surrounding for a period of seven days

As shown in Figure 4.15 the temperature of the pipe wall fluctuated in a cyclic pattern while the temperature of the room did not fluctuate in the same pattern and was approximately constant during each day. It can further be shown from Figure 4.15 that the temperature of the pipe was higher during the night compared to the temperature in the mornings. This is mainly due to the increase in flow during the daytime (this building is a commercial property). Reduced flow at night results in higher residence time for the water in the pipe, therefore it has a lesser cooling effect on the pipe and the pipe becomes warmer (room temperature was higher than the pipe). This effect was especially prominent during the weekends (the last two days in Figure 4.15), where the usage of water was minimal as the building was occupied by only a few people. Therefore the residence time of the water in the pipe was high, which resulted in a higher pipe wall temperature.

4.6 Summary

In this chapter sensor requirements for pipeline monitoring were identified. Non-invasive installations, ease of installation and adequate accuracy were the main requirements for sensors used in pipeline monitoring.

Pressure and temperature of the pipe were identified as the main two parameters that can be used to identify leaks or potential defects in pipes. A sudden dramatic change or a gradual change in the steady pressure of a pipeline during night (nightline pressure) can potentially be used to detect bursts or developing leaks in distribution networks. Similarly temperature can be used to detect local temperature abnormalities caused by leaks or to monitor the environment of the pipe (avoid freezing).

Common pressure sensors used for pipeline pressure monitoring require access to the medium inside the pipe via a tapping or a valve. This can potentially damage the structural integrity of the pipe and increase the cost and complexity of the installation. In this chapter a novel non-invasive relative pressure sensor based on FSR technology was designed, developed and validated. The operational domain and parameters affecting the performance of the proposed pressure sensing method were identified and analysed. Furthermore, FEA analysis was carried out to verify the developed analytical model (Equation (4.6)). Results from this study showed a high correlation between the FEA model and the analytical model. A series of tests were also carried out to compare the performance of the FSR based pressure sensor assembly. These tests showed a high linearity in the response of the FSR based pressure sensor in the static test. In the dynamic test the results from the FSR based pressure sensors closely correlated with the reference direct pressure sensor. The FSR sensor exhibited rate dependant error when it was subjected to rapid pressure changes. However this does not affect the final

intended application of these sensors (i.e. daily pressure change monitoring). The feasibility of the temperature sensors for pipeline monitoring by measuring the pipe wall temperature and surrounding environment of the pipe was studied and analysed in this chapter. Results from laboratory trials showed that the difference in temperature between the pipe and its surroundings can be used as an indication of flow in the pipe. This in conjunction with relative pressure measurements can be potentially used to detect faults and abnormalities in the distribution network.

The next chapter of this thesis describes the application of the sensors developed in this chapter for detecting leaks in pipes. The leak/burst detection capabilities of the FSR based pressure sensor were studied in the laboratory and in field trials. Additionally, the potential of temperature data combined with pressure data to detect abnormal pressure changes from normal daily variations is demonstrated in the next chapter.

5

PIPELINE FAILURE DETECTION USING WUSN

Contents

Overview of the chapter

The focus of this chapter is on the use of the FSR relative pressure sensor (and temperature sensors) for pressure monitoring and burst detection in pipelines. During the research described in this chapter burst detection capabilities of the FSR based relative pressure sensor were studied via laboratory tests and extended field trials. Nodes designed in this research were also deployed during these trials in order to study their performance. The experimental setup and methodology used in both of these tests are described in detail in this chapter. The long-term field trials are also described and the performance of the node and the FSR based pressure sensor during these trials are analysed and described in this chapter.

5.1 Introduction

In order for the WUSN developed in this research to be feasible for use in pipeline monitoring, its sensors should be capable of detecting leaks/bursts in the pipeline. Additionally, a successful implementation of a WUSN should also have the capability to localise the detected defect to facilitate maintenance or repairs.

During this research, capabilities of the sensors and nodes developed were tested and analysed in laboratory and field trials. A laboratory based test setup was designed and developed in order to test the capabilities of the FSR based relative pressure sensor for burst detection and localisation. Furthermore, nodes developed during this research (version 2.0) were connected to a FSR based pressure sensor assembly and temperature sensor and were deployed in an industrial leak test facility, where they monitored the pressure and temperature for a period of approximately 6 months. Both of the mentioned tests (laboratory and field trials) are discussed in detail in the following sections of this chapter.

5.2 Laboratory trials

The pressure sensing capabilities of the FSR sensors were validated separately via tests described in Chapter 4 of this thesis. However, in order for them to be suitable for pipeline motioning, their leak detection and localisation were also required to be tested and analysed under controlled laboratory conditions.

5.2.1 Experimental setup

As a part of this research a laboratory based test bed was designed and developed to simulate leaks/bursts in pipes. This test rig was a 10m long U shaped water pipe made from five 2m long, 40mm diameter PVC pipes with 1.9mm wall thickness (Figure 5.1a). Water was circulated in the pipe by an electric pump connected to the pipe section via a common hosepipe. Water was also discharged from the pipe section to a storage bin via a hosepipe; from here it was pumped back into the system. The pump used for these tests was capable of producing up to 3 bar of pressure. A hole with a diameter of 10mm was placed in the middle of the U section of the system in order to act as a simulated sudden leak/burst. This hole was plugged with a rubber insert, which would pop out after a random amount of time, resulting in a simulated leak/burst in the system (Figure 5.1b). The experimental setup used for the leak detection tests and its main components are shown in Figure 5.1a and Figure 5.1b.

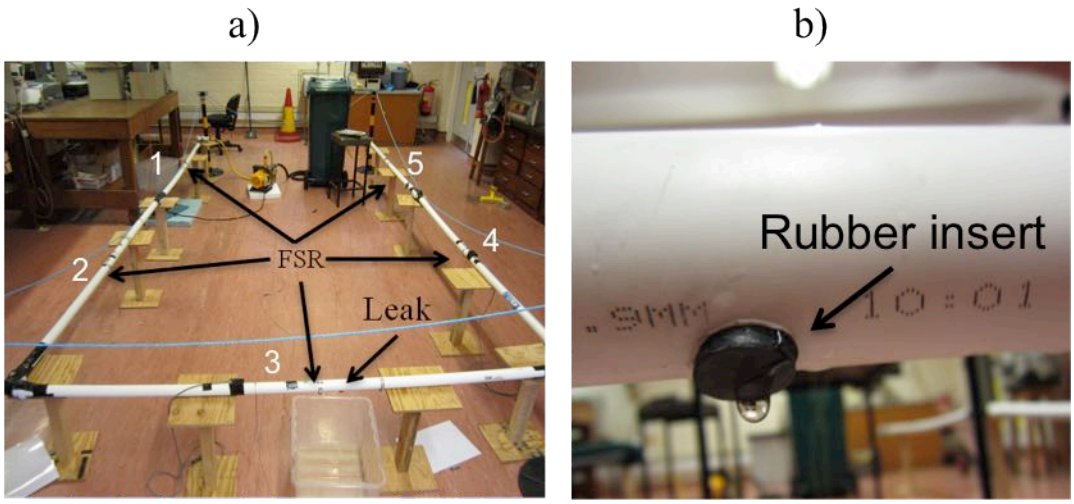

Figure 5.1 a) Experimental setup used for laboratory leak tests and its components b) Close-up of the leak with rubber insert.

As can be shown in Figure 5.1a five FSR sensors were also installed on the pipe at 1, 3, 5, 7 and 9 metres along the pipe. Sensors 1, 2 and 3 were placed upstream of the leak and sensors 4 and 5 were placed downstream of the leak. This helped to analyse the effect of the location

of the leak on the output of the FSR based pressure sensors, which potentially could be used to locate the leak. A stainless steel Jubilee clip with a thickness of 2mm was used to fix the FSR sensors on the pipe. The FSR sensors were connected to a voltage divider circuitry with a source voltage of 5V and a fixed reference resistance of 300Ω. A Labjack data acquisition device (Labjack U3) was used to record the output signal from the voltage divider circuit at a sampling rate of 1kHz. The high sampling rate in these tests was used to identify the capabilities of the FSR sensor at a wide range of sampling rates. The WUSN nodes developed in this research were not used during these tests in order to isolate the leak detection capabilities of the FSR based relative pressure sensors from the performance characteristics of the node.

5.2.2 Results and discussions

Leak detection tests were repeated multiple times (minimum 5 repeats) in order to ensure repeatability and reliability of the results. Data from all of the sensors attached to the pipe were successfully measured during the tests. As mentioned previously in Chapter 4, the proposed leak detection method is intended for relative pressure measurement; therefore, measurements taken from the FSR based sensors are normalised based on their maximum stabilised pressure and baseline (zero pressure) values. The relative nature of the readings removes the need for precise calibration of the sensor, which in turn will result in easier and lower cost installation. However, a rough calibration at the time of installation by means of adjusting the clips' initial tension is required to ensure that the outputs of the sensors are in the range of the analog to digital converter (normally 0-5V). Figure 5.2 illustrates an example of the normalised output of the sensors during a leak test (more examples are presented in Appendix B).

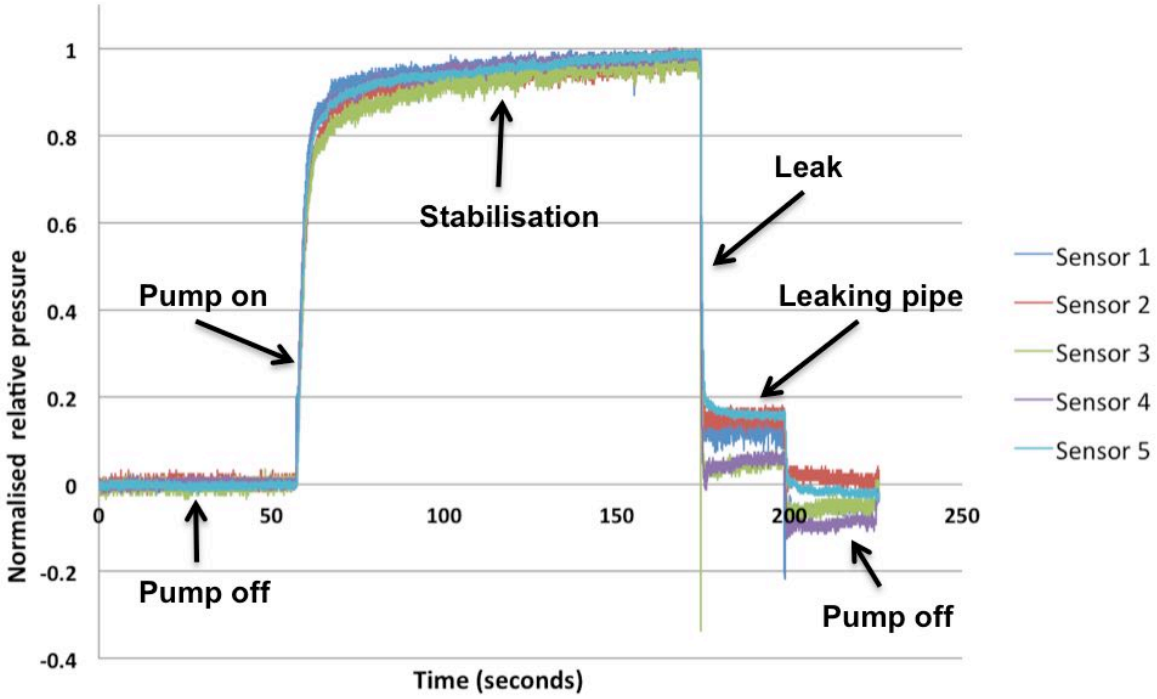

Figure 5.2 Example of the normalised relative pressure output from the five sensors during a leak test

Four main stages of the experiment (pump on, stabilisation, leak/burst and pump off) are clearly visible from the output of the sensors. It can be clearly seen in Figure 5.2 that the pressure increased in the pipes from the baseline as the pump was started. The burst/leak event is also clearly visible in the data, as the relative pressure suddenly dropped as the rubber insert was forced out of the hole due to pressure. Finally, the drop in pressure due to switching off the pump is shown in the output of the sensors. Figure 5.2 clearly shows that the simulated burst/leak can be detected from the output of the sensor. The location of the simulated leak is not clearly determinable from Figure 5.2 as all sensors seem to respond similarly to the leak. However, further analysis of the data at the time of the leak showed that sensors 1, 2 and 3, which are upstream of the leak, have a different pressure profile compared to sensors 4 and 5 during the leak incident. Figure 5.3 shows a close up of the output of the sensors during the leak event (taken from Figure 5.2).

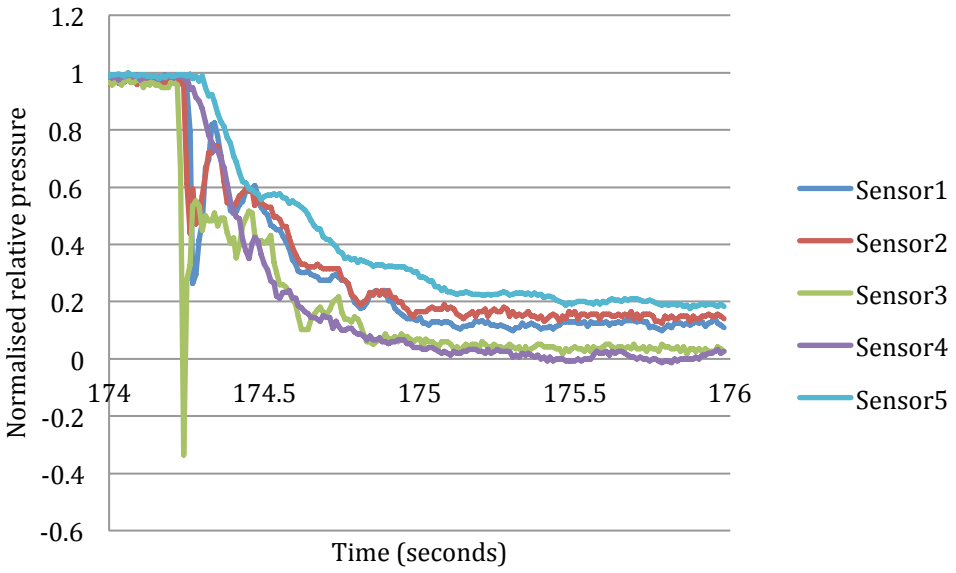

Figure 5.3 The close up of the normalised pressure at the time of leak taken from Figure 5.2.

As can be seen from Figure 5.3 sensors 4 and 5 show a more gradual drop in the relative pressure compared to sensors 1, 2 and 3; which show a rapid drop in relative pressure as the rubber insert is forced out of the hole. This difference can be used to locate the zone in which leak had happened (i.e. between sensors 3 and 4). The first derivative of the relative pressure output of the sensors can be used to compare rate of change in the output of the sensors. Figure 5.4 illustrates the average of minimum value of the first derivative of the normalised relative pressure for the sensors 1-5 based on five repetitions (Appendix B). Error bars in Figure 5.4 are based on the standard deviation of the results from these repetitions.

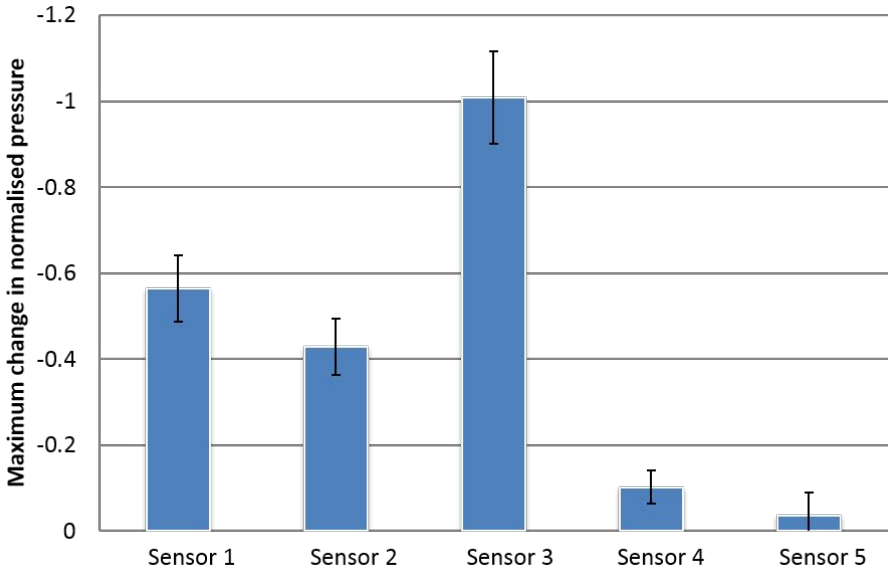

Figure 5.4 Maximum rate of change in normalised pressure

As can be seen from Figure 5.4 the rate of pressure drop is higher in sensors upstream of the leak (sensors 1, 2 and 3) compared with sensors downstream of the leak (sensors 4 and 5). Moreover it can be seen from Figure 5.4 that the rate of change in sensor 3 (closest sensor to the leak) is higher than the rate of change in the other sensors. This is to be expected as sensor 3 was placed very close to the burst and is affected by the localised pressure drop in addition to the systematic pressure drop caused by the burst. However from Figure 5.4 there appears to be no trend between the amplitude of the pressure drop and distance for the sensors downstream of the leak. However time analysis of the data during the leak event showed that the order in which the sensors respond to the burst depends on their distance from the leak. Figure 5.5 shows the normalised relative pressure output of the sensors at the time of the leak and the delay of each sensor responding to the leak based on their location.

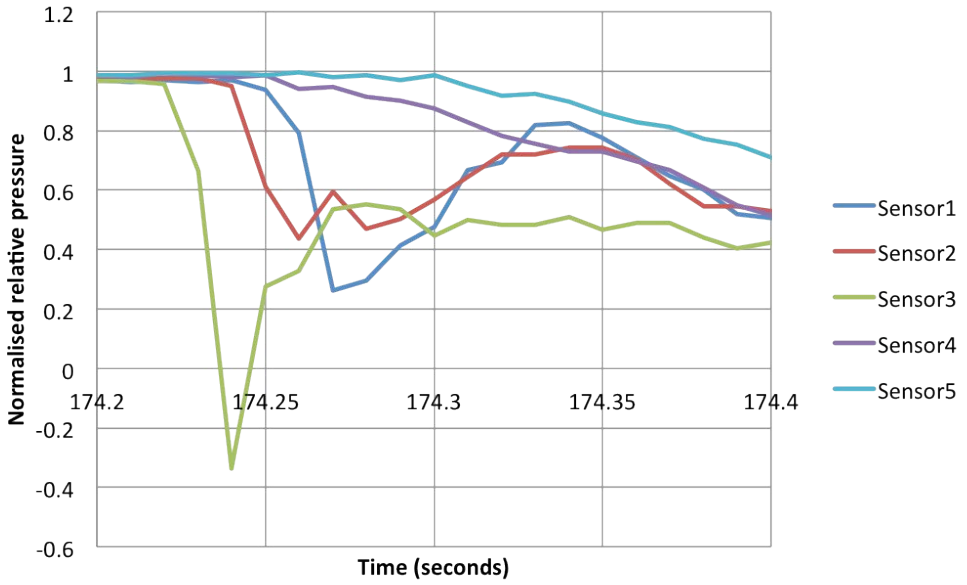

Figure 5.5 Delay of the output of the sensors depending of their location

As can be seen from Figure 5.5 as expected sensor 3 (closest to the leak) responded to the leak first followed by sensor 2 (≈20ms delay) and sensor 1 (≈30ms delay). Sensors 4 and 5 had a much slower response to the leak at ≈50ms delay and ≈90ms delay respectively. This shows that it is feasible to detect the location of the leak based on response time difference between the sensors where a high sampling rate (≥100Hz) is possible. These tests were repeated multiple times (see Appendix B) to investigate the repeatability of the results. All of the repeat tests showed similar trends to ones presented in Figure 5.4 and Figure 5.5. In addition, Li (2014) carried out these tests on a similar test rig and obtained similar results to ones presented in this thesis. A hybrid sampling rate can be used where a high sampling rate is not feasible. In this method an interrupt is configured to react to the drop in the output of the sensors and activate a higher sampling rate. Based on the reaction time of the interrupt an initial section of the pressure drop profile will be lost. However this partial pressure drop profile can still be used to detect difference between the response of the sensors based on their location.

5.3 Field trials

The performance and capabilities of the nodes and sensors developed in this research were evaluated by deploying them in a near real life condition on an industrial leak test training facility. Version 2.0 of the node, FSR based relative pressure sensors and temperature sensors were deployed in the field trials. These field trials were also used to study other parameters affecting the overall reliability and performance of the systems in real life conditions, such as corrosion, ease of installation and water proofing. The methodology, experimental setup, results and discussion regarding these tests are described in the following sections of this chapter.

5.3.1 Test facility

A water industry[1] leak test and training facility was used for the purpose of field trials in this research. Some of the main advantages of this facility were its live connection to the mains water supply network, availability of multiple pipe dimensions and materials, and facility to control the pressure and create known leaks in the system. Figure 5.6 shows an aerial photograph of the test facility used in this research, with the pipe and sensor nodes locations noted.

[1] Severn Trent Water, Lake House test facility

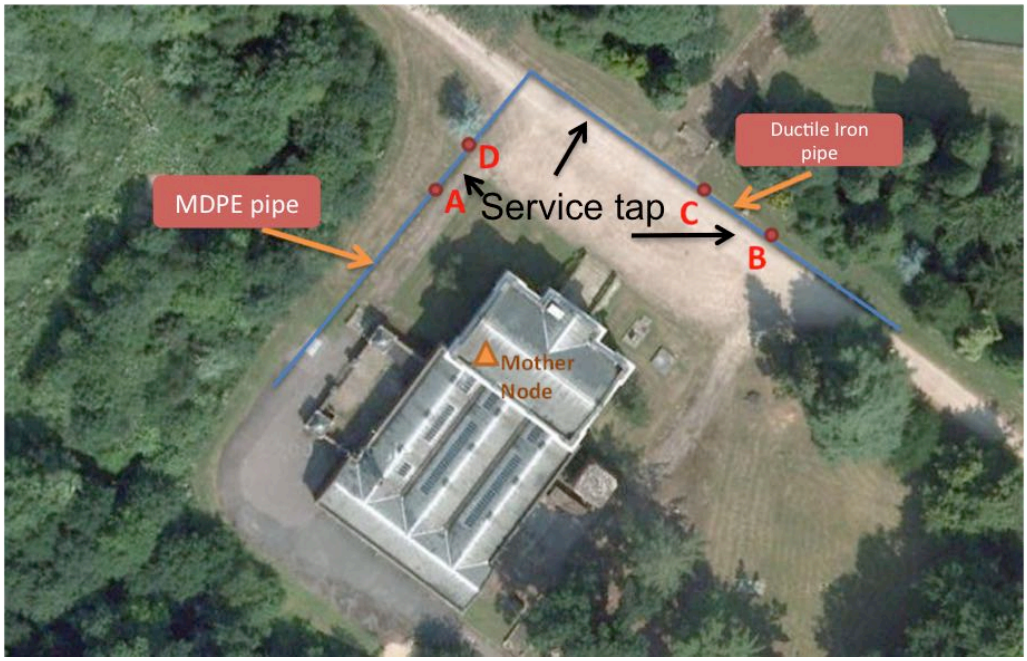

Figure 5.6 Aerial photograph[1] of the test facility with the location of the pipes and sensor nodes shown

As can be seen in Figure 5.6 a section of MDPE pipe with a diameter of 90mm and a section of ductile iron pipe with a diameter of 100mm were selected for these trials. The pressure of these pipes could be regulated by a pressure release valve (PRV). The developed WUSN nodes (version 2.0) and their associated sensors were installed at four locations on the pipes (points A to D in Figure 5.6). The mother node and logging equipment were placed in the building close to the nodes. Operating service taps, which are noted in Figure 5.6, could be used to simulate leaks in the system. This facility is mainly used for valve training and these service taps are used during this training. The relevance of this will become apparent when the data is presented later in this chapter.

As mentioned earlier, the pipe network in this facility is connected to the mains water supply network. This was beneficial for the purposes of this research, as daily pressure variation due

[1] Google earth, Google, USA

to variation in demand by the commercial and residential properties nearby were present on the system, which made these trials closer to a real life application.

5.3.2 Nodes setup and installation

Version 2.0 of the node was used for the purpose of these trials. Two temperature sensors[1] (same as ones used in tests described in Chapter 4) and one FSR based relative pressure sensor were connected to each node. One of the temperature sensors was placed in contact with the pipe (with a plastic wire tie) to measure the pipe wall temperature, while the other temperature sensor was placed approximately 30cm away from the pipe in order to measure the temperature of the soil surrounding the pipe. For both the plastic and metallic pipes the FSR sensors were attached to the pipe via a stainless steel jubilee clip. Figure 5.7 shows a photograph of one node, C, being installed on the metallic pipe.

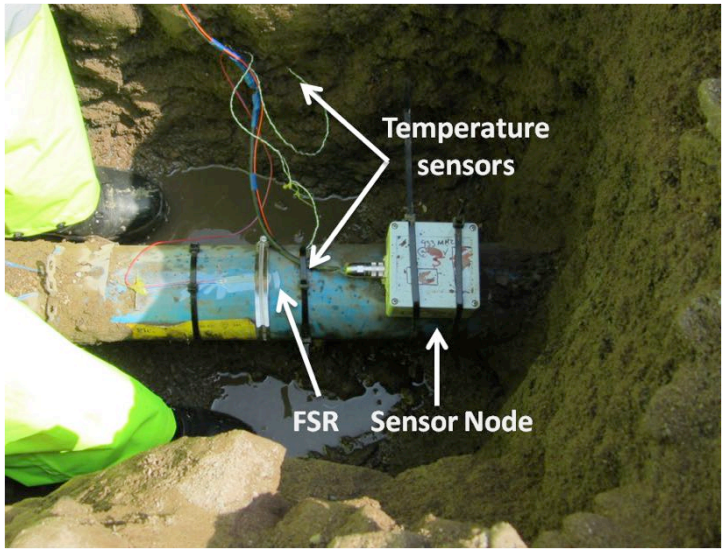

Figure 5.7 Installation of node C and its sensors on the metallic pipe

[1] LM35, analog temperature sensors

The holes required for accessing the pipes and installing the sensors and nodes were created by a dry vacuum excavation technique using a specialist company. The non-invasive nature of this technique ensured that the existing pipes and tree roots were not damaged during the installation. Figure 5.8 shows the vacuum excavation process.

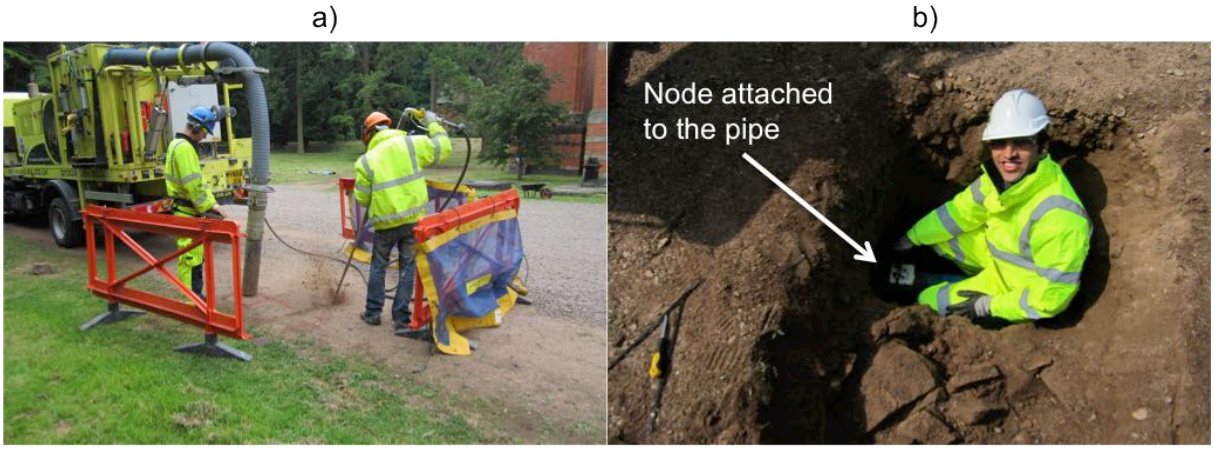

Figure 5.8 a) Vacuum excavation technique used during the field trials, b) Installations

The nodes were installed in two different variations. Three of the nodes (nodes A, B and D) were placed above the ground with an umbilical cord connecting them to their sensors attached to the pipe under the ground; while one of the nodes (node C) was attached to the pipe via plastic wire ties. This enabled the performance of the sensors to be separately analysed and monitored from the performance of the nodes. Additionally, placing some of the nodes above ground ensured that a potential failure of the nodes would not result in total failure of the experiment; as the nodes can be replaced, repaired or modified when required. Placing one of the nodes in the ground enabled the performance of the nodes in an environment that would be closer to their final application to be studied. Batteries could not be buried with the nodes due to health and safety and environmental considerations such as danger of build up of hydrogen gas in the battery enclosure and potential harm to the environment in case of leakage of battery chemicals in the ground. Therefore, a lithium

polymer battery was placed above ground (in an enclosure) to power each node. A 80mm x 100mm, 1W solar panel with a charging circuitry was used to charge the batteries. Figure 5.9 shows a schematic of the above ground and underground sensor node arrangements and a photograph of the node installed in the field.

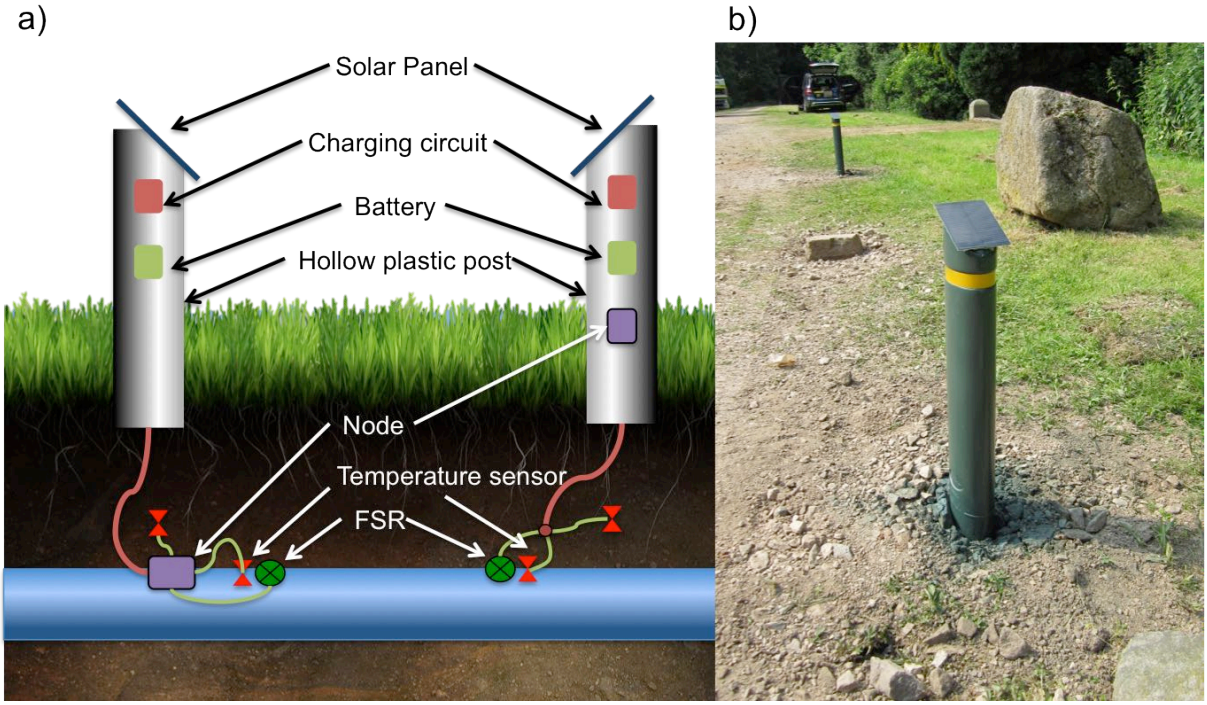

Figure 5.9 a) Schematic of the over ground and underground node arrangements, b) Installed node in the field

Each node was programmed to measure all of the sensors attached to it and the voltage of its battery every 1,027 seconds (approximately 17 minutes) and transmit them wirelessly to the mother node. Each message from the nodes contained their node ID (same as location ID) and data ID (message counter), followed by the four measured parameters (comma separated).

Data received from the nodes at the mother node were time stamped and stored locally on the hard drive of the laptop connected to the mother node. The laptop was also connected to the Internet via a 3G mobile broadband connection. This allowed the laptop to be remotely accessed via the Internet (TeamViewer) and also backup the data in the Cloud (Dropbox).

Due to the transmission range issues caused by poor transmission through soil, node C could not directly communicate with the mother node. Therefore, a commercially available (Logomatic SD) local SD card data logger was attached to an RF transceiver and was placed inside the battery enclosure of node C to record the data from this node. Figure 5.10 shows the setup for the mother node.

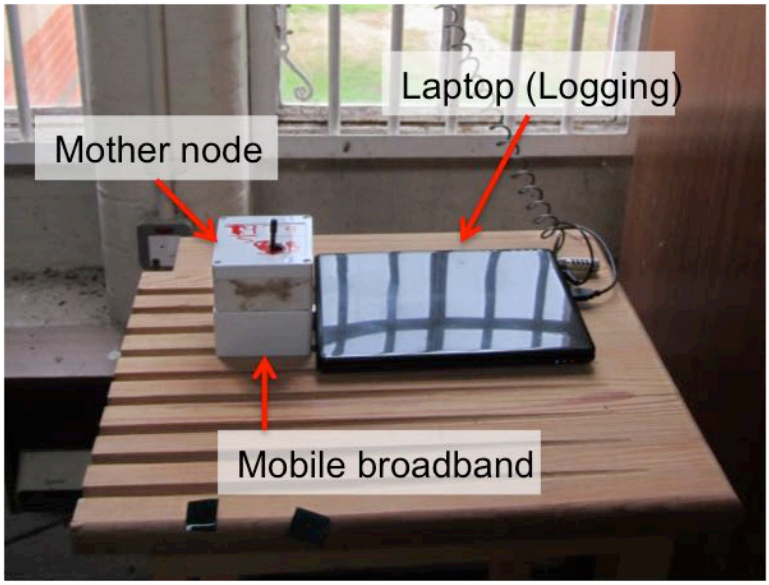

Figure 5.10 Setup of the mother node used in the field trials

One of the main challenges for the deployment of the nodes and sensors was protecting them from the harsh environment (for example, corrosion and water damage). Standard waterproofing techniques such as low-pressure moulding, potting and epoxy dipping are commonly used for ruggedisation of electronics in harsh environments. However, these techniques cannot be used for waterproofing the FSR sensors, as they will interfere with their operation. A suitable waterproofing method for the FSR sensor should be able to protect it from environment while maintaining its operational characteristics such as its flexibility and the ability to transfer the contact pressure on to the sensor part of the FSR. The method used should also maintain the low thickness of the FSR sensor in order for it to have minimal

impact on the contact pressure distribution between the clip and the pipe. For the purpose of the field trials, the FSR sensors are ruggedized by a process of lamination. This method satisfies both the low thickness and flexibility requirements which are essential for the operation of the FSR sensors. During this process the FSR sensor was laminated by two layers of clear plastic (thermal lamination). The exit point for the wires attached to the FSR sensor was also sealed with epoxy in order to stop water penetrating into the sensor through the surface of the cables. Figure 5.11 shows a laminated FSR sensor used in the field trials.

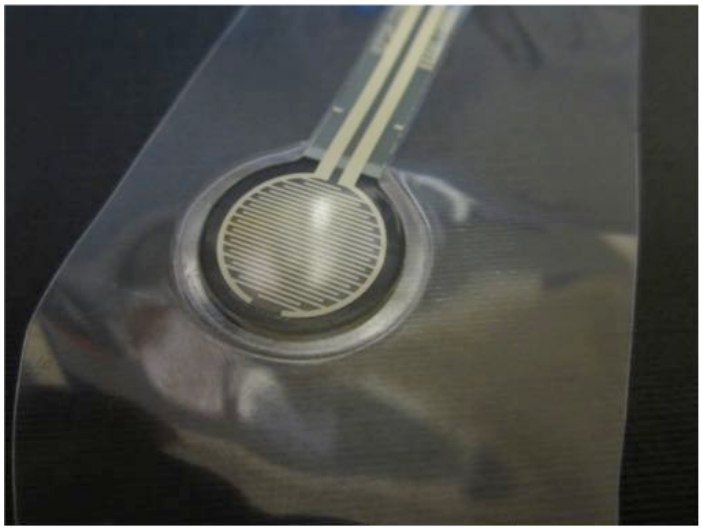

Figure 5.11 Laminated FSR

The temperature sensors used in the field trials were ruggedized by covering their contacts with epoxy. Node C, on the pipe (underground), was sealed and ruggedized by placing it into an IP65 box and sealing the lid with silicon sealant. Multiple humidity absorber sachets were also placed into the box to avoid condensation of the humidity in the box damaging the node (Figure 5.12). The other nodes, which were placed above ground, were sprayed with multiple layers of sealant and were placed in the above ground container (post) to protect them from the environment.

Figure 5.12 Sealing of node C

5.3.3 Results and discussion

During the field trials, the nodes on both the metallic and plastic pipes were able to successfully monitor the relative pressure and temperature data and transmit them to the mother node (with the exception of node C, where its data was stored locally).

The nodes and their sensors were installed on 16th -18th of June 2013 and the logging of the nodes started on 3rd of July 2013[1]. Despite efforts in waterproofing and ruggedisation, during the monitoring period some of the nodes/sensors failed due to corrosion or water damage. Damaged nodes were repaired/replaced where possible; however, damaged sensors could not be repaired, as re-excavation of the site was not possible. Additionally, for a period of approximately four weeks (09/08/2013-11/09/2013) data were not recorded on the laptop due to a power cut to the laptop and the mother node. Due to a fault in the local logger of node C, data from this node were not time stamped. The SD logger also ceased to operate six weeks after installation. For these two reasons the results from node C are not presented in this

[1] As of 9th July 2014 the FSR sensors were still operational, however all of the nodes and temperature sensors have ceased functioning.

thesis. All data from all the other nodes are presented and discussed in this section. The transmission success rate of the nodes was calculated without accounting for the physical failures of the node or the issue with the laptop. This is done by calculating the ratio between the number of missing packets (calculated via packet counter ID) and total packets received from each node. Figure 5.13 illustrates the data collected by node A (attached to the MDPE pipe).

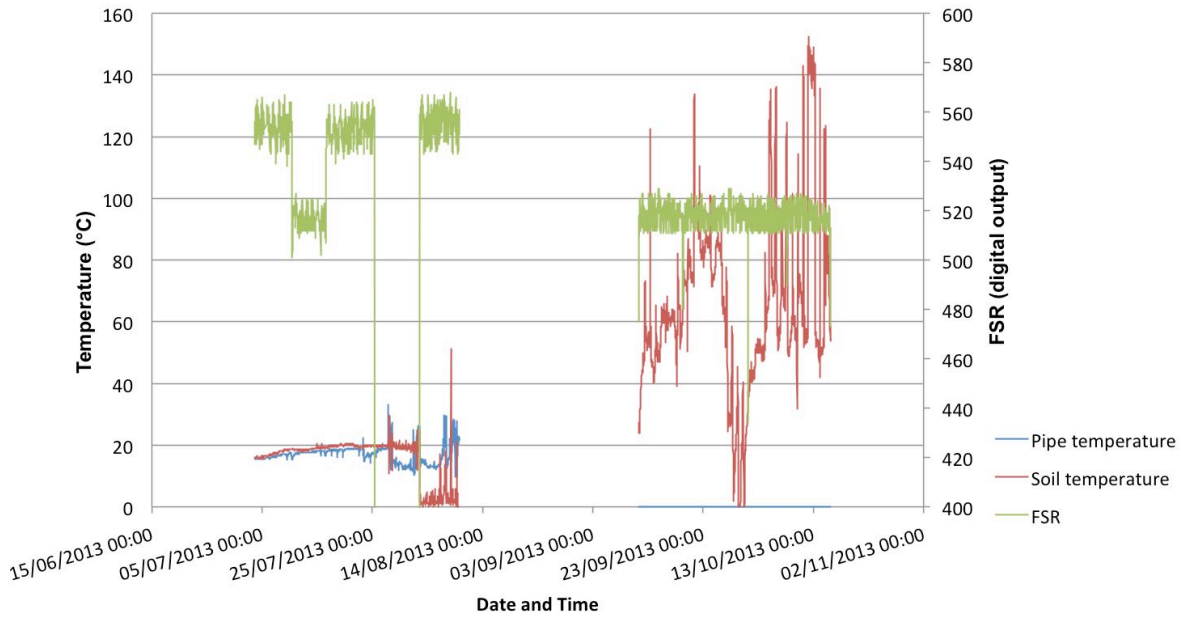

Figure 5.13 Data collected by node A attached to the MDPE pipe

As shown in Figure 5.13, the temperature sensors connected to the node became unreliable after approximately 4 weeks; this was mainly due to corrosion of the node's temperature sensors and their contacts. However, the FSR sensor was not affected by corrosion and performed without any issues during the monitoring period with an exception of a week (25/07/2013-02/08/2013) where the contacts of the FSR were disconnected from the node due to corrosion. It can also be seen from Figure 5.13 that the proposed relative pressure sensor successfully recorded pressure fluctuation and systematic pressure changes in the system. In

addition node A had a high transmission success rate of 98.61%. These data are further analysed in detail later in this section. Figure 5.14 illustrates the data from node B (attached to the ductile iron pipe).

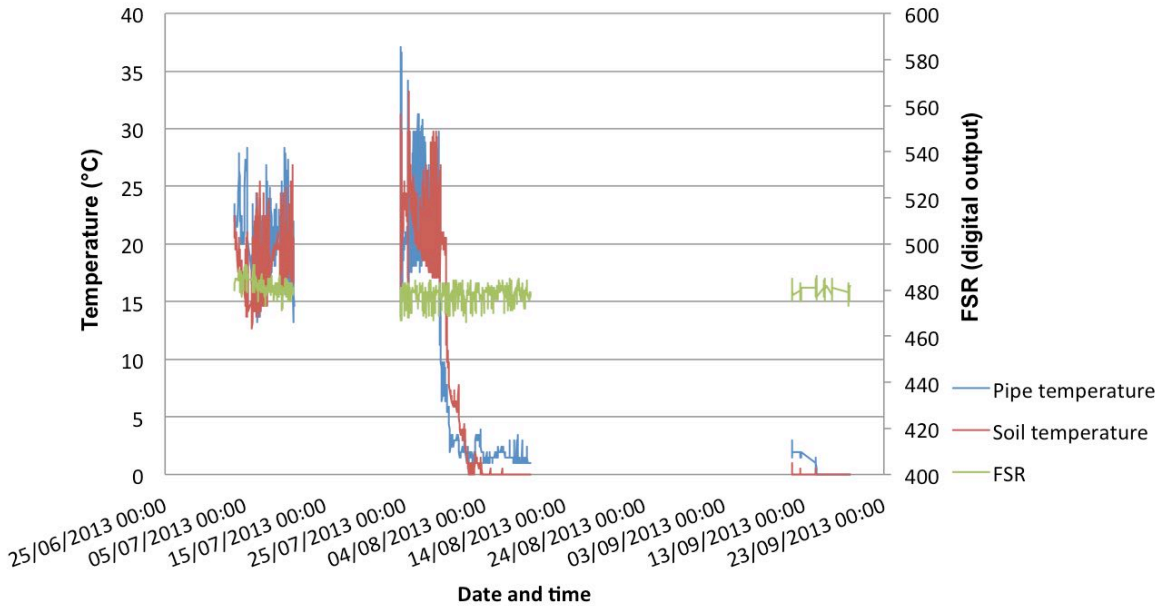

Figure 5.14 Data collected by node B attached to the ductile iron pipe

As shown in Figure 5.14, the temperature sensors attached to node B were damaged by corrosion shortly after installation and before logging began. This also indicated an issue with the sealing method used for the temperature sensors. However, the FSR sensor attached to the node was not affected by corrosion and performed without any issue during the monitoring period. The node itself suffered from a failure (due to corrosion of the MCU pins) for a period of approximately two weeks (11/07/2013-24/07/2013) this resulted in a gap in the data for that period. Furthermore node B had a significantly lower (48.28%) transmission success rate compare to node A. This was potentially due to the fact that Node B was the furthest node from the mother node (Figure 5.6).

Data captured from sensor node D attached to the MDPE pipe during the monitoring period are presented in Figure 5.15.

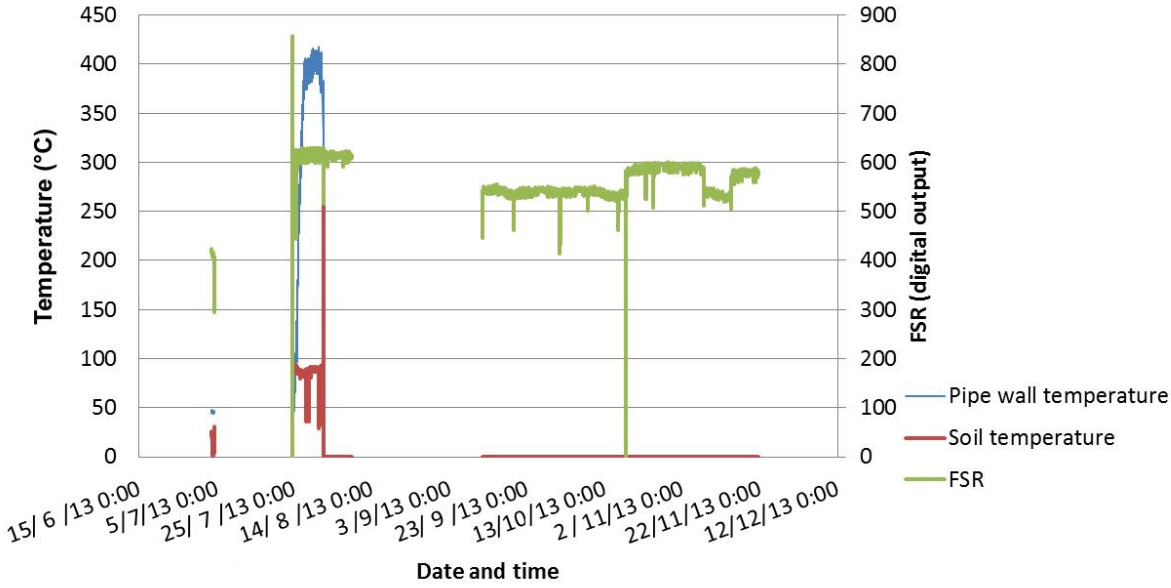

Figure 5.15 Data collected by node D attached to the MDPE pipe

Node D exhibited issues in the power supply unit (V supply) early on after installation, which was related to its solar panel charging circuitry. This issue was resolved on 24/07/2013 by replacing the charging circuit and battery of the node. The temperature sensors were also damaged due to corrosion before the start of logging, similar to node B. Despite initial problems of node D it had the highest transmission success rate (98.64%) amongst the nodes.

As shown in Figure 5.13 and Figure 5.15 relative pressure data from both of these nodes showed multiple systematic step changes in the internal pressure of the pipes. Figure 5.16 shows the comparison between the normalised pressure values from node A and node D.

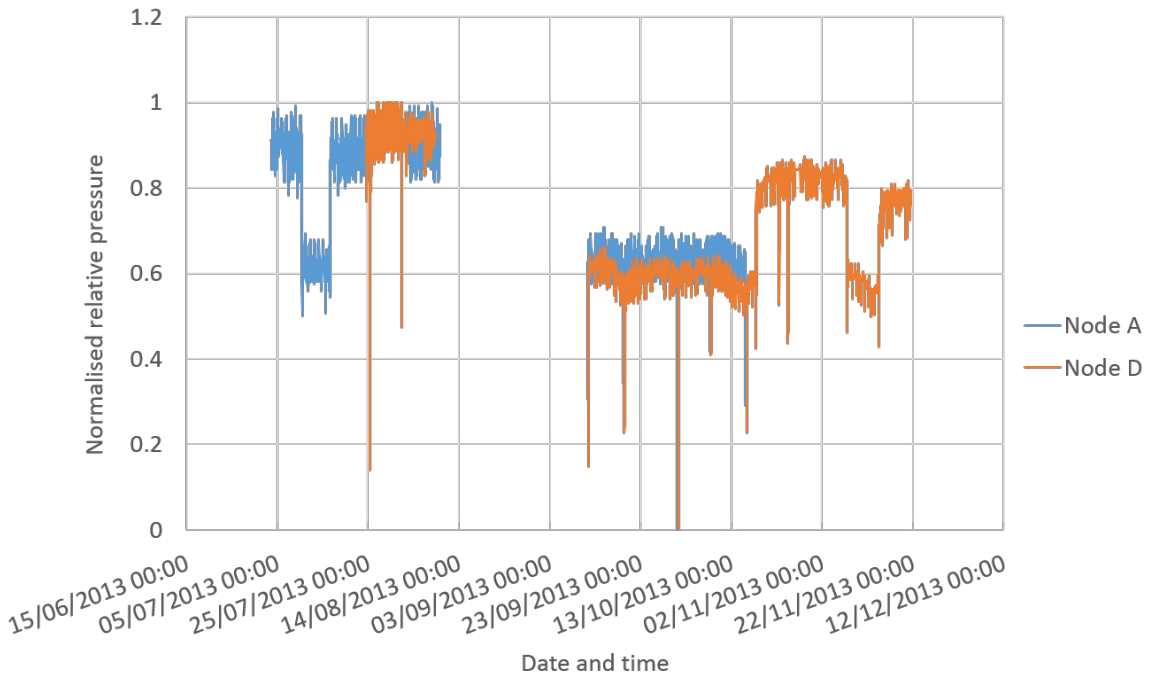

Figure 5.16 Comparison of measure relative pressure from node A and node D

As shown in Figure 5.16 relative pressure readings from node A and node D correlate with each other and the systematic pressure change (before and after the gap in the data) was registered by both of the nodes. In addition both nodes had a similar normalised response to the pressure changes. It is also shown in Figure 5.16 that both of the sensors registered large negative spikes in the data. These were caused by large transients and systematic depressurisation of the pipes.

Corrosion of the nodes was one of the main challenges during the field trials. Figure 5.17 shows an example of the corrosion on the sensor nodes despite the protective layer.

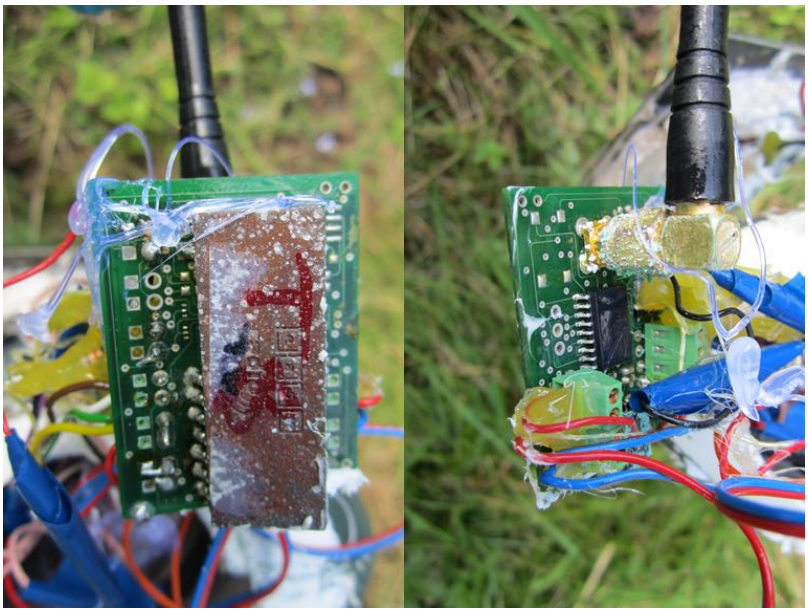

Figure 5.17 Example of corrosion of the nodes

It can be seen from Figure 5.17, that the contacts on the node are completely damaged by corrosion. The nodes ceased to operate after approximately 9 months. They were not repaired/replaced by new nodes due to a failure of the majority of the sensors and difficulties in accessing the site. However, the FSR sensors attached to the pipe were investigated on 9th July 2014, separately from the node. This investigation showed that despite damage to the node and temperature sensors, all of the FSR sensors attached to nodes were fully functional.

Data from the nodes were also studied in more detail to assess the capabilities of the FSR based relative pressure sensor for leak detection. Valve training was carried out on the test facility during the monitoring period of the field trials. During these training sessions, service taps were opened and closed, which simulated random leaks in the system. These leaks were visible in the data collected by the nodes. Figure 5.18 illustrates the normalised pressure data[1] and temperature readings from node A (attached to the MDPE pipe) for a duration of 20 days.

[1] Relative pressure data are filtered using default "rloess" filter in Matlab to remove outliers.

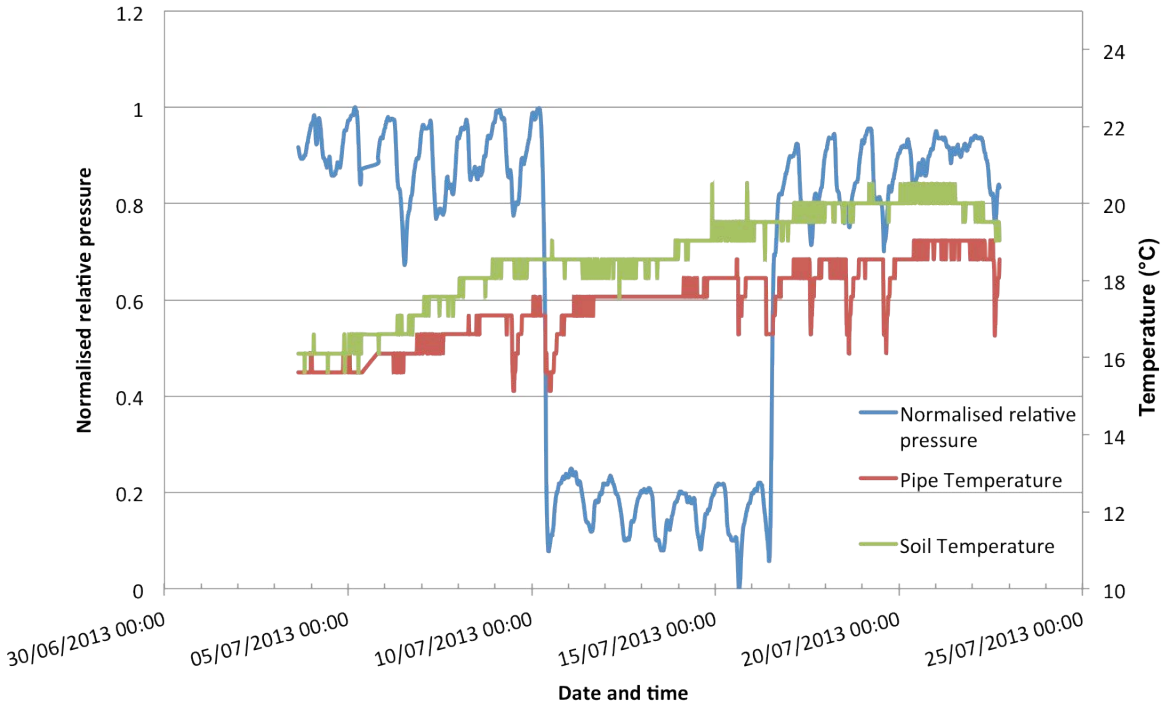

Figure 5.18 Relative pressure and temperature readings for a period of 20 days

As can be seen in Figure 5.18, daily pressure variations due to fluctuations in demand are clearly visible from the output of the relative pressure sensor. The relative pressure data identified a sudden systematic pressure drop approximately on 10th July 2013. Later, after contact with the site supervisor, this pressure drop was identified as being introduced by the site staff in order to carry out maintenance. This was very encouraging as it illustrated that the relative pressure sensors were able to clearly identify the systematic pressure drop in the pipes. The pressure was restored to the normal state after seven days, which was also registered by the sensor node system. During the period presented in the Figure 5.18 daily fluctuations of normalised relative pressure had an average peak-to-peak range of 0.12. Additionally, it can be seen in Figure 5.18 that the relative the pressure sensor showed pressure drops outside of the mentioned average daily fluctuation limit. These were later identified to be the valve training, which simulated leaks in the system. Figure 5.19 illustrates

pressure and temperature readings for a five-day period, where during the first three days, valve training was carried out at the test facility.

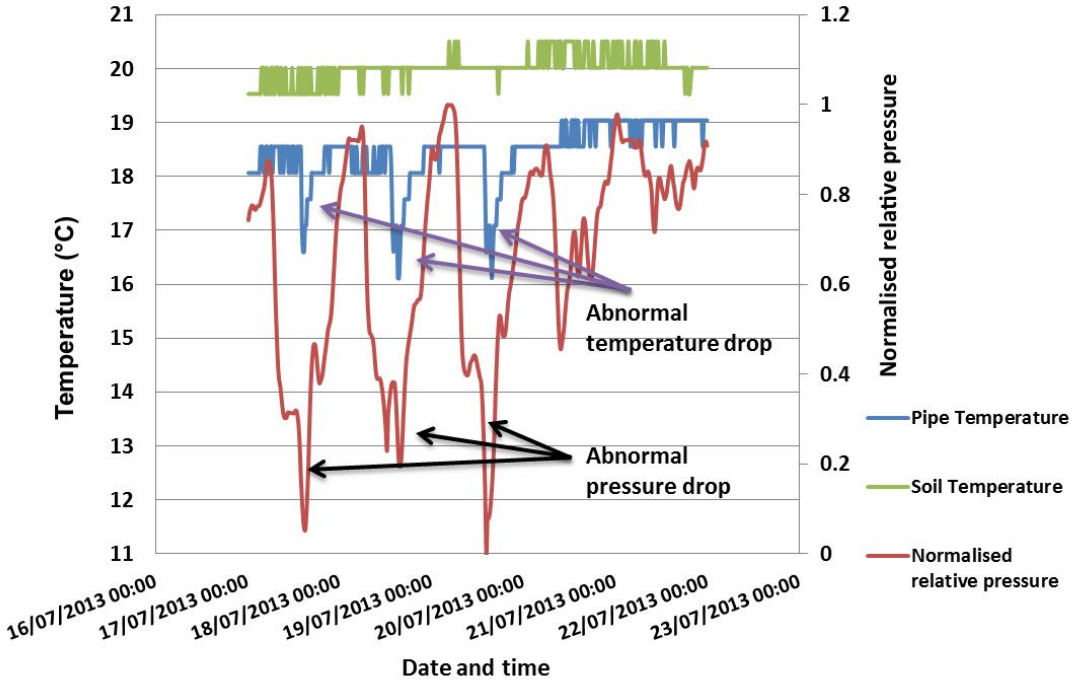

Figure 5.19 Correlation between relative pressure drop and pipe wall temperature for node A (Sadeghioon et al., 2014a)

It can be seen from Figure 5.19 that the simulated leaks during the valve training are detectable in the relative pressure readings as abnormal pressure drops out of daily pressure variation limits (0.40-0.95). In addition, the pipe wall temperature readings also showed a drop in pipe temperature at the same time as the drop in relative pressure, which were not present in the soil temperature readings. In contrast, this temperature drop was not present in the data for the last two days, despite a drop in relative pressure values (daily fluctuations) as it was a weekend and no leak tests were carried out. This effect was also evident in other periods in which valve training was carried out. Figure 5.20 illustrates pressure and temperature readings for a three-day period, where during the last day, valve training was carried out at the test facility.

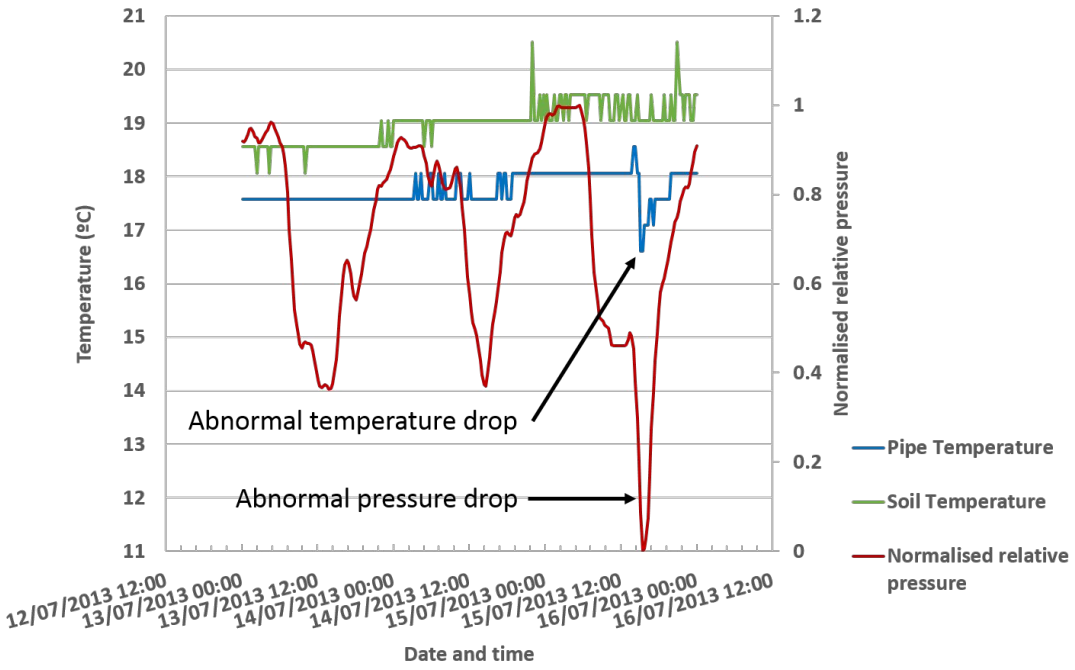

Figure 5.20 Correlation between relative pressure drop and pipe wall temperature during leak training for node A

It can be seen from Figure 5.20 that similar to measurements presented in Figure 5.19, the leak created on the last day (15/07/2013) during valve training was registered as an abnormal pressure drop out of the daily limit. In addition, similar to Figure 5.19 the leak in the pipe caused a rapid drop in the pipe wall temperature, which were not present in the soil temperature readings.

The rapid change in the pipe wall temperature was caused by a sudden change in the flow rate of water in the pipe. As mentioned previously in Chapter 4, a change in the flow rate of the water inside the pipe results in a change in its residence time. A sudden increase in the flow results in a higher cooling rate and therefore reduces the temperature of the pipe wall. As the soil is not a good heat conductor (compared to a pipe), this rapid change in pipe wall temperature is not apparent in the temperature of the soil. This shows a potential for relative pressure readings in combination with temperature readings to be used to detect leaks and differentiate them from normal pressure variations. In addition, long lasting small leaks can

potentially change the daily temperature profile of the surrounding soil compared to other locations, which could be detected by the temperature sensors at the proximity of the leak. Temperature readings can also help suppliers (i.e. water companies) with proactive asset management of their pipeline network during colder seasons.

5.4 Summary

In this chapter, the capabilities of an FSR based relative pressure sensor for leak detection are studied by means of laboratory and field trials. In addition to the proposed relative pressure sensors, the feasibility of using temperature readings and temperature differential (between pipe wall and surrounding) for leak detection were tested and analysed in the field trials.

A closed loop pressurised test bed (10m length) in the laboratory was developed in order to test the leak detection and localisation capabilities of the FSR based relative pressure sensor. Five FSR sensors were installed on the test bed (at 2m intervals). A leak was simulated in the pipe (at 5m) at a random time and the outputs of all the FSR sensors were measured simultaneously via a data acquisition device. Based on the results from these tests, it was shown that the FSR sensors were capable of measuring the pressure changes in the pipe during all stages of the test. The pressure drop caused by the simulated leak was clearly identifiable from the output of the FSR sensors under these test conditions. Further investigation of the output of the FSR sensors at the exact time of the leak event showed a more gradual drop in pressure for sensors downstream of the leak, compared to those that were placed upstream of the leak. The difference in the pressure profile can potentially be used to locate the leak zone (i.e. between two nodes).

The developed node (version 2.0), FSR based relative pressure sensors and temperature sensors were deployed in an industrial test facility. These field trials were carried out in order to test their individual performance as well as the performance of the complete system in a realistic environment. Four nodes were installed during the field trials. Each node was connected to two temperature sensors and an FSR based relative pressure sensor. Data from the nodes were transmitted to a mother node in a building close to the nodes. The mother node was responsible for time stamping and logging the data from the nodes.

One of the main challenges in deployment of the nodes in field trials was waterproofing and ruggedisation of the nodes. A method of waterproofing FSR sensors was developed based on a laminating technique. This proved to provide adequate protection for the FSR sensors while maintaining their flexibility and low footprint. The temperature sensors were waterproofed by epoxy encapsulation. However, this technique proved unable to provide the required protection for the sensors, as all the temperature sensors failed within 2 months after installation. During the field trials some of the nodes failed due to corrosion and required repair/replacement, despite being protected by multiple layers of sealant.

Results from the field trial showed that the system overall was able to successfully monitor the required parameters for an extended period of time. Node A and D exhibited high transmission success rates of 98.61% and 98.64%, while node B had a significantly lower success rate of 48.28%. The FSR sensors successfully registered systematic pressure changes and daily pressure fluctuation in the pipes. The FSR sensor also registered abnormal pressure fluctuations caused by leaks created during valve training (blind test). This further validated the use of the relative pressure measurement for leak detection in pipes. Additionally, the pipe wall temperature readings also showed a clear drop at the time of the leak training, which was not present in the soil temperature readings. This is very promising as temperature differential

measurements could be used to distinguish pressure drops caused by leaks from the normal pressure fluctuations.

As indicated in this chapter and Chapter 2, RF transmission through soil is challenging. The next chapter of this thesis describes an improved model for approximating RF signal attenuation in soil. This model is compared with existing models. In addition, multiple field tests are carried out in order to investigate the performance of the proposed and existing models for estimating RF propagation in soil.

6

RF PROPAGATION IN SOIL

Contents

Chapter overview

The focus of this chapter is to study the RF propagation in soil. In this chapter, the methodology used for the RF transmission trials are described and the results from these trials are presented. In addition a modification to the existing method for the extraction of the real and imaginary parts of the complex permittivity from the TDR waveform is proposed. These results are also discussed and compared with existing models for RF transmission through soil.

6.1 Introduction

WUSN are a subcategory of common WSN. As was mentioned in Chapter 2, WUSN have potential for a variety of applications such as precision agriculture, mine monitoring, and pipeline monitoring. Environmental differences between WUSN and common WSN impose a variety of challenges on successful implementation of WUSN. In terrestrial WSN, communication between nodes mainly happens through air, while in WUSN, Underground-to-Underground (UG2UG) communication is entirely through the ground. Drastic differences between the dielectric properties of air and the ground creates a need for a completely different wave propagation model for WUSN. Previously due to the high attenuation (shorter range) of RF signals in soil, WUSN with UG2UG communication paths were considered not feasible (Silva, 2010). However, a sharp decrease in price of electronics due to rapid advances in this field and the mass production of the devices with similar technologies have made dense deployment of WUSN technically and economically more feasible. As was mentioned in Chapter 2 there is a large discrepancy between existing models for prediction of RF attenuation in the ground. In addition an accurate model for the prediction of attenuation of RF signals in ground is essential for the design of the WUSN (i.e. node spacing).

Vuran and Silva (2009) classifies underground communication in WUSN, based on their application and environment, into two main categories of wireless communication networks for mines and tunnels and wireless communication in buried WUSN. Although wireless communication in mines and tunnels sometimes need to partially travel through the ground, most of the time the travel path is completely through air. This makes the attenuation model for wireless communication in mines and tunnels similar to those of above ground networks (Silva, 2010).

Silva and Vuran (2009) additionally categorise buried WUSN based on their burial depth in to two subcategories of topsoil WUSN (0-300mm depth) and subsoil WUSNs (>300mm depth). This categorisation is necessary due to the difference in soil parameters between these regions and the effect of the soil-air boundary (surface of the soil) on the signal path and its attenuation. The distance to the surface of the soil (burial depth) greatly affects the attenuation of the signal, as at shallower depths the effects of reflected signals are stronger (Silva, 2010). Generally underground RF communication is composed of direct path (node to node) and reflected path (reflected from the ground surface). An increase in the burial depth of the nodes will significantly reduce the effect of the reflected path on the overall signal attenuation. Therefore the signal can be assumed to follow a direct path (Akyildiz et al., 2009). Figure 6.1 shows the schematic of the direct path and reflected path and their total length.

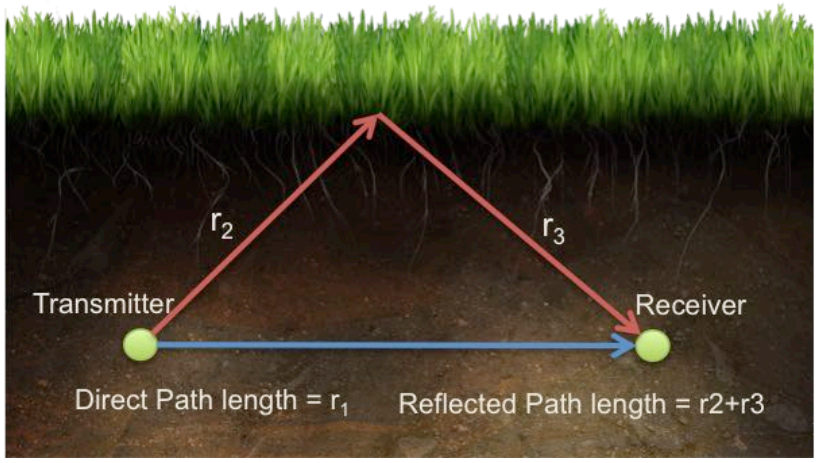

Figure 6.1 Schematic of direct path and reflected path and their total length.

The focus of this thesis and this chapter, however, will be on attenuation of the RF signals in the subsoil region as the majority of the water pipelines are deployed in this region (0.5-1.0m). Although internode communication in WUSN for pipeline monitoring is entirely

through soil, at some point these data packets are required to be transmitted to the surface to be relayed to the user therefore some of the nodes (i.e. mother nodes) use the Underground-to-Aboveground (UG2AG and AG2UG) communication channel. Therefore, based on the location of the nodes, communications in WUSN for pipeline monitoring can be divided into two main categories of AG2UG (or UG2AG) and UG2UG paths. Attenuation of RF signals in both of these paths is highly dependent on the dielectric properties of soil.

6.1.1 Dielectric properties of soil

Craig, (2004) defines soil as "*any uncemented or weakly cemented accumulation of mineral particles formed by the weathering of rocks, the void space between the particles containing water and/or air.*". Soil therefore can be classified as a complex mixed dielectric medium, which consists of air, water (bound and free) and bulk soil (Silva, 2010). Models which are used to predict the attenuation of the EM signals in soil rely on three key dielectric parameters of soil, which are complex dielectric permittivity, electrical conductivity and magnetic permeability of soil.

Dielectric permittivity is a complex value which represents the ability of the dielectric medium to permit an electric field and is defined by Equation (6.1) (Van-Dam et al., 2005; Curioni, 2013).

$$\varepsilon^* = \varepsilon' - j\varepsilon'' \tag{6.1}$$

Where ε^* is the complex dieelectric prermitivity, ε' is the real part of complex permittivity (storage of energy), ε'' is the imaginary part of complex permittivity (relaxation and dispersive losses) and $j = \sqrt{-1}$. The permittivity of a medium is commonly described by relative permittivity ε_r, which is the ratio of the real part of permitivilty to the permittivity of

free space. The permittivity of soil is mainly dependent on the frequency of the EM wave, soil water content, electrical conductivity, and soil composition. Various models have been proposed in the literature to estimate the permittivity of soil based on other measurable parameters (Peplinski et al., 1995a, 1995b; Van-Dam et al., 2005; Mironov and Dobson, 2004). As was mentioned earlier attenuation of EM signals in soil is highly affected by its complex permittivity and therefore the accuracy of these models ultimately affects the accuracy of the propagation estimation models. A comprehensive review of the methods used for the prediction of soil dielectric properties was produced by van Dam et al. (2005). A common method of extraction of the real and imaginary parts of the complex permittivity from time domain reflectometry waveform (TDR) was introduced by Topp et al. (2000). This method is based on estimation of the effective frequency of the TDR in soil (Curioni, 2013). In this method, the effective frequency is estimated based on the rise time of the signal at the end of the TDR (Topp et al., 2000). Figure 6.2 shows a typical TDR waveform and rise time t_r and travel time t_1 of the signal.

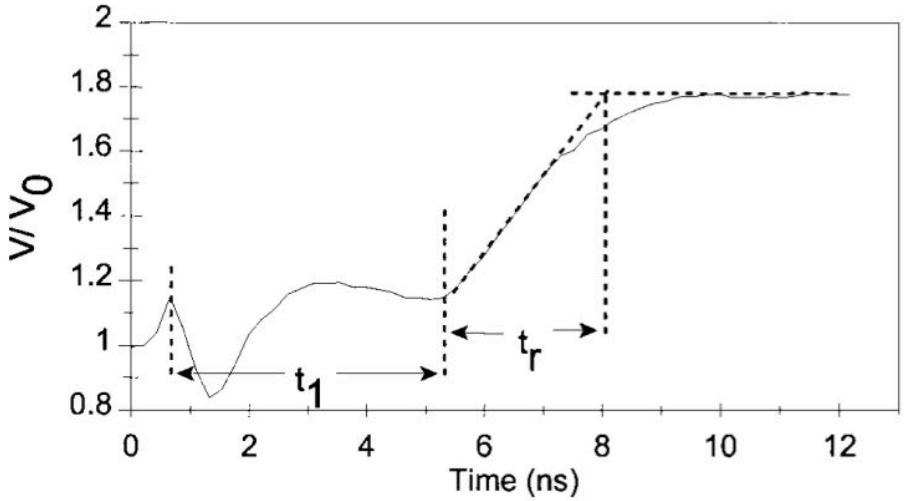

Figure 6.2 An example of Time Domain Reflectometry (TDR) waveform showing rise time t_r and travel time t_1 of the signal

However in practice multiple reflections at the end of the probe makes choosing the top line for calculating the rise time very difficult. This issue was also pointed out by Curioni (2013) and Evett and Parkin (2005). In order to overcome this issue it is proposed that the steady state value of the waveform after the reflections have levelled out be used for the calculations of the rise time. This method can potentially eliminate inaccuracies caused by the multiple reflections of the waveform at the end of the probe and provide a robust method for calculation of the rise time. The mentioned steady state value is commonly used for calculation of Bulk Electrical Conductivity (BEC) of the soil (Curioni, 2013). Figure 6.3 illustrates a typical waveform with end reflections and proposed method of calculation of the rise time. In this figure apparent length was calculated assuming that the velocity of the signal was equal to the velocity of light in a vacuum.

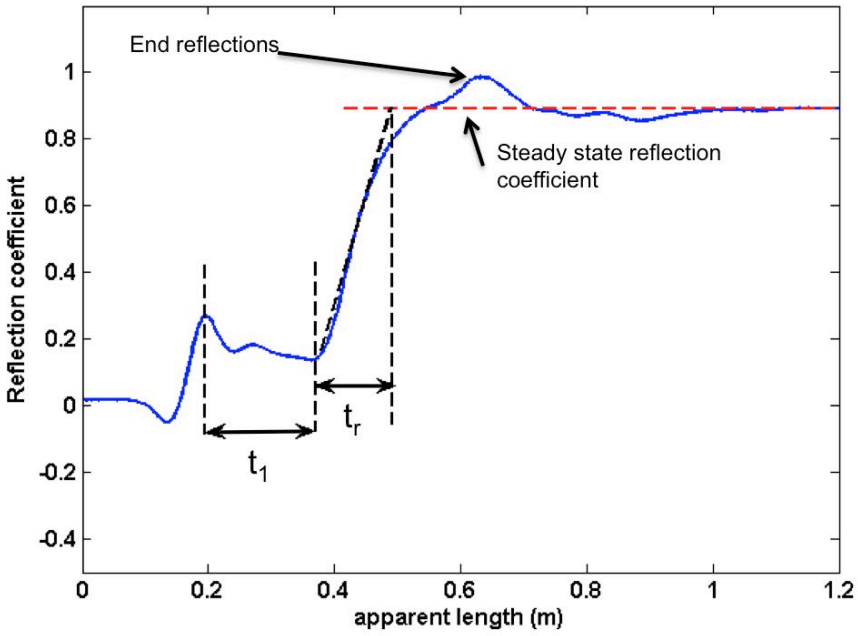

Figure 6.3 An example of TDR waveform with end reflections, showing the proposed steady state reflection line for calculation of rise time t_r and travel time t_1 of the signal

The performance of the proposed method for estimation of the real and imaginary parts of the complex permittivity of the soil as an input for modified Friis model is investigated in section 6.3 of this chapter.

Another main dielectric parameter of the soil is its electrical conductivity. The electrical conductivity of a medium can be described as the capability of the material to conduct electrical current (Curioni, 2013) and is represented by σ. Similar to permittivity, electrical conductivity is also dependent on frequency. Static electrical conductivity σ_{dc} affects the imaginary part of the complex permittivity and the relation between the ε'' and σ_{dc} is given by Equation (6.2) (Robinson et al., 2003).

$$\varepsilon''(f) = \varepsilon_p''(f) + \frac{\sigma_{dc}}{2\pi f \varepsilon_0} \tag{6.2}$$

Where ε_p'' is the dipolar losses due to relaxation, f is the frequency (Hz) and ε_0 is the permittivity of free space.

The magnetic permeability of a medium is described as the magnetisation capability of that material when it is exposed to a magnetic field. Similar to permittivity it is also a complex value and it is commonly expressed as a ratio to the magnetic permeability of free space and is called relative magnetic permeability (Curioni, 2013). The relative magnetic permeability of soil is considered to be 1 for the most common types of soil (Chaamwe et al., 2010), although some soil types (i.e. iron-oxide rich soils) have higher magnetic permeability.

6.2 RF propagation field trials

During this research two RF propagation field trials were carried out at different locations in order to evaluate the performance of existing models for RF propagation in a closer to real life environment. Moreover, despite the potential of WUSN, very few field trials have been

carried out in order to investigate underground communications (Silva and Vuran, 2010). During tests presented in this thesis only the UG2UG communication (in the subsoil region) of the nodes was investigated. The methodology and setup of these trials is described in detail in the following sections of this chapter.

6.2.1 Test arrangement

The first set of RF propagation trials was carried out in an area adjacent to an agricultural farm in the Leighton Buzzard area and the second set of tests were carried out in an open area in the test facility (Severn Trent Water, Lake House) described in Chapter 5. For ease of referencing these locations are referred to as locations A and B respectively in the later parts of this chapter. Differences in composition, condition and properties of the soil in these two locations were used to investigate the propagation of RF signals transmitted by the nodes and the results were compared with the previously described (Chapter 2) RF propagation models.

6.2.1.1 Location A trials

These tests can be divided into two sections of vertical and horizontal tests. In the vertical tests, a hole with a diameter of approximately 300mm and depth of 500mm was created using a hydraulic post borer. The latest version of the node (version 2.0) was used as a transmitter (at two operational frequencies of 868MHz and 433MHz). The node was placed at the bottom of the hole. The hole then was backfilled (via manual compaction plate) and a handheld RF spectrum analyser was place on top of the hole and was covered by the topsoil and grass which was removed prior to digging the hole. The handheld RF spectrum analyser (RFExplorer 3G-Combo) was used to measure the strength of the signal transmitted by the node. This procedure was repeated for all burial depths of 200, 400 and 600 mm and measurements taken for both transmission frequencies. Figure 6.4 illustrates the schematic of the setup of these tests.

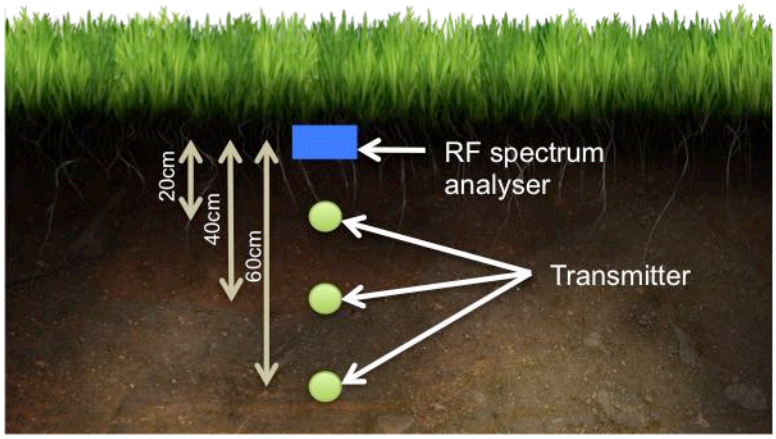

Figure 6.4 Schematic of the vertical test setup at location "A"

In the horizontal tests the RF spectrum analyser (same unit as the vertical tests) was buried at a depth of 500mm and the senor node was buried at a same depth with horizontal spacings of 2.50m, 3.75m and 5.00m from the spectrum analyser. The transmitter (same unit as the vertical tests) was initially placed at the 5m distance and was moved closer to the transmitter at each stage in order to avoid disturbance caused in the soil by the prior holes affecting the measurements. These tests were only carried out at 433MHz operating frequency due to the damage caused to the 868MHz transmitter during vertical tests. Figure 6.5 illustrates a schematic of the horizontal test setup.

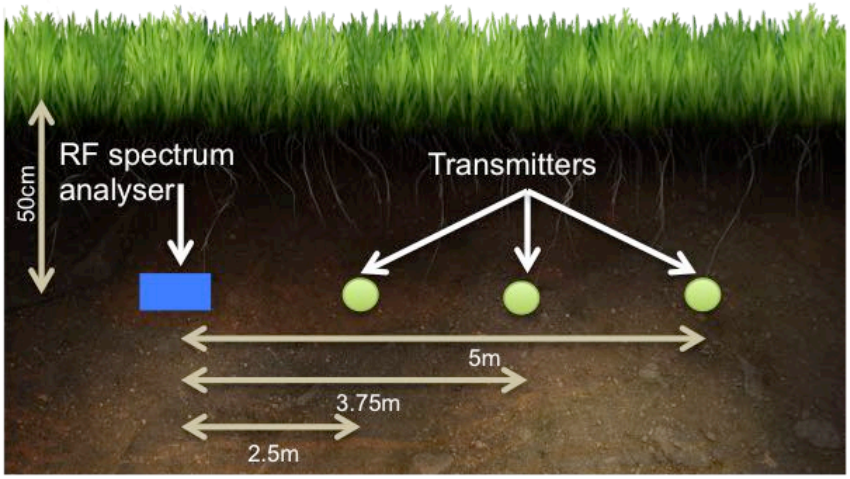

Figure 6.5 Schematic of the horizontal RF tests at location "A"

In both of tests (vertical and horizontal) data from the spectrum analyser was transferred to a laptop on the surface via a shielded USB cable.

6.2.1.2 Location B trials

The overall setup of these trials was similar to the horizontal tests at location “A” with a few differences. For these tests six holes with approximately 600mm spacing between them were created in the ground using a dry vacuum excavation technique. Additionally, these tests were carried out for two different depths of 500mm and 900mm with both the transmitter (node) and the receiver at same depth. Two different spectrum analysers were used for measurement of signal intensity in these trials. These spectrum analysers were connected to the receiver antenna placed in the ground via a shielded coaxial cable. Figure 6.6 illustrates the schematic of the setup used in these trials.

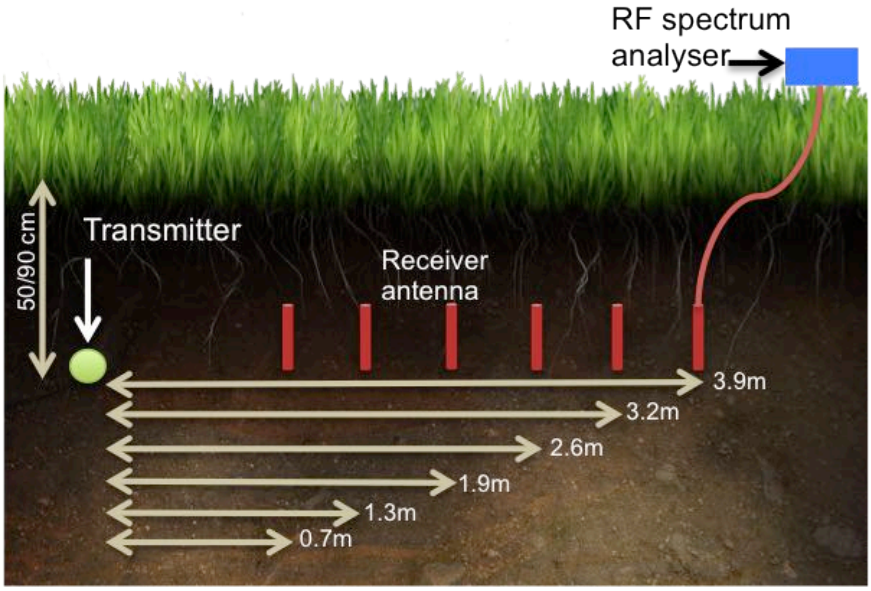

Figure 6.6 Test setup schematic for location "B"

6.2.2 Soil characterisation

During all of the RF field trials soil samples were taken from each hole location and at multiple depths to further analyse the characteristics of the soil and their effect on RF propagation. The key parameters tested were moisture content, particle size distribution, permittivity and conductivity. The dry sieving method based on British Standard 1377-2 (BSI, 1990) was used in order to obtain a distribution profile of the sample. The gravimetric water content (GWC) of the samples was measured by the oven drying method. The volumetric water content, permittivity and conductivity of the samples were obtained using Time Domain Reflectometry (TDR) methods described in Curioni (2013) and Topp et al. (2000). Results of the characterisation tests are given in section 6.3 of this chapter.

6.2.3 Factors affecting the field trials

Due to the complex nature of RF propagation in soil it is important that factors negatively affecting the results from the field trials are identified in order to minimise their effect (Silva,

2010; Silva and Vuran, 2010). The main factors affecting field trials carried out during this research are:

- Antenna orientation
- Excavation process (soil disturbance)
- Instrumentation characteristics

In terrestrial WSN, the orientation of the antennas does not significantly affect the communication (in short range), however in WUSN the high attenuation of signals compared to air makes the orientation of the antennas crucial (Silva and Vuran, 2010). For the purpose of this research during all the trials the antennas of the transmitter and the receiver were placed in the soil parallel to each other (0 degrees). This ensured that the results from the trials are not affected by change in the orientation of the antenna and their comparability is not jeopardised.

The excavation process was the most time consuming and labour intensive stage of the trials. During the field trials the transmitter and receiver were required to be buried and retrieved multiple times at various depths (up to 900mm). This makes manual excavation of the holes not feasible. During the initial set of RF field trials (location "A") a hydraulic post borer was used to create the holes necessary for burial of the instruments. Figure 6.7 illustrates a photograph of the posthole borer used for these tests.

Figure 6.7 Hydraulic posthole borer used at location "A"

However, this method exhibited some drawbacks. The main issue was that the maximum hole depth achievable by this method was limited to 600m which made testing the RF transmission at a normal depth of water distribution pipelines not possible. In addition, due to the invasive nature of this method instruments were damaged during the process of retrieval. The final issue was that the excavation process using the hydraulic posthole borer required significant physical effort due to the weight of the equipment and the soil. A vacuum excavator was used in the field trials at location “B” in order to overcome these issues. This method allowed deeper holes to be excavated and did not pose any risk to the instruments. Figure 6.8 shows a photograph of the vacuum excavator used for the field trials and the holes created for the RF transmission tests.

Figure 6.8 Vacuum excavator used for the trials at location "B" and the holes created for the RF tests.

Regardless of the method used for excavation, some considerations should be taken into account during the excavation process to ensure repeatability and reliability of the results. Any form of excavation will disturb the soil; therefore it is crucial that the soil excavated from the holes is compacted back on top of the instruments in order to reflect the initial conditions of the soil as closely as possible. During the field trials a compaction plate was used after refilling the holes to restore the initial density of the soil. As was mentioned earlier, soil is a complex medium and is composed of multiple layers. The properties and composition of the soil can vary significantly with depth (layers) therefore it is important that digging process is carried out in multiple stages in order to avoid mixing the layers during backfilling and potentially affecting the result.

The characteristics of the instruments used in the field trials also greatly affected the reliability and comparability of the results. An ideal RF measurement instrument will have no measurement error however in reality this is not the case. Measurement errors, and tolerances

of each of the components used in the trials will affect the end results. Part-to-Part error is one of the main issues that can affect the results. Due to manufacturing tolerances, similar parts such as antennas and transceivers will exhibit small differences in their performance characteristics (i.e. sensitivity, gain or output power). In order to avoid these variations affecting the comparability of results, the same instruments (for example antennas and nodes) were used in all the trials where possible[1].

Results from the measurements at both of the locations and comparison with the existing models are presented together in the next section of this chapter.

6.3 Results and discussion

6.3.1 Results from Location "A"

During the field trials at location "A" each signal intensity reading was repeated 5 times to investigate the reliability of the measurement. The classification of the soil at location "A" based on the results from the particle size distribution tests (Appendix C) and the results from the water content test and dielectric values of the soil samples taken from this location are presented in Table 6.1.

Table 6.1 Location "A" soil characteristics

Location	Classification	GWC	ε'	ε''	σ_{DC} (mS/m)
A	Gravelly SAND, C_U=2.00, C_K=0.99	12.97%	7.14	1.31	2.32

[1] The RF Spectrum analyser used in the first set of trials was damaged by the posthole borer during retrieval and was replaced by another spectrum analyser for the rest of the tests.

Figure 6.9 illustrates the signal intensity measurements with respect to depth (vertical tests) at location "A"[1].

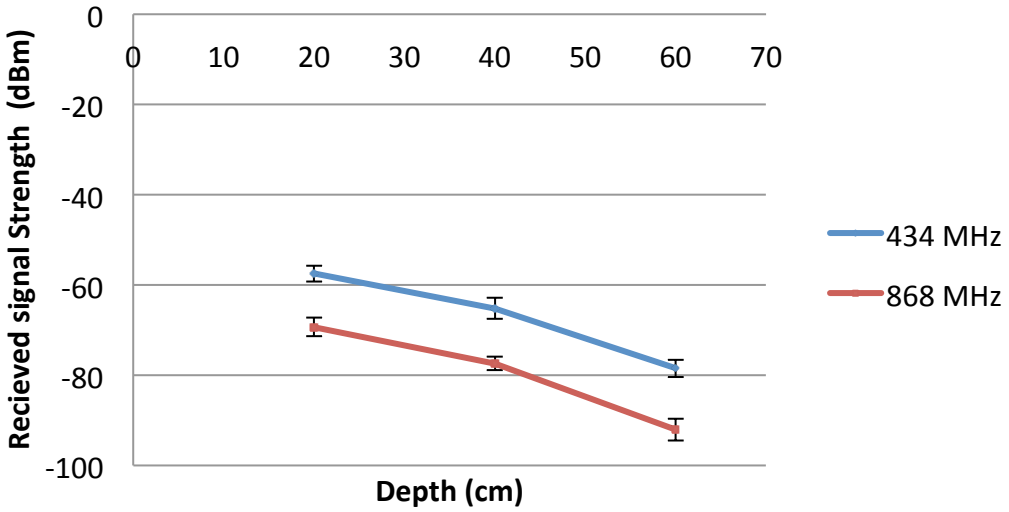

Figure 6.9 Received signal strength for the vertical tests, location "A"

The offset that can be seen in Figure 6.9 is caused by the difference between the transmission power of the 433MHz (10dBm output) and 868MHz (0dBm output) radio module. The attenuation values for the vertical tests are calculated based on using the signal intensity at 200mm depth as a reference. These are presented in Figure 6.10 (433MHz) and Figure 6.11 (868 MHz) and are compared with the CRIM-Fresnel, the modified-Friis model and the modified-Friis model (based on values from proposed TDR method).

[1] The error bars in this figure represent the standard deviation in the readings.

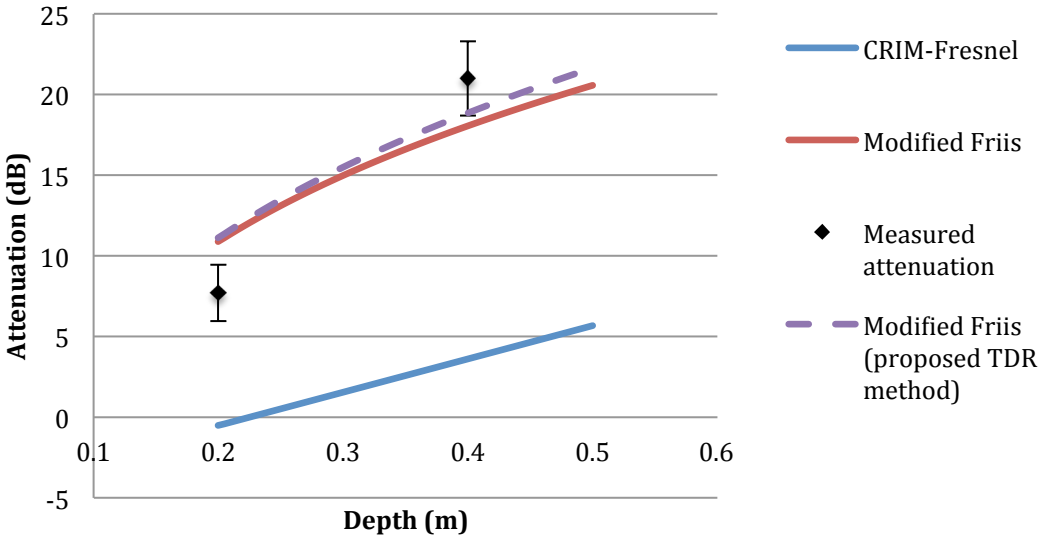

Figure 6.10 Comparison of the measured attenuation with the propagation models at 433MHz (location "A")

As shown from Figure 6.10 none of the models perfectly fit the measured data. The CRIM-Fresnel model especially underestimates the attenuation of signal (RMSE=13.59), while the modified Friis model performs significantly better (RMSE=3.06). However the modified-Friis model based on the proposed TDR method had the best performance (RMSE=2.85) amongst the compared methods.

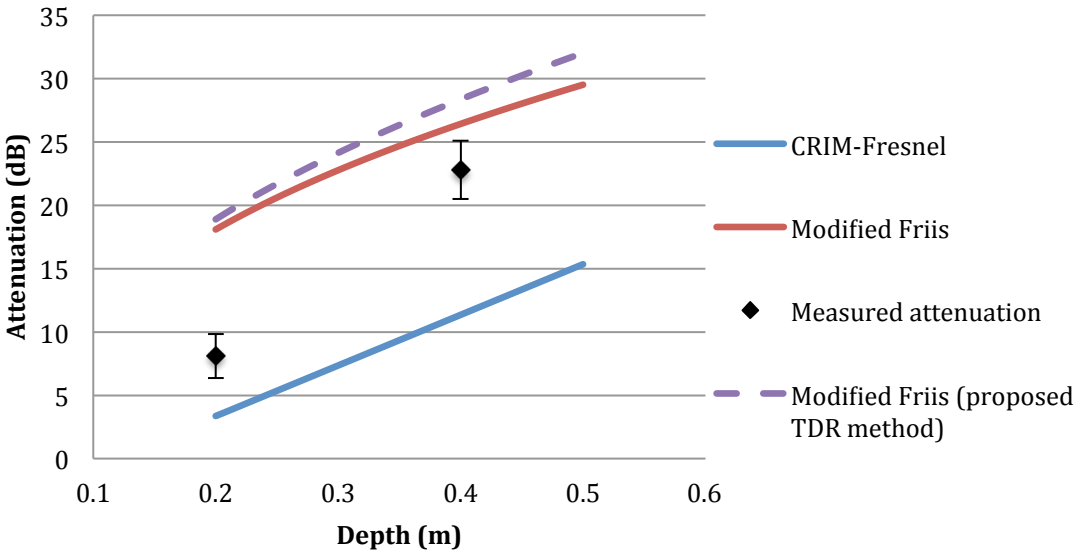

Figure 6.11 Comparison of measured attenuation with propagation models at 868MHz (location "A")

As can be seen from Figure 6.11, and similar to Figure 6.10, none of the models provided an accurate estimation of the signal attenuation for the 868 MHz signal. In addition similar to the results at 433MHz signal frequency CRIM-Fresnel was less accurate (RMSE=14.87) than modified Friis model (RMSE=8.76). However unlike the result at 433MHz the proposed modified-Friis method had a higher error (RMSE= 10.04) in estimation of the attenuation of the signal in soil.

Unfortunately, due to damage caused by the posthole borer on the spectrum analyser, the results from the horizontal test proved to be unreliable and are not presented in this thesis.

6.3.2 Results from Location "B"

Based on the results from Location "A" and the damage caused to the spectrum analyser, two higher performance spectrum analysers (Antritsu MS2721A and TTi-PSA2702) with higher accuracy and repeatability were chosen for the RF measurements at location "B". The RF measurements at each position were taken by both the RF spectrum analysers and were repeated 3 times. These results are then logarithmically averaged for use in the further analysis. Moreover, multiple reference measurements by both the spectrum analysers (in air) were used to ensure comparability of the results from these devices (as a calibration reference for the results). The TTi spectrum analyser exhibited a higher noise bed compared to the Antrisu, therefore measurements with values lower than -99 dBm were only carried out using Anritsu spectrum analyser.

During trials at location "B" multiple soil samples were taken from both depths of 500mm and 900mm. These samples were analysed using the same techniques used in characterisation of soil samples from location "A". Results these test are presented in Table 6.2.

Table 6.2 Classification and properties of the soil at location "B"

Location	Classification	GWC	ε'	ε''	σ_{DC} (mS/m)
B(500mm depth)	Gravelly SAND, C_U=9.43, C_K=0.42	17.02%	11.78	1.96	3.74
B(900mm depth)	Gravelly SAND, C_U=7.87, C_K=0.51	20.18%	19.30	4.33	7.61

As can be seen from Table 6.2 the soil samples at 900mm depth had a higher GWC compared to 500mm depth. Figure 6.12 illustrates the measured signal intensity at different horizontal distances from the transmitter for the 500mm and 900mm depths. Despite the similar classification of the samples from 500mm and 900mm depth, the particle size distribution tests showed a difference between the compositions of the soil at these depths, with the

samples from 900m depth showing a higher cumulative percentage of finer particles compared to the samples from 500m depth (see Appendix C). These differences in the water content and composition of the soil result in higher permittivity values for the soil at 900mm depth compared to 500mm depth. Figure 6.12 shows the measured signal strength at different horizontal distances for burial depth of 50 and 90cm.

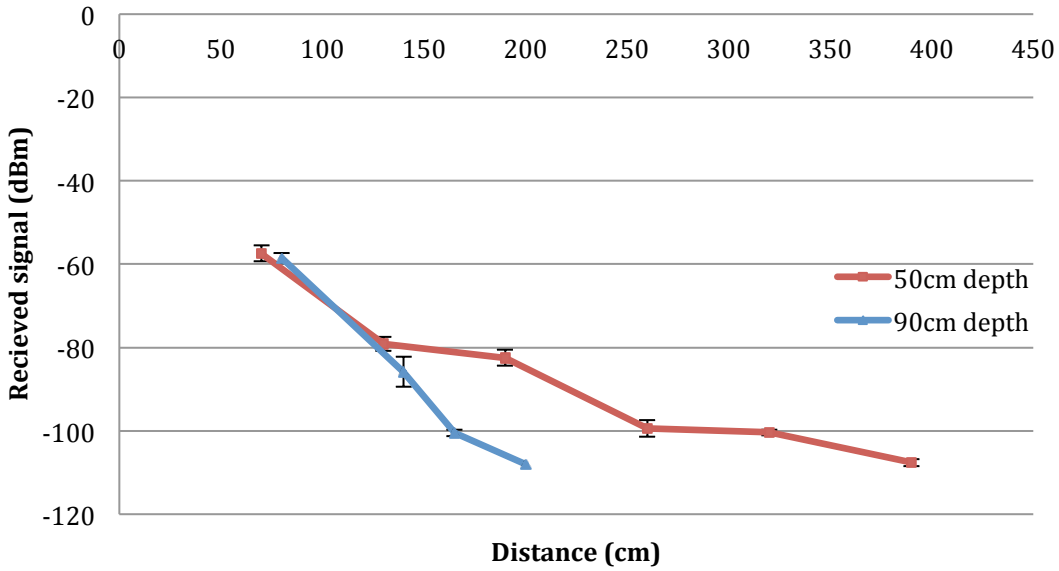

Figure 6.12 Received signal strength for 50cm and 90cm depths at different horizontal distances

As can be shown from Figure 6.12, the measurements shows a higher attenuation rate for the signal when the transmitter is buried at 90 cm compared to 50cm. This is mainly due to the previously mentioned difference in the soil moisture content and higher permittivity values. The relative attenuation of the signal is calculated for signal transmissions at 50cm and 90cm with the first measurement used as a reference. Figure 6.13 and Figure 6.14 illustrates the attenuation of the signal at 90cm and 50cm depth compared with the predicted values by the CRIM-Fresnel, modified-Friis model and modified-Friis model based on proposed TDR method.

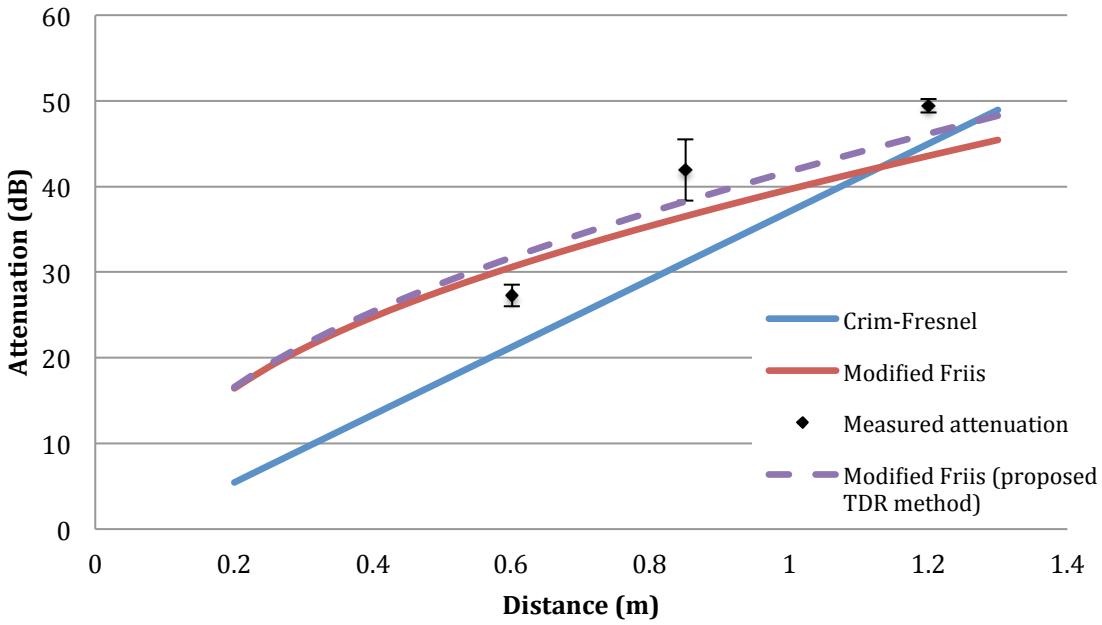

Figure 6.13 Measured attenuation of transmission at a depth of 90cm at location "B"

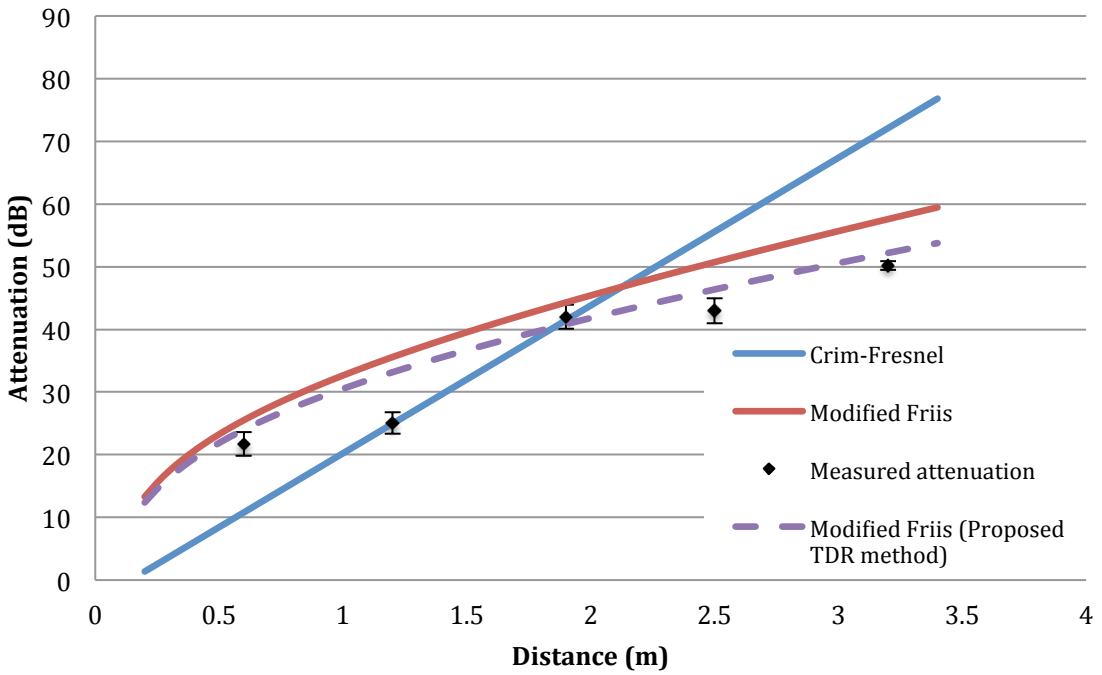

Figure 6.14 Measured attenuation of transmission at a depth of 50cm at location "B"

As can be seen from Figure 6.13 and Figure 6.14 all of the RF propagation models failed to provide an acceptable prediction (R^2 >0.95) for the attenuation of the signal in the soil.

However, the modified-Friis model provided a better approximation ($RMSE_{50cm}$=7.00, $RMSE_{90cm}$=4.97) for signal attenuation at both depths compared to the CRIM-Fresnel model ($RMSE_{50cm}$=12.31, $RMSE_{90cm}$=7.56). However, at both depths the modified-Friis model based on the proposed TDR method had the best performance ($RMSE_{50cm}$=4.19, $RMSE_{90cm}$=3.82) in estimation of the signal attenuation. In addition the linear estimation provided by the CRIM-Fresnel model was not inline with the trend of the measured values at both depths.

6.4 Summary

In this chapter the main RF propagation models for the prediction of signal attenuation in soil are compared with measured attenuations during field trials and a new modification to the modified-Friis model is proposed.

Due to the multilayer nature of the soil and possible significant variation between the dielectric parameters of the soils in each layer, buried WUSN can be divided into two main categories of subsoil and topsoil networks.

The main dielectric properties of the soil which affect RF propagation in soil are permittivity, electrical conductivity and magnetic permeability. Methods for estimation and calculation of the dielectric properties of soil (i.e. permittivity) are described. A new modification to the method of the extraction of the real and imaginary parts of the complex permittivity from TDR waveform for usage in a modified-Friis attenuation model is proposed. The link budget formula for transmission modelling is described. The modified Friis and CRIM-Fresnel models are the main techniques used for estimation of RF attenuation in soil.

The RF propagation through soil was tested at two locations with different soil compositions and conditions in order to investigate the accuracy of the existing RF propagation models. The process of excavation proved to be the most challenging aspect of the trials. Two

different techniques (hydraulic post hole borer and vacuum excavation) were used for creating the holes necessary for burial of the nodes and antennas. The hydraulic post borer proved not to be suitable due to its operational limitation and invasiveness. Vacuum excavation proved to be the more suitable technique and was used exclusively at location “B”.

Factors that could potentially negatively affect the results from the trials were thought to be antenna orientation, excavation process (soil handling) and instruments characterises. Measures were taken in order to minimise effect of these and ensure reliability of the results.

Comparison of the measured attenuation of the signal in the soil with the predicted values calculated from the CRIM-Fresnel and modified-Friis models showed that neither are these models provide an accurate estimation of signal attenuation, which is inline with (Yoon, 2013). However, the modified-Friis model provided more accurate estimations compared to the CRIM-Fresnel model. Comparison of the measured attenuation values with the new proposed modification to the modified-Friis model showed improvements in estimation accuracy of the modified-Friis model in three of the tests conditions (total of 4 test conditions).

The next chapter of this thesis concludes the research carried out during this project and summarises the key findings presented in this thesis. Additionally, recommendations for future work are presented in the next chapter.

7

CONCLUSIONS AND RECOMMENDATIONS FOR FUTURE WORK

Contents

Chapter overview

This chapter presents conclusions and key findings of the research carried out during this project. Additionally recommendations for future work are presented in this chapter.

7.1 Conclusions

This thesis presented the design, development and trials of a non-invasive WUSN for pipeline monitoring. Based on the review of the literature concerning NDE methods for pipeline monitoring, it was apparent that none of the existing methods is suitable for long-term permanent monitoring of pipelines due to their high power consumption or their survey based design. Amongst the reviewed NDE techniques, WUSN were identified as a suitable platform for pipeline monitoring. However, review of the current state of the art in WUSN for pipeline monitoring showed that due to their high power consumption and use of invasive sensors none of the existing systems provide a non-invasive long-term monitoring solution for pipeline monitoring. Power consumption, non-invasive sensing and underground connectivity (lack of requirement to access the interior of the pipe) are the main challenges for a successful WUSN for pipeline monitoring.

Due to the multi-disciplinary nature of this problem a holistic approach was chosen to address these challenges. Figure 7.1 shows the main challenges of this research and outlines the key outcomes of this project.

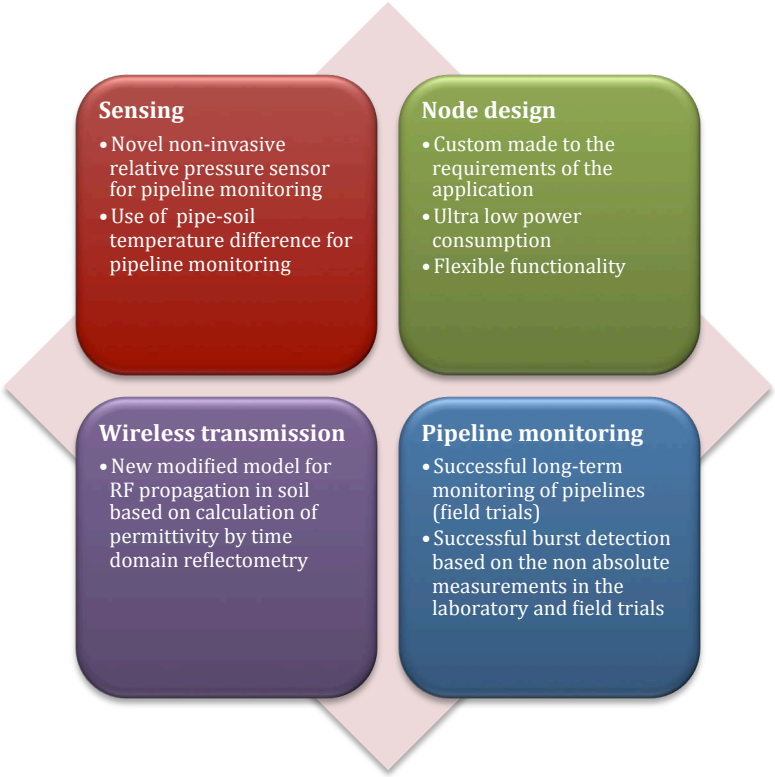

Figure 7.1 Main aspects of the project and the key outcomes of each of the sections

A custom wireless sensor node was designed and developed by the author based on design requirements identified for long-term pipeline monitoring. The design of the hardware and software of the node were refined during multiple stages of design, prototyping and testing in order to achieve ultra-low power consumption (<10μW[1]) while maintaining the functionality of the nodes. Pressure is one of the main parameters in pressurised pipeline monitoring. Commonly, pressure sensors require access to the medium inside the pipe (i.e. via tapings). In order to remove this requirement a novel non-invasive relative pressure sensor was designed and developed as a part of this research. The non-invasive nature of this sensor combined with its ease of installation (lower costs) makes it a more suitable option for use in WUSN. The performance of the proposed relative pressure sensor was investigated by comparing its response to a conventional direct pressure sensor. A laboratory pipe test bed with the ability

[1] Based on one transmission every 6 hours

to simulate pipe failure was developed in order to investigate the leak detection and localisation capabilities of the proposed pressure sensor. The complete WUSN developed during this research was tested at an industrial leak training test facility where pipelines were monitored continuously for a period of 6 months. In addition, existing models for the prediction of RF propagation in the soil, as one of the main challenges in WUSN, were reviewed and investigated via two separate field trials. A new modification to the method of the extraction of the real and imaginary parts of the complex permittivity from TDR waveform for usage in the modified-Friis model is proposed in order to increase its accuracy for the prediction of EM wave attenuation in soil. The key findings from the research presented in this thesis are summarised below:

- The frequency of measurements and transmission (duty cycle) of the nodes was identified as the main factor in reducing the power consumption of the nodes. A lower system duty cycle allows the nodes to spend more of their time in "sleep" mode which in turn greatly reduces the overall power consumption as power consumption in "sleep" mode is significantly lower than other stages of the operation. Based on the results from the power consumption tests on the final version of the node, reducing the duty cycle from every 5 minutes to every 6 hours decreased the power consumption of the node by over 90%. However, the relationship between the duty cycle of the node and the average overall power consumption is not linear and at longer sleep periods the overall power consumption of the node is dominated by the energy consumed during "sleep" period and any further increase in the "sleep" period does not have a significant effect on the overall power consumption of the node. Therefore a reduction in power consumption of the nodes in "sleep" mode is crucial in order to reduce the overall power consumption of the node. PIC microcontrollers with nanoWatt

technology were chosen in this research for their ultra-low power consumption during "sleep" mode, while maintaining the ability to wake up based on a watchdog timer.

- The effect of the operating parameters (supply voltage and operating frequency) of the nodes on their overall power consumption was investigated by laboratory tests on the final version of the node (version 2.0). Based on these tests the supply voltage directly affects the overall power consumption of the node during both the "sleep" and "on" periods. In contrast, the MCU clock frequency inversely affects the power consumption of the node during the "on" period by reducing computation time and therefore shortening the length of time that the node spends at this stage. Based on the results from the power consumption tests the latest version of the node had a power consumption of 5.25μW for one measurement and transmission every 15 minutes and 1.31μW for one measurement and transmission every six hours. This ultra-low power consumption was achieved by careful component selection during the hardware design stage and an efficient firmware design. This achievement makes it possible for the nodes to use low output harvesting techniques for continuous operation, or have a long operational lifetime (>15 years) on batteries.
- A non-invasive novel relative pressure sensor based on measurement of change in contact pressure between a clip and the pipe, caused by change in internal pressure was designed and developed. The material properties and geometry of the pipe and clip were identified as the main parameters affecting the response of the pressure sensors. The results from an analytical evaluation of the sensor node assembly showed that the proposed sensor has a larger operational domain when applied to plastic pipes compared to metallic pipes due to the lower Young's Moduli of plastic pipes compared with metallic pipes. However, the geometry and material of the clip can be

modified in order to compensate for the change in the material properties of the pipes. An FEA model was developed in order to investigate the response of the sensor assembly for different geometrical and material properties. The results from this model were compared with the analytical model and showed an acceptable accuracy for the analytical model (95.71%).

- Static and dynamic pressure tests were carried out to compare the output of the proposed sensor with a direct commercial pressure sensor. The results from these tests showed a high correlation between the sensors with $R^2>0.95$ for both tests. Based on the static tests the FSR sensors exhibited a linear response to pressure, however the dynamic tests showed a rate dependent error caused by large pressure changes. This, however, does not negatively affect the performance of the proposed sensor for its final application as it will be used to measure at lower sampling rates.
- A closed loop pipe test bench was developed during this project in order to investigate the leak detection and localisation capabilities of the FSR sensor. The results from these tests showed that the FSR sensor was capable of detecting the pressure drop caused by the simulated failure event. Moreover, these results demonstrated that the FSR sensors upstream of the simulated burst had a more sudden pressure drop profile compared to the ones downstream of the burst. This information can be used to detect the zone in which the pipe has failed.
- The use of temperature sensors for pipeline monitoring was investigated during this project. The results from the trials at the University of Birmingham and long-term monitoring at the leak test facility showed that a temperature difference between the pipe wall and its surroundings can be used to extract useful information regarding the flow in the pipe. An increase in the flow of the water in the pipe results in shorter

residence time of water, which in turn changes the cooling or heating effect of the water in the pipe based on the temperature of the water compared to the temperature of pipe environment.

- The developed WUSN and FSR based relative pressure sensors were deployed in a leak test facility for a period of 6 months in order to investigate the performance of the system in a more realistic environment. Based on the results from these trials, the WUSN were successfully able to monitor the sensors (FSR relative pressure and temperature) associated to them. The ruggedisation and waterproofing of the temperature sensors and nodes proved to be challenging as some of the nodes were needed to be replaced during the monitoring period due to corrosion, despite the water proofing efforts. In addition, the temperature sensors also suffered from rapid corrosion in the soil and failed shortly after installation (approximately 8 weeks), which further highlighted the importance of ruggedisation. However, the FSR sensors, and the method recommended in this research for their waterproofing, proved to perform successfully and therefore FSR sensors were not affected by corrosion problems. During this research a star network (single-hop) configuration was used during trials. Additional research is required to optimise the communication protocols for underground wireless communication in order to increase the reliability of connections while maintaining low power consumption and to enable multi-hop networks with longer range and reliability.
- The results from the field trials showed that the proposed system was capable of monitoring daily pressure fluctuations in the pipe that were caused by changes in demand on the network. In addition, systematic changes to the pressure of the network (i.e. due to maintenance) were also registered by the proposed WUSN system and the

relative pressure sensors. Furthermore, the proposed relative pressure sensors successfully registered abnormal pressure drops caused by leaks in the system during valve training sessions.

- The temperature data from the field trials showed a difference between the pipe's wall and its surrounding soil (on average≈1°C). In addition, the results showed a drop in the temperature of the pipe wall (i.e. increase in temperature difference up to 4°C) during the leak tests due to an increase in flow. It is suggested that temperature drop could be used in combination with the relative pressure readings in order to detect failures in the pipe by separating abnormal pressure drops from normal pressure variations in the pipe network.
- A comparison of the existing models for RF propagation in soil (modified-Friis and CRIM-Fresnel) showed a high discrepancy between the predicted values of attenuation obtained from these models. Moreover, mistakes in the published literature regarding the Modified-Friis model decreased the reliability of the published results on the validation of this model. In order to address these issues two field trials were carried out to investigate the performance of these models. The results from these trials showed that neither of the existing models was able to predict the attenuation of the signal in soil with an acceptable accuracy (>95%) when compared to the measured attenuation. The modified-Friis model (with corrected equations), however, had a better accuracy compared to the CRIM-Fresnel model.
- A modification to the method for extracting real and imaginary parts of permittivity by TDR is proposed in this thesis. It was also proposed to replace the dielectric mixing formula (Peplinski) used in the Modified-Friis method with the values extracted by TDR. The results from the two trials showed an improvement in the accuracy of the

Modified-Friis model by adaptation of the proposed method. However, the proposed modifications to the method of extracting the permittivity values from the TDR waveforms were tested on limited soil samples. In order to validate this method further tests are required on an extended range of soil compositions and conditions.

- Underground RF communication was thoroughly researched and it is found to be not appropriate as a means of data transmission for buried WSNs. This is largely due to the high absorption of EM signals in soil which results in short internode distances (range) and therefore increases in cost of deployment due to the higher number of required nodes and excavations. In addition, variations in soil conditions and compositions can significantly affect the absorption of EM signals, which also makes reliable communication for WUSNs nodes challenging. These variations need to be considered in calculations of the range, which results in further reductions of the internode distance.

7.2 Recommendations for future work

A number of recommendations are identified in this section based on the research presented in this thesis.

- Any permanent buried monitoring system for water pipelines is expected to have a long operational life due to high costs of excavations and replacements. Therefore the longevity of the electronics and the effects of ageing on the sensors needs to be studied further.
- The temperature measurements of the pipe wall and the surrounding soil presented in this thesis covered a short period of time (4 weeks). Longer-term monitoring of the pipe wall and its surrounding soil temperatures (>1 year) would provide useful

information on seasonal changes of the temperature differential between the pipe and its surrounding soil. This, in conjunction with monitoring of flow and pressure in the pipe, could also be used to further investigate the feasibility and reliability of using temperature differentials for leak detection.

- The novel relative pressure sensor presented in this thesis was only tested on limited pipe diameters and materials (four combinations in total), therefore further tests on different pipe materials and dimensions is recommended in order to investigate and validate the performance of the proposed relative pressure sensors.
- The results from the dynamic pressure tests showed a rate dependency error in the output of the proposed pressure sensor. More controlled dynamic tests with various rates of pressure change need to be carried out to further characterise this error. These tests can potentially help to further understand the operational domain and capabilities of the FSR sensors.
- The attenuation of electromagnetic signals increase in soils with an increase in frequency, therefore, WUSN can benefit from a low frequency transceiver (<100MHz). This will increase the internode range, which can result in lower overall system adaptation cost for suppliers due to lower equipment and excavation costs. In addition, more research needs to be carried out on alternative non-invasive methods of communication in WUSN for pipeline monitoring such as acoustic communication through the pipe wall.
- The performance of the existing RF propagation models and the new proposed modification to the Modified-Friis model in soil were tested on two different soil types. It is recommended to extend these trials by testing the performance of these models in more soil types with varying conditions (i.e. water content). This will help

to better understand the attenuation of EM signals in soil. This will also benefit the design of WUSN (i.e internode distance prediction). In addition, this can provide useful information for other NDE techniques based on electromagnetic signals (for example GPR) by providing better prediction of the behaviour of these methods in different soil types and conditions (i.e. prediction of effective depth of GPR measurements).

References

Ahadi, M. & Bakhtiar, M.S., (2010) Leak detection in water-filled plastic pipes through the application of tuned wavelet transforms to Acoustic Emission signals. *Applied Acoustics*, 71(7), pp.634–639.

Akyildiz, I.F. & Stuntebeck, E.P., (2006) Wireless underground sensor networks: Research challenges. *Ad Hoc Networks*, 4(6), pp.669–686.

Akyildiz, I.F., Su, W., Sankarasubramaniam, Y. & Cayirci, E., (2002) Wireless sensor networks: a survey. *Computer Networks*, 38, pp.393–422.

Akyildiz, I.F., Sun, Z. & Vuran, M.C., (2009) Signal propagation techniques for wireless underground communication networks. *Physical Communication*, 2(3), pp.167–183.

Akyildiz, I.F. & Vuran, M.C., (2010) *Wireless Sensor Networks 1st ed.*, Wiley.

Al-Barqawi, H. & Zayed, T., (2006) Condition rating model for underground infrastructure sustainable water mains. *Journal of Performance of Constructed Facilities*, (May), pp.126–136.

Atherton, D., (1995) Remote field eddy current inspection. *Magnetics*, IEEE Transactions on.

Atzori, L., Iera, A. & Morabito, G., (2010) The Internet of Things: A survey. *Computer Networks*, 54(15), pp.2787–2805.

Balachander, D., Rao, T.R. & Mahesh, G., (2013) RF Propagation Investigations in Agricultural Fields and Gardens for Wireless Sensor Communications. In *Proceedings of 2013 IEEE Conference on Information and Communication Technologies*. pp. 755–759.

BenSaleh, M.S., Qasim, S.M., Obeid, A.M. & Garcia-Ortiz, A., (2013) A review on wireless sensor network for water pipeline monitoring applications. *2013 International Conference on Collaboration Technologies and Systems (CTS)*, pp.128–131.

Berardi, L., Giustolisi, O., Kapelan, Z. & Savic, D.A., (2008) Development of pipe deterioration models for water distribution systems using EPR. *Journal of Hydroinformatics*, 10(2), p.113.

Bogena, H.R., Herbst, M., Huisman, J. a., Rosenbaum, U., Weuthen, A. & Vereecken, H., (2010) Potential of Wireless Sensor Networks for Measuring Soil Water Content Variability. *Vadose Zone Journal*, 9(4), pp.1002–1013.

Bogena, H.R., Huisman, J. a., Meier, H., Rosenbaum, U. & Weuthen, A., (2009) Hybrid Wireless Underground Sensor Networks: Quantification of Signal Attenuation in Soil. *Vadose Zone Journal*, 8(3), pp.755–761.

Bond, A., Mergelas, B. & Jones, C., (2004) Pinpointing leaks in water transmission mains. *Proceedings of ASCE Pipeline 2004*, pp.1–10.

Bowman, J., (1997) A Review of the Electrofusion Joining Process for Polyethylene Pipe Systems. *Polymer Engineering & Science*, 37(4).

BSI, (1990) *BS 1377-2 Methods of test for soils for civil engineering purposes: Part 2: Classification tests*, London : British Standards Institution.

Cawley, P., Lowe, M., Alleyne, D., Pavlakovic, B. & Wilcox, P., (2003) Practical long range guided wave inspection-applications to pipes and rail'. *Materials Evaluation*, 61(1), pp.66–74.

Chaamwe, N., Liu, W. & Jiang, H., (2010) Wave Propagation Communication Models for Wireless Underground Sensor Networks. *Communication Technology (ICCT), 2010 12th IEEE International Conference on*, pp.9–12.

Chang, Y.C., Lai, T. Te, Chu, H.H. & Huang, P., (2009) PipeProbe: Mapping Spatial Layout of Indoor Water Pipelines. *2009 Tenth International Conference on Mobile Data Management: Systems, Services and Middleware*, (3), pp.391–392.

Chen, Y., Wang, Q., Chang, M. & Terzis, A., (2011) Ultra-Low Power Time Synchronization Using Passive Radio Receivers. In *Information Processing in Sensor Networks (IPSN), 2011 10th International Conference on*. pp. 235–245.

Cheung, L., Soga, K., Amatya, B., Wright, P., Bennett, P.J., Kobayashi, Y. & Cheung, L.L.K., (2010) Optical fibre strain measurement for tunnel lining monitoring. *Proceedings of the ICE - Geotechnical Engineering*, 163(3), pp.119–130.

Christin, D., Reinhardt, A., Mogre, P.S. & Steinmetz, R., (2009) Wireless Sensor Networks and the Internet of Things : Selected Challenges. In *Proceedings of the 8th GI/ITG KuVS Fachgespräch Drahtlose Sensornetze*. pp. 31–33.

Costello, S.B., Chapman, D.N., Rogers, C.D.F. & Metje, N., (2007) Underground asset location and condition assessment technologies. *Tunnelling and Underground Space Technology*, 22(5-6), pp.524–542.

Craig, R.F., (2004) *Craig's Soil Mechanics*. 7th ed., London: Taylor & Francis.

Crocco, L., Prisco, G., Soldovieri, F. & Cassidy, N.J., (2009) Early-stage leaking pipes GPR monitoring via microwave tomographic inversion. *Journal of Applied Geophysics*, 67(4), pp.270–277.

Curioni, G., (2013) *Investigating the seasonal variability of electromagnetic soil properties using field monitoring data from Time-Domain Reflectometry probes* By. University of Birmingham.

Dane, J.H. & Topp, C., (2002) Methods of soil analysis: Part 4, Madison, *WI: Soil Science Society of America*, Inc.

Deivasigamani, A., Daliri, A., H. Wang, C. & John, S., (2013) A Review of Passive Wireless Sensors for Structural Health Monitoring. *Modern Applied Science*, 7(2), pp.57–76.

Department for Environment Food and Rural Affairs, (2011) *Environmental Statistics – Key Facts*, London.

Drinking Water Inspectorate, (2013) *DWI PR14 Guidance-Lead in Drinking Water*,

Elson, J. & Römer, K., (2003) Wireless sensor networks: A new regime for time synchronization. *ACM SIGCOMM Computer Communication Review*, 33(1), pp.149–154.

Evett, S.R. & Parkin, G.W., (2005) Advances in Soil Water Content Sensing. *Vadose Zone Journal*, 4(4), p.986.

Fletcher, R. & Chandrasekaran, M., (2008) SmartBallTM: A New Approach in Pipeline Leak Detection. In *2008 7th International Pipeline Conference*. pp. 117–133.

Frank, A., Pinter, G. & Lang, R.W., (2009) Prediction of the remaining lifetime of polyethylene pipes after up to 30 years in use. *Polymer Testing*, 28(7), pp.737–745.

Friis, H., (1946) A note on a simple transmission formula. *proc. IRE*, (1), pp.254–256.

Galvagni, A. & Cawley, P., (2012) Guided wave permanently installed pipeline monitoring system. In *Review of progress in quantitative nondestructive evaluation* pp. 1591–1598.

Gao, Y., Brennan, M., Joseph, P., Muggleton, J. & Hunaidi, O., (2005) On the selection of acoustic/vibration sensors for leak detection in plastic water pipes. *Journal of Sound and Vibration*, 283(3-5), pp.927–941.

Ghazanfari, E., Pamukcu, S. & Suleiman, M.T., (2011) A Radio Propagation Model for Wireless Underground Sensor Networks. *2011 IEEE Global Telecommunications Conference - GLOBECOM 2011*, pp.1–5.

Hancke, G., (2012) Industrial wireless sensor networks: A selection of challenging applications. In Antennas and Propagation (EUCAP), *2012 6th European Conference on*. pp. 64–68.

Heim, P.M., (1979) Conducting a leak detection search. *Journal of Amercian Water Works Association*, pp.66–69.

Hieu, B., Choi, S., Kim, Y.U., Park, Y. & Jeong, T., (2011) Wireless transmission of acoustic emission signals for real-time monitoring of leakage in underground pipes. *KSCE Journal of Civil Engineering*, 15(5), pp.805–812.

Hoàng, E.M. & Lowe, D., (2008) Lifetime prediction of a blue PE100 water pipe. *Polymer Degradation and Stability*, 93(8), pp.1496–1503.

Hunaidi, O., (2000) Detecting Leaks in Water-Distribution Pipes. *Construction Technology Update*, 40, pp.1–8.

Hunaidi, O. & Giamou, P., (1998) Ground-penetrating radar for detection of leaks in buried plastic water distribution pipes. In *Seventh International Conference on Ground-Penetrating Radar* pp. 27–30.

Hurst, N., Bellamy, L., Geyer, T. & Astley, J., (1991) A classification scheme for pipework failures to include human and sociotechnical errors and their contribution to pipework failure frequencies. *Journal of Hazardous Materials*, 26, pp.159–186.

Ikram, W., Stoianov, I. & Thornhill, N.F., (2010) Towards a radio-controlled time synchronized wireless sensor network: A work in-progress paper. *2010 IEEE 15th Conference on Emerging Technologies & Factory Automation (ETFA 2010)*, pp.1–4.

Interlink Electronics, (2010) *FSR Force Sensing Resistors Integration Guide*,

Jiles, D.C., (1990) Review of magnetic methods for nondestructive evaluation (Part 2). *NDT International*, 21(5), pp.83–92.

Jin, Y. & Eydgahi, A., (2008) Monitoring of Distributed Pipeline Systems by Wireless Sensor Networks. In *Proceedings of The 2008 IAJC-IJME International Conference*. pp. 1–10.

Khulief, Y. a., Khalifa, A., Ben-Mansour, R., Habib, M. a., Mansour, R. Ben & Ben Mansour, R., (2012) Acoustic Detection of Leaks in Water Pipelines Using Measurements inside Pipe. *Journal of Pipeline Systems Engineering and Practice*, 3(2), pp.47–54.

Kim, J.H., (2011) *Sensor-based autonomous pipeline monitoring robotic system*. Louisiana State University.

Kingajay, M. & Jitson, T., (2008) Real-time Laser Monitoring based on Pipe Detective Operation. In Proc. of World Academy of Science, *Engineering and Technology*, vol. 32, pp. 127-132, Aug. 2008. pp. 121–126.

Kleiner, Y. & Rajani, B., (2002) Forecasting variations and trends in water-main breaks. *Journal of infrastructure systems*, 8(4), pp.122–131.

Lai, T., Chen, W. & Li, K., (2012) TriopusNet: automating wireless sensor network deployment and replacement in pipeline monitoring. *Proceedings of the 11th international conference on Information Processing in Sensor Networks*, pp.61–71.

Lai, T., Chen, Y., Huang, P. & Chu, H., (2010) PipeProbe: a mobile sensor droplet for mapping hidden pipeline. *Proceedings of the 8th ACM Conference on Embedded Networked Sensor Systems*, pp.113–126.

Lambert, A., (1994) Accounting for losses: The bursts and background concept. *Water and Environment Journal*, pp.205–214.

Lambert, V. & Hirner, W., (2002) Losses from water supply systems: standard terminology and recommended performance measures. *Voda i sanitarna tehnika*, (3).

LeChevallier, M., Gullick, R. & Karim, M., (2003) The potential for health risks from intrusion of contaminants into the distribution system from pressure transients. *Journal of Water Health*, 1, pp.3–14.

Li, H.N., Li, D.S. & Song, G.B., (2004) Recent applications of fiber optic sensors to health monitoring in civil engineering. *Engineering Structures*, 26(11), pp.1647–1657.

Li, I., Kumar, A., Beard, S.J., Zhang, D.C. & Layer, A.S., (2012) State-of-the-art pipeline structural health monitoring systems. *Sensors*.

Li, L., Vuran, M. & Akyildiz, I., (2007) Characteristics of underground channel for wireless underground sensor networks. *In The Sixth Annual Mediterranean Ad Hoc Networking WorkShop*. Corfu, Greece, pp. 92–99.

Li, M. & Liu, Y., (2009) Underground coal mine monitoring with wireless sensor networks. *ACM Transactions on Sensor Networks*, 5(2), pp.1–29.

Li, M. & Liu, Y., (2007) Underground Structure Monitoring with Wireless Sensor Networks. *2007 6th International Symposium on Information Processing in Sensor Networks*, pp.69–78.

Li, Y., (2014) *Using sensor systems to detect leaks in water pipes*. University of Birmingham.

Liu, Z. & Kleiner, Y., (2013) State of the art review of inspection technologies for condition assessment of water pipes. *Measurement*, 46(1), pp.1–15.

Logsdon, S.D., (2005) Soil Dielectric Spectra from Vector Network Analyzer Data. *Soil Science Society of America Journal*, 69(4), p.983.

López-higuera, J.M., Cobo, L.R., Incera, A.Q. & Cobo, A., (2011) Fiber Optic Sensors in Structural Health Monitoring. *Journal of lightwave technology*, 29(4), pp.587–608.

Lowe, M.J.S., Alleyne, D.N. & Cawley, P., (1998) Defect detection in pipes using guided waves. *Ultrasonics*, 36(1-5), pp.147–154.

Makar, J.M., (2000) A preliminary analysis of failures in grey cast iron water pipes. *Engineering Failure Analysis*, 7(1), pp.43–53.

Makar, J.M. & Kleiner, Y., (2000) *Maintaining water pipeline integrity*,

Maraiya, K., Kant, K. & Gupta, N., (2011) Application based Study on Wireless Sensor Network. *International Journal of Computer Applications*, 21(8), pp.9–15.

Metje, N., Chapman, D.N., Cheneler, D., Ward, M. & Thomas, A.M., (2011) Smart Pipes—Instrumented Water Pipes, Can This Be Made a Reality? *Sensors*, 11(8), pp.7455–7475.

Metje, N., Chapman, D.N., Rogers, C.D.F. & Henderson, P., (2008) Optical Fibre Sensors For Remote Monitoring of Tunnel Displacements - Prototype Tests in the Laboratory. *Structural Health Monitoring – An international journal*, 7(1), pp.51–63.

Microchip Technology Inc., (2009) *PIC Microcontroller Low Power Tips ' n Tricks*,

Mironov, V., (2004) Spectral dielectric properties of moist soils in the microwave band. In *Geoscience and Remote Sensing Symposium, 2004. IGARSS'04. Proceedings*. pp. 3474–3477.

Mironov, V. & Dobson, M., (2004) Generalized refractive mixing dielectric model for moist soils. *Geoscience and Remote Sensing, IEEE Transactions*, 42(4), pp.3556–3558.

Misiunas, D., (2005) *Failure Monitoring and Asset Condition Assessment in Water Supply Systems*. Lund University.

Misiunas, D., (2008) Failure Monitoring and Asset Condition Asssessment in Water Supply Systems. *In The 7th International Conference "Environmental engineering": Selected papers*. Vilnius, pp. 1–8.

Misiunas, D., Lambert, M., Simpson, A. & Olsson, G., (2005) Burst detection and location in water distribution networks. *Water Science and Technology: Water Supply*, 5, pp.71–80.

Mohamad, H., Soga, K. & Bennett, P., (2011) Monitoring Twin Tunnel Interaction Using Distributed Optical Fiber Strain Measurements. *Journal of geotechnical and geoenvironmental engineering*, 138(8), pp.957–967.

Muggleton, J.M. & Brennan, M.J., (2004) Leak noise propagation and attenuation in submerged plastic water pipes. *Journal of Sound and Vibration*, 278(3), pp.527–537.

Muggleton, J.M., Brennan, M.J., Pinnington, R.J. & Gao, Y., (2006) A novel sensor for measuring the acoustic pressure in buried plastic water pipes. *Journal of Sound and Vibration*, 295(3-5), pp.1085–1098.

Myles, A., (2011) Permanent Leak Detection on Pipes using a Fibre Optic Based Continuous Sensor Technology. In *Pipelines 2011: A Sound Conduit for Sharing Solutions ASCE 2011*. pp. 744–754.

Nakhkash, M., (2004) Water leak detection using ground penetrating radar. In Ground Penetrating Radar, 2004. GPR 2004. *Proceedings of the Tenth International Conference on*. Delft, The Netherlands, pp. 525–528.

Nikles, M., (2009) Long-distance fiber optic sensing solutions for pipeline leakage, intrusion and ground movement detection. *In Fiber Optic Sensors and Applications VI.* SPIE, pp. 731602–731613.

Ozevin, D. & Yalcinkaya, H., (2013) New Leak Localization Approach in Pipelines Using Single-Point Measurement. *Journal of Pipeline Systems Engineering and Practice*, (8), pp.1–8.

Pelletier, G., Mailhot, A. & Villeneuve, J., (2003) Modeling water pipe breaks-three case studies. *Journal of water resources planning and management*, pp.115–123.

Peplinski, N., Ulaby, F.T. & Dobson, M.C., (1995a) Corrections to "Dielectric Properties of Soils in the 0.3-1.3-GHz Range." *IEEE Transactions on Geoscience and Remote Sensing*, 33(6), p.1340.

Peplinski, N., Ulaby, F.T. & Dobson, M.C., (1995b) Dielectric properties of soils in the 0.3-1.3-GHz range. *IEEE Transactions on Geoscience and Remote Sensing*, 33(3), pp.803–807.

Rajani, B. & Kleiner, Y., (2004) *Non-destructive inspection techniques to determine structural distress indicators in water mains*.

Rajeev, P., Kodikara, J., Chiu, W.K. & Kuen, T., (2013) Distributed Optical Fibre Sensors and their Applications in Pipeline Monitoring. *Key Engineering Materials,* 558, pp.424–434.

Rizzo, P., (2010) Water and Wastewater Pipe Nondestructive Evaluation and Health Monitoring: A Review. *Advances in Civil Engineering*, 2010, pp.1–13.

Robinson, D.A., Jones, S.B., Wraith, J.M., Or, D. & Friedman, S.P., (2003) A Review of Advances in Dielectric and Electrical Conductivity Measurement in Soils Using Time Domain Reflectometry. *Vadose Zone Journal*, 2(4), pp.444–475.

Rogers, P. & Grigg, N., (2009) Failure assessment modeling to prioritize water pipe renewal: two case studies. *Journal of Infrastructure Systems*, (September), pp.162–171.

Sadeghioon, A.M., Metje, N., Chapman, D. & Anthony, C., (2014a) SmartPipes: Smart Wireless Sensor Networks for Leak Detection in Water Pipelines. *Journal of Sensor and Actuator Networks*, 3(1), pp.64–78.

Sadeghioon, A.M., Walton, R., Chapman, D., Metje, N., Anthony, C. & Ward, M., (2014b) Design and Development of a Nonintrusive Pressure Measurement System for Pipeline Monitoring. *Journal of Pipeline Systems Engineering and Practice*, 5(3), pp.3–6.

Saul, A.J., Unwin, D.M. & Boxall, J.B., (2003) Data mining and relationship analysis of water distribution system databases for improved understanding of operations performance. *In Advances in Water Supply Management*. Taylor & Francis.

Schmitt, C., Pluvinage, G., Hadj-Taieb, E. & Akid, R., (2006) Water pipeline failure due to water hammer effects. *Fatigue & Fracture of Engineering Materials and Structures*, 29(12), pp.1075–1082.

Shinozuka, M., Chou, P.H., Kim, S., Kim, H.R., Yoon, E., Mustafa, H., Karmakar, D. & Pul, S., (2010) Nondestructive Monitoring of a Pipe Network using a MEMS-Based wireless network. In *Proceedings of SPIE Conference on Smart Structures & Materials/NDE*. San Diego, pp. 1–12.

Silva, A.R., (2010) *Channel characterization for wireless underground sensor networks*. University of Nebraska - Lincoln.

Silva, A.R. & Vuran, M.C., (2010) Development of a Testbed for Wireless Underground Sensor Networks. *EURASIP Journal on Wireless Communications and Networking*, (1), pp.1–14.

Silva, A.R. & Vuran, M.C., (2009) Empirical Evaluation of Wireless Underground-to-Underground *Communication* in Wireless Underground Sensor Networks, *Distributed Computing in Sensor Systems,* Springer Berlin / Heidelberg.

Sinha, S.K., Iyer, S.R. & Bhardwaj, M.C., (*2003*) Non-contact ultrasonic sensor and state-of-the-art camera for automated pipe inspection. *In Sensors, 2003. Proceedings of IEEE*. pp. 493–498.

Sinha, S.K. & Knight, M.A., (2004) Intelligent system for condition monitoring of underground pipelines. *Computer-Aided Civil and Infrastructure Engineering*, 19, pp.42–53.

Sñgrov, S., Baptista, J.F.M., Conroy, P., Herz, R.K., Legau, P., Moss, G., Oddevald, J.E., Rajani, B. & Schiatti, M., (1999) Rehabilitation of water networks Survey of research needs and on-going efforts. *Urban Water*, 1, pp.15–22.

Sonyok, D., Zhang, B. & Zhang, J., (2008) Applications of Non-Destructive Evaluation (NDE) in Pipeline Inspection. *In Pipelines 2008 Pipeline Asset Management: Maximizing Performance of our Pipeline Infrastructure*. pp. 1–10.

Stajano, F., Hoult, N., Wassell, I., Bennett, P., Middleton, C. & Soga, K., (2010) Smart bridges, smart tunnels: Transforming wireless sensor networks from research prototypes into robust engineering infrastructure. *Ad Hoc Networks*, 8(8), pp.872–888.

Stoianov, I., Nachman, L., Madden, S., Tokmouline, T. & Csail, M., (2007) PIPENET: A wireless sensor network for pipeline monitoring. In *6th International Symposium on Information Processing in Sensor Networks, IPSN 2007. IEEE*, pp. 264–273.

Stokes, V., (1989) Joining Methods for Plastics and Plastic Composites: An Overview. *Polymer Engineering & Science*, 29(19).

Sun, Z., Wang, P., Vuran, M.C., Al-Rodhaan, M.A., Al-Dhelaan, A.M. & Akyildiz, I.F., (2011) MISE-PIPE: Magnetic induction-based wireless sensor networks for underground pipeline monitoring. *Ad Hoc Networks*, 9(3), pp.218–227.

Tanimola, F. & Hill, D., (2009) Distributed fibre optic sensors for pipeline protection. *Journal of Natural Gas Science and Engineering*, 1(4-5), pp.134–143.

Topp, G., Zegelin, S. & White, I., (2000) Impacts of the real and imaginary components of relative permittivity on time domain reflectometry measurements in soils. *Soil Science Society of America*, 1252, pp.1244–1252.

Trinchero, D., Fiorelli, B., Galardini, A. & Stefanelli, R., (2009) Underground Wireless Sensor Networks. In *Wireless and Microwave Technology Conference, 2009. WAMICON '09. IEEE 10th Annual*. Clearwater, pp. 1–3.

Van-Dam, R.L., Borchers, B. & Hendrickx, J.M.H., (2005) Methods for prediction of soil dielectric properties: a review. *Defense and Security*, 5794, pp.188–197.

Vuran, M.C. & Akyildiz, I.F., (2010) Channel model and analysis for wireless underground sensor networks in soil medium. *Physical Communication*, 3(4), pp.245–254.

Vuran, M.C. & Silva, A.R., (2009) Communication Through Soil in Wireless Underground Sensor Networks – Theory and Practice. In *Sensor Networks, Signals and Communication Technology*. Berlin Heidelberg, pp. 309–347.

Weimer, D., (2001) Water loss management and techniques. *The German Technical and Scientific Association for Gas and Water*.

Whittle, A., Allen, M., Preis, A. & Iqbal, M., (2013) Sensor networks for monitoring and control of water distribution systems. *In The 6th International Conference on Structural Health Monitoring of Intelligent Infrastructure*.

Yan, S.Z. & Chyan, L.S., (2010) Performance enhancement of BOTDR fiber optic sensor for oil and gas pipeline monitoring. *Optical Fiber Technology*, 16(2), pp.100–109.

Ye, G. & Soga, K., (2012) Energy Harvesting from Water Distribution Systems. *Journal of Energy Engineering*, 138(1), pp.7–17.

Yoon, S., (2013) *Wireless Signal Networks : A Proof of Concept for Subsurface Characterization and A System Design with Reconfigurable Radio*, Lehigh University.

APPENDICES

Appendix A: Sensor nodes

Figure A.1 Version 0.5 of the node

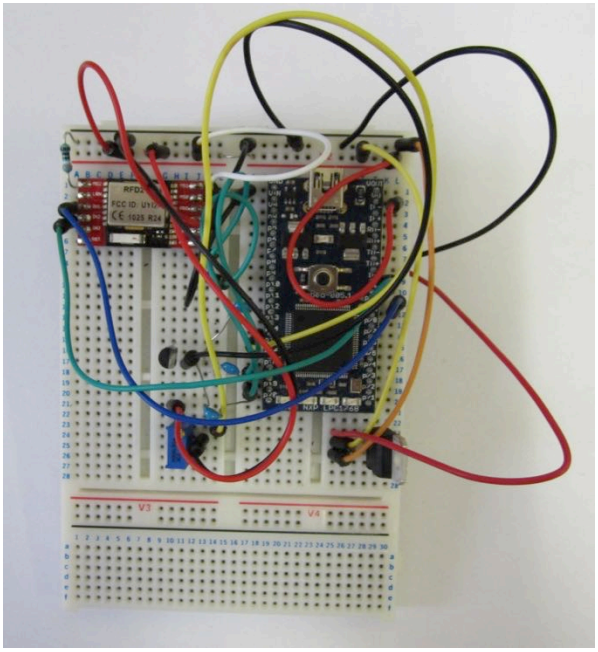

Figure A.2 Version 1.0 of the node.

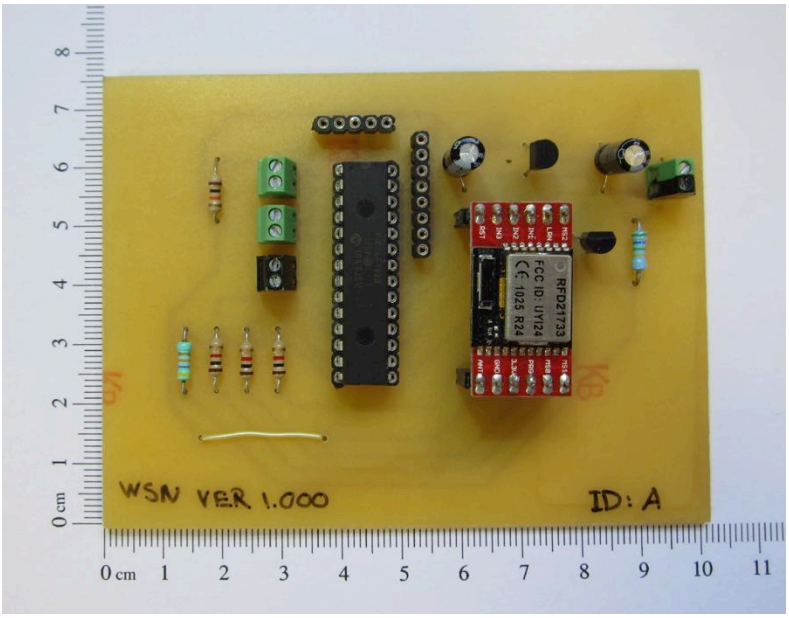

Appendix B: Laboratory leak test

The following are more examples of the normalised pressure readings during laboratory leak tests described in Section 5.2:

Figure B.1 Normalised output of the FSR sensor during leak test example1

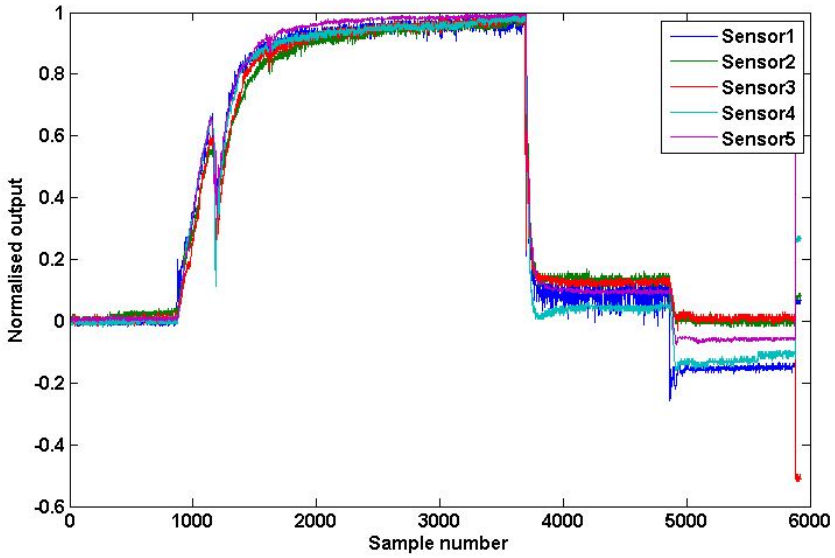

Figure B.2 Normalised output of the FSR sensor during leak test example2

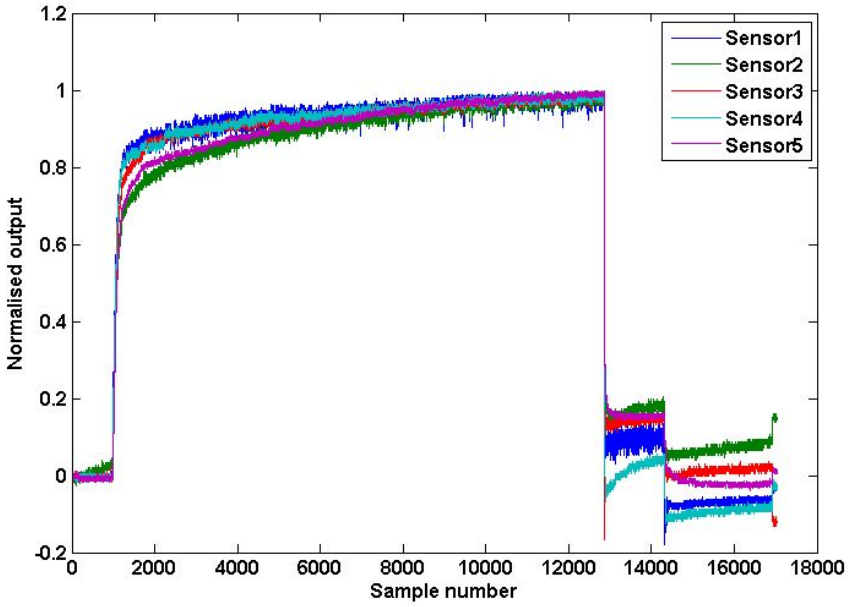

Figure B. 3 Normalised output of the FSR sensor during leak test example 3

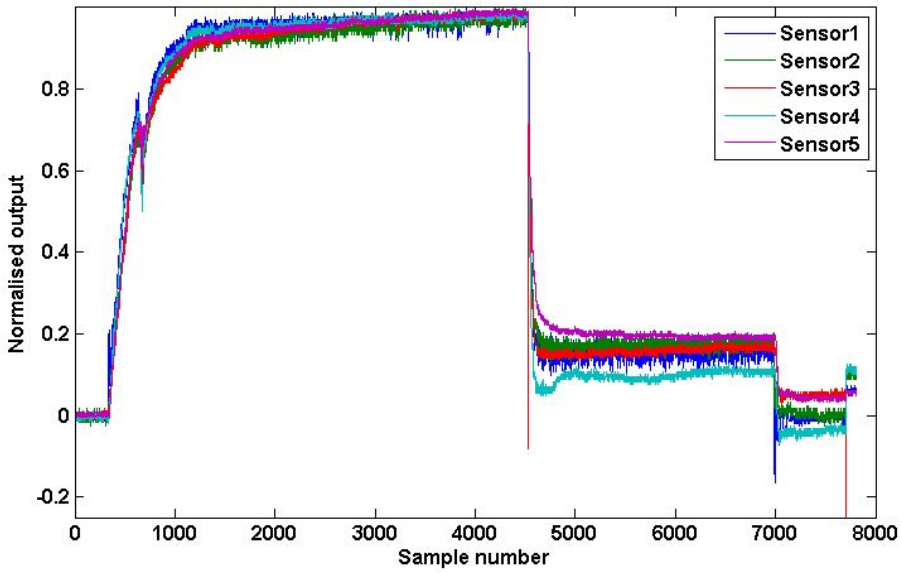

Figure B.4 Normalised output of the FSR sensor during leak test example 4

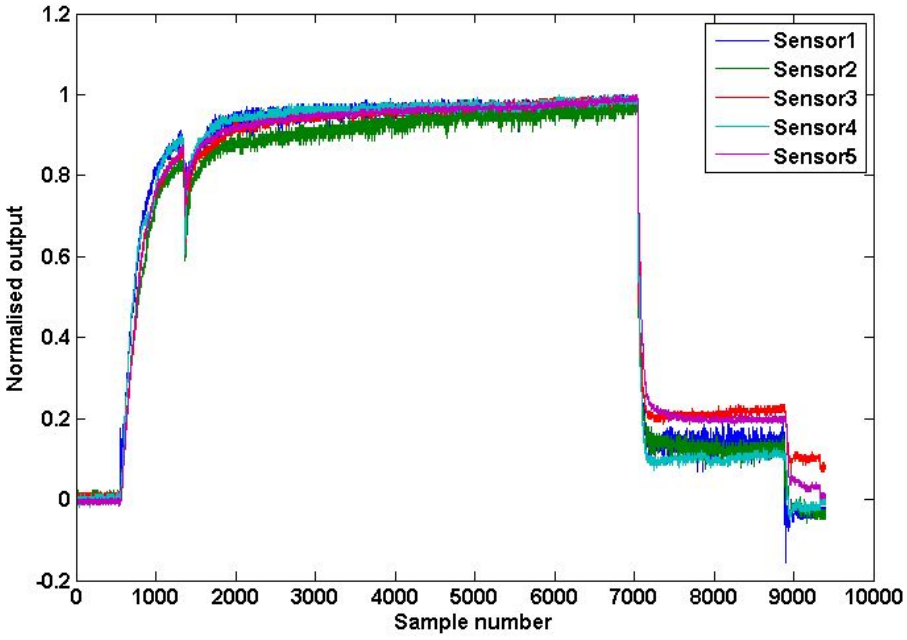

Appendix C: Particle size distribution curves

Figure C.1 Particle size distribution curve for samples from location A and B